ABLATION MODELING OF THERMAL PROTECTION SYSTEMS OF BLUNT-NOSED
BODIES AT SUPERSONIC FLIGHT SPEEDS

A THESIS SUBMITTED TO
THE GRADUATE SCHOOL OF NATURAL AND APPLIED SCIENCES
OF
MIDDLE EAST TECHNICAL UNIVERSITY

BY

BUĞRA ŞİMŞEK

IN PARTIAL FULFILLMENT OF THE REQUIREMENTS
FOR
THE DEGREE OF MASTER OF SCIENCE
IN
MECHANICAL ENGINEERING

JANUARY 2013

Approval of the Thesis:

ABLATION MODELING OF THERMAL PROTECTION SYSTEMS OF BLUNT-NOSED BODIES AT SUPERSONIC FLIGHT SPEEDS

submitted by **BUĞRA ŞİMŞEK** in partial fulfillment of the requirements for the degree of **Master of Science in Mechanical Engineering Department, Middle East Technical University** by,

Prof. Dr. Canan Özgen
Dean, Graduate School of **Natural and Applied Sciences**   _____

Prof. Dr. Suha Oral
Head of Department, **Mechanical Engineering**   _____

Prof. Dr. Hafit Yüncü
Supervisor, **Mechanical Engineering Dept., METU**   _____

Examining Committee Members:

Prof. Dr. M. Haluk Aksel
Mechanical Engineering Dept., METU   _____

Prof. Dr. Hafit Yüncü
Mechanical Engineering Dept., METU   _____

Prof. Dr. Hüseyin Vural
Mechanical Engineering Dept., METU   _____

Assist. Prof. Dr. Ahmet Yozgatlıgil
Mechanical Engineering Dept., METU   _____

Assist. Prof. Dr. Barbaros Çetin
Mechanical Engineering Dept., Bilkent University   _____

Date: **24.01.2013**

I hereby declare that all information in this document has been obtained and presented in accordance with academic rules and ethical conduct. I also declare that, as required by these rules and conduct, I have fully cited and referenced all material and results that are not original to this work.

Name, Last name   : Buğra Şimşek

Signature   :

ABSTRACT

ABLATION MODELING OF THERMAL PROTECTION SYSTEMS OF BLUNT-NOSED
BODIES AT SUPERSONIC FLIGHT SPEEDS

Şimşek, Buğra
M.S., Department of Mechanical Engineering
Supervisor: Prof. Dr. Hafit Yüncü

January 2013, 73 pages

The objective of this thesis is to predict shape change due to ablation and to find temperature distribution of the thermal protection system of a supersonic vehicle under aerodynamic heating by using finite element method. A subliming ablative is used as thermal protection material. Required material properties for the ablation analyses are found by using DSC (Differential Scanning Calorimetry) and TGA (Thermogravimetric Analysis) thermal analysis techniques. DSC is a thermal analysis technique that looks at how a material's specific heat capacity is changed by temperature and TGA is a technique in which the mass of a substance is monitored as a function of temperature. Moreover, oxyacetylene ablation tests are conducted for the subliming ablative specimens and measured recession values are compared with the analytically calculated values. Maximum difference between experimental results and analytical results is observed as 3% as seen in Table 7. For the finite element analyses, ANSYS Software is used. A numerical algorithm is developed by using programming language APDL (ANSYS Parametric Design Language) and element kill feature of ANSYS is used for simulation of ablation process. To see the effect of mesh size and time step on the solution of analyses, oxyacetylene test results are used. Numerical algorithm is also applied to the blunt-nosed section of a supersonic rocket which is made from subliming ablative material. Ablation analyses are performed for the nose section because nose recession is very important for a rocket to follow the desired trajectory and nose temperature is very important for the avionics in the inner side of the nose. By using the developed algorithm, under aerodynamic heating, shape change and temperature distribution of the nose section at the end of the flight are obtained. Moreover, effects of ablation on the trajectory of the rocket and on the flow around the rocket are examined by Missile DATCOM and CFD (computational fluid dynamics) analysis tools.

Keywords: Ablation, Thermal Protection System, Subliming Ablative

ÖZ

SÜPERSONİK HIZDA UÇAN KÜT BURUNLU HAVA ARAÇLARI ISI KALKANI SİSTEMLERİNİN AŞINMA MODELLEMESİ

Şimşek, Buğra
Yüksek Lisans, Makine Mühendisliği Bölümü
Tez Yöneticisi: Prof. Dr. Hafit Yüncü

Ocak 2013, 73 sayfa

Bu tezin amacı süpersonik hızlarda uçan bir hava aracının ısı koruma sisteminin, aerodinamik ısınma altındaki ablasyona bağlı şekil değişimini ve sıcaklık dağılımını sonlu elemanlar yöntemi kullanarak bulmaktır. Isı kalkanı malzemesi olarak süblimleşebilir bir ablatif kullanılmıştır. Aşınma analizleri için gerekli olan malzeme özellikleri ve aşınma ölçütleri DSC ve TGA yöntemleri kullanılarak bulunmuştur. DSC malzemenin özgül ısı kapasitesinin sıcaklığa bağlı değişimini ,TGA ise malzemenin ağırlığının sıcaklığa bağlı değişimini ölçebilen termal ölçüm yöntemleridir. Oksiasetilen ablasyon testlerinde ablatif malzemenin aşınma miktarları ölçülmüş, sonuçları analitik sonuçlarla karşılaştırılmıştır. Test sonuçları ile analitik sonuçlar arasındaki fark, Tablo 7'de görüldüğü gibi maksimum %3'tür. Sonlu eleman analizleri için ANSYS yazılımı kullanılmıştır. Aşınma simülasyonu için APDL (ANSYS Parametrik Tasarım Dili) program dili kullanılarak nümerik bir algoritma hazırlanmış olup eleman öldürme özelliği aşınma için kullanılmıştır. Eleman boyutu ve zaman aralığının analiz sonuçlarına etkisini görebilmek amacıyla oksiasetilen test sonuçları kullanılmıştır. Nümerik algoritma, süpersonik bir roketin süblimleşebilir ablatiften üretilmiş olan burun bölgesine de uygulanmıştır.Analizlerde burun bölgesinin kullanılma sebebi roket için burun aşınmasının istenen yörüngenin takip edilmesinde önemli etkisinin olmasıdır. Ayrıca burun kısmında yer alan aviyonik sistemler için sıcaklığın kritik seviyelere yükselmemesi gerekmektedir. Geliştirilen algoritma yardımıyla, uçuş süresi boyunca maruz kalınan aerodinamik ısınma altında, burun kısmının uçuş sonunda gösterdiği şekil değişikliği ve bu kısımda görülen sıcaklık dağılımı elde edilmiştir. Ayrıca aşınmanın roket menzili ve roket çevresindeki akış üzerindeki etkisi Missile DATCOM ve HAD (hesaplamalı akışkanlar dinamiği) analiz araçları ile incelenmiştir.

Anahtar Kelimeler: Ablasyon, Isı Kalkanı Sistemleri, Süblimleşebilen Ablatif

To My Parents

ACKNOWLEDGEMENTS

TABLE OF CONTENTS

x

LIST OF TABLES

LIST OF FIGURES

NOMENCLATURE

$\{a\}$ — Thermal gradient vector

c_p — Constant pressure specific heat capacity

$[C_e^t]$ — Element specific heat matrix

$\{F^a\}$ — Vector of applied load

$\{F_i^{nr}\}$ — Vector of resisting load

h — Heat transfer coefficient

k — Specific heat capacity ratio

k_x — Conductivity in x direction

$[K]$ — Coefficient matrix

$[K_e^{tb}]$ — Element diffusion conductivity matrix

$[K_e^{tc}]$ — Element convection surface conductivity matrix

$[K_e^{tm}]$ — Element mass transport conductivity matrix

M_1 — Mach number of flow at upstream of a shock wave

$\dot{m}$ — Mass ablation rate of the ablative material

Pr — Prandtl number

Q_a — Heat of ablation of ablative material

q''' — Heat generation rate per unit volume

q_s'' — Stagnation point heat flux

q_w'' — Heat flux to surface

$\{Q_e^c\}$ — Element convective surface heat flow vector

$\{Q_e^f\}$ — Element mass flux vector

$\{Q_e^g\}$ — Elemental heat generation load.

$\{q\}$ — Heat flow matrix

r — Recovery factor

$\{R\}$ — Residual vector

$\dot{s}$ — Recession rate of an ablative material

T — Temperature

T_r — Adiabatic wall temperature

T_w — Wall temperature

T_0 — Stagnation temperature

T_1 — Temperature of flow at upstream of a shock wave

T_2 — Temperature of flow at downstream of a shock wave

T_∞ — Free stream temperature

u_∞ — Free stream velocity

v_x — x-velocity component of flow

v_y — y-velocity component of flow

v_z — z-velocity component of flow

α — Diffusivity

Δ — Mesh size

δ — Shock detachment distance

ε — Emissivity of the surface

μ_e — Absolute viscosity of flow at the edge of the boundary layer

μ_w — Absolute viscosity of flow immediately adjacent to the wall

ρ_a — Density of ablative material

ρ_e — Density of flow at the edge of the boundary layer

ρ_w — Density of flow immediately adjacent to the wall

ρ_1 — Density of flow at upstream of a shock wave

ρ_2 — Density of flow at downstream of a shock wave

ρ_∞ — Free stream density

σ — Stefan-Boltzmann constant

CHAPTER 1

INTRODUCTION

"...re-entry...is perhaps one of the most difficult problems one can imagine...It is certainly a problem that constitutes a challenge to the best brains working in these domains of modern aero physics...possible means [include] mass transfer cooling, consisting of a coating that sublimates or chemically dissociates..."
Theodore von Karman   [1]

1.1 Background

At hypersonic or supersonic flight speeds, produced shock wave and viscous dissipation effects increase the temperature of the gases adjacent to the high-speed vehicle's surface. Temperature of the gases can reach elevated values at which dissociation or even ionization of the gases occur [2]. An increase in the temperature of the adjacent gases causes heat flux to the relatively cooler surface and this heating process is called *Aerodynamic Heating*. In the field of aerospace, one of the most important design considerations is aerodynamic heating. Structural parts and electronic equipments of the vehicle have limited operating temperatures; therefore, it is compulsory for the designer to minimize the heat conducted into the body to prevent failure of the high-speed vehicle due to high thermal loads.

Thermal protection systems minimize the heat conducted into the body to prevent the failure of the body. There are many types of thermal protection systems which are explained in this thesis in detail. Selection of thermal protection system depends on many parameters such as trajectory, maximum velocity, geometry and cost of system application.

Ablation is one of the most widely used processes on the thermal protection systems. In this process, energy is rejected from the body by mass loss. Mass loss can be achieved by phase change, decomposition, oxidation or chemical erosion. During these processes, energy is absorbed; therefore, energy conducted into the body is reduced. Moreover, mass injection into the boundary layer, just outside the surface, decreases the heating value due to *blockage effect* which is explained in this thesis in detail [1].

During design phase, determination of thickness of the insulation is very important. Smaller thickness than required causes the vehicle to explode at the mission due to high temperature levels seen in warhead section, or to fail to follow trajectory due to drastic change at its nose section because of high levels of recessions. However, larger thickness than required can increase cost and weight of the vehicle which is undesirable. As a result, optimum thickness for the ablative material should be determined at the design phase of high-speed air vehicles.

To determine the thickness of the thermal protection systems, characterization of the insulation material should be performed and thermal analyses should be conducted to find and examine the temperature distribution on the components. These analyses are only possible by use of computer tools that can model ablation process.

1.2 Scope of the Thesis

Teflon is one of the widely used ablative materials used in the nose sections of the high-speed rockets in aerospace. In this thesis, ablative performance of Teflon was conducted under oxyacetylene ablation tests and a computer tool was developed to simulate the ablation process of Teflon under high heat fluxes. Computer tool was developed by using *ANSYS Parametric Design Language (APDL)*. Results of analyses and tests were compared to validate the computer tool. Computer tool was also applied to the nose section of a rocket by using available aerodynamic heating values. Recession due to ablation and temperature distribution at the end of flight were obtained. Effects of ablation on the trajectory and flow are also examined.

1.3 Purpose of the Thesis

The objective of this thesis is to predict the shape change due to ablation and to find temperature distribution of the thermal protection system of a supersonic vehicle under aerodynamic heating by using finite element method. Material characterization and oxyacetylene ablation tests for Teflon are also conducted for this study. By using material characterization and test results, a numerical algorithm is developed. The study will provide a tool that can model ablation process under known aerodynamic heating; therefore, design of missiles and rockets at high flight velocities will be modified and improved. It is well known fact that the success of a missile or rocket mission on the target depends on the correct evaluation of the thermal loads on the vehicle. It is also believed that this study will be one of the milestones of the space projects in which ablation analyses are compulsory to design thermal protection systems of satellites or re-entry vehicles.

1.4 Outline of the Thesis

The chapters are organized as follows. In Chapter 2, brief explanations about aerodynamic heating and thermal protection systems are given. In Chapter 3, literature survey on the corresponding field is introduced. In Chapter 4, detailed information about DSC (Differential Scanning Calorimetry) and TGA (Thermogravimetric Analysis) thermal analysis techniques are given and DSC and TGA results of Teflon are supplied. In Chapter 5, governing equations and computational domains for the thermal analyses are given. In Chapter 6, numerical approaches to an ablation problem are described and methodology of the developed numerical algorithm is presented. In Chapter 7, oxyacetylene ablation test results of Teflon are given and results are compared with the theoretical values. In Chapter 8, developed numerical algorithm is applied to the test specimens. Moreover, developed algorithm is applied to the nose section of a rocket and temperature and recession distributions are presented for the end of the flight. Results of trajectory simulations and CFD analyses are also given in this chapter. In Chapter 9, summary and conclusions of this thesis study and recommendations for the future works are given. In Appendix section, detailed information about ANSYS solver is given.

CHAPTER 2

AERODYNAMIC HEATING AND THERMAL PROTECTION SYSTEMS

In this chapter, detailed information about aerodynamic heating and thermal protection systems is given.

2.1 Aero-thermodynamics

"*Aero-thermodynamics*" is a scientific and technical discipline in which aerodynamics and thermodynamics are combined. The word "aero" represents the field of *aerodynamics* and rest of the term stands for *thermodynamics*. It is Italian air force general and aeronautical engineer General G. Arturo Crocco who is the first used the term aero-thermodynamics in 1931 and it is Theodore von Karman who introduced and propagated the term in the United States in 1940 [2].

In 1949, Ludwig Prandtl defined aerodynamics as a term which is used for problems arising from flight and other topics involving the flow of air [3]. Aerodynamics has been developing over the past two centuries since Sir George Cayley published his studies as three part treatise "On Aerial Navigation". In his triple paper, he studied on the basic principles of the aero-thermodynamics. He designed a fixed-wing aircraft and he separated propulsion system and tail systems for an airplane. To illustrate his studies, helicopter design from "On Aerial Navigation" is given in Figure 1[4].
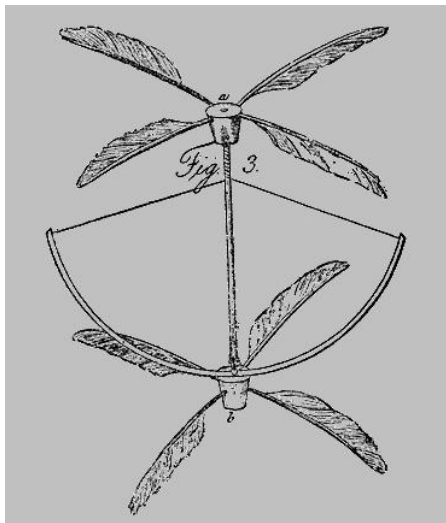
Figure 1: George Cayley's Helicopter Design from "On Aerial Navigation" [4]

Aerodynamics studies were based on assumptions of low-speed incompressible flow in which mechanical laws are valid. However, with the advent of high-speed flight in the 1940s, energy became the one of the most important parameters that governs the flow. This consideration wed the science of thermodynamics to the science of the aerodynamics [2].

Aero-thermodynamics assumed calorically perfect gas flow until 1960s. In this assumption, specific heat capacity of gases, constant pressure c_p and at constant volume c_v, are constant and their ratio k, is equal to 1.4 for air. By the principles of this first classical aero-thermodynamics, temperature ratio across a normal shock wave ahead of high velocity air vehicle can be calculated analytically or can be found in a standard table. Analytically temperature ratio is given as [5]:

$$\frac{T_2}{T_1} = \frac{\left[2kM_1^2 - (k-1)\right]\left[(k-1)M_1^2 + 2\right]}{(k+1)^2 M_1^2} \tag{2.1}$$

where T_2 is the temperature of the flow at downstream of a shock wave, T_1 is the temperature of the flow at up-stream of a shock wave, k is the ratio of specific heat capacities and M_1 is the mach number of flow at up-stream of a shock wave. If this equation is applied to the Apollo 11 spacecraft, some interesting results can be reached.

Apollo 11, the spaceflight which landed the first humans on the Moon, returned from the mission on July 24, 1969 and at an altitude of 53 km at which atmospheric temperature is 283 K; its speed was 11.2 km/s. [2]. By using above equation, temperature at the immediately downstream of the shock wave can be found nearly 58000 K which is too high and totally incorrect. Therefore, a new aero-thermodynamics principle is required for high mach numbers as high as 36, as seen in Apollo 11 trajectory, in which k is not constant. Chemical reactions in the flow and molecular vibrations should be considered in this *new aero-thermodynamics*. High temperature effects in shock layers are concentrated by this "newer" aero-thermodynamics [2].

A shock wave is very thin region since its thickness is in the order of nearly 10^{-5} cm, and flow properties can change drastically across it. Just ahead of a blunt-nosed body, flying at supersonic or hypersonic flight speeds, detached bow shock wave appears. This wave converts the kinetic energy associated with the flight speed into internal energy of the gas, yielding very high temperatures in the shock layer close to the nose of the body. In addition, at the downstream of the nose region, viscous dissipation effects also increase the temperature of the flow. The behavior of the flow directly depends on the magnitude of the temperature [2].
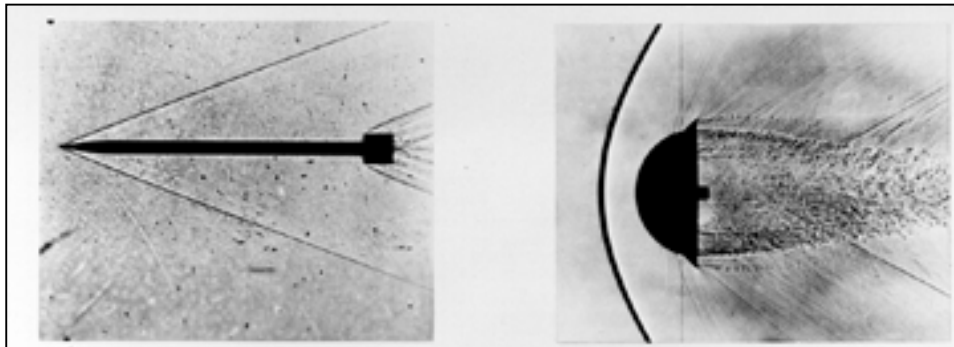
Figure 2: Contrast of Shock Waves for Slender and Blunt Nosed Vehicles [6]

In modern aero-thermodynamics, contrary to classical aero-thermodynamics, k is not constant at elevated temperatures (above 800 K [2]). Moreover, the thermodynamic properties of the flow are completely different. The transport properties are different also. If the temperature is too high, the flow is in plasma form due to ionization of the molecules of the gases. For air, chemical reaction effects become important at some critical temperature levels. Temperature ranges of dissociation and ionization for air is given in Figure 3 [2].
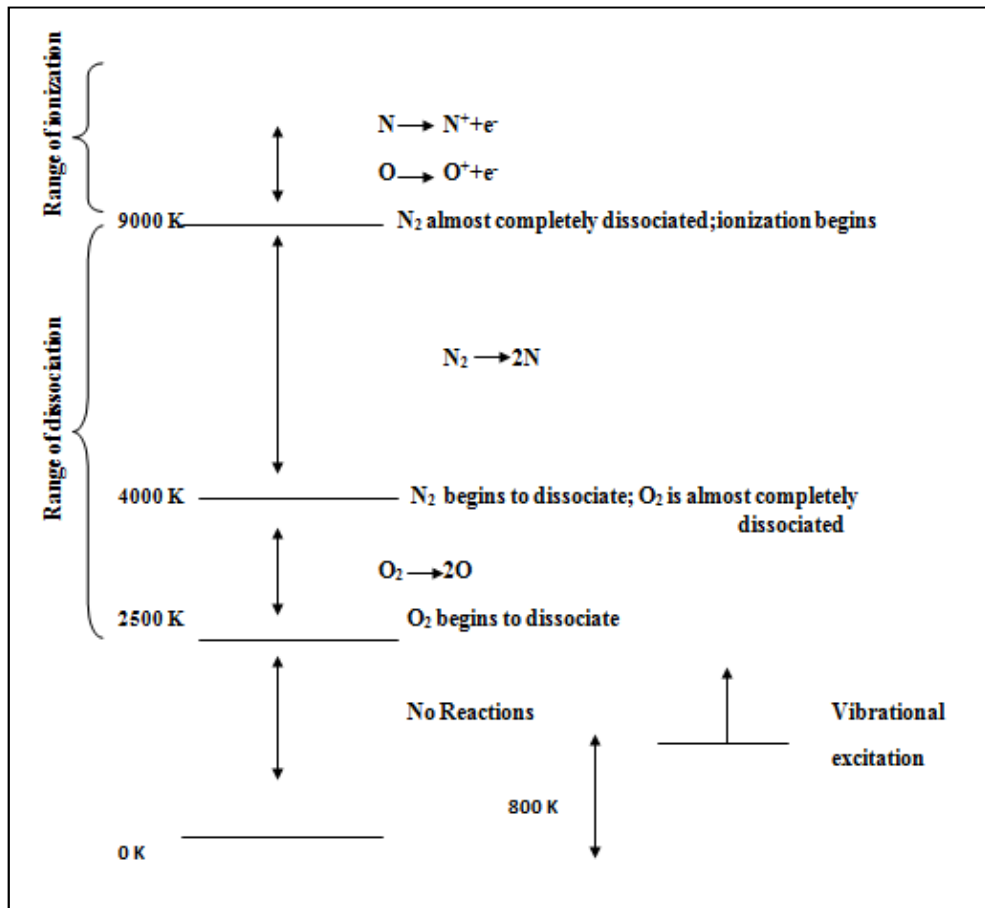
Figure 3: Ranges of Excitation, Dissociation, and Ionization for Air at Pressure of 1-atm [2]

As seen in Figure 3, at a temperature of 800 K, energy of the molecules becomes significant. Although this is not a chemical reaction, it affects the properties of the gases in flow. At 2000 K, O_2 begins to dissociate and at 4000 K, N_2 begins to dissociate. Above 9000 K, flow is in plasma form including O, O^+, N^+ and electrons. For high-speed air vehicles, such as some kind of rockets and missiles, trajectory and velocity history are very critical to the engineer to predict the characteristics of the flow since temperature seen in the flow is a direct result of the velocity and trajectory of the flight.

Aero-thermodynamics classifies gases in three different types. First one is *real gas* in which intermolecular forces are important and must be accounted for; second one is *calorically perfect gas* which has constant specific heat capacities, c_p and c_v, and constant ratio of specific heat capacities, k.

Third one is the *ideal gas* and c_p and c_v of this kind of gas are functions of temperature only. The assumption of an ideal gas is suitable for most of the aerodynamic problems since real gas assumption requires high pressures and low temperatures [2].

Equilibrium of the gases in flow is one of the most important conditions that engineers deals with. In thermodynamic equilibrium condition, gas properties are identical with the ones at their equilibrium values under corresponding temperatures at every point of the flow [2]. For equilibrium condition, it is assumed that the gas has had enough time for collisions to occur. In non-equilibrium condition, there is no enough time for collisions to occur. To illustrate, when the flow passes through a shock wave, pressure and temperature suddenly increase and fluid particles have to seek new properties under these new pressure and temperatures. However, up to reach this new properties, fluid particles will be moved in a path in which non-equilibrium condition is valid. Therefore, behind the shock waves there is a region where non-equilibrium conditions for the flow are seen. If the density of the air is high enough, there will be sufficient collisions between the air molecules; so, equilibrium condition is quickly achieved [2].

2.2 Aerodynamic Heating

Aerodynamic heating of a blunt body is a consequence of flow of air at high-speed around it. Kinetic energy of the motion is converted into heat within the boundary layer of air surrounding the body due to internal friction and compressibility effects [7]. Heating is a function of fluid density, body velocity, temperature or enthalpy difference between surface and boundary layer gases and size or sharpness of the moving body [8].

Before examining the effect of mentioned parameters on the aerodynamic heating it is better to define *adiabatic wall temperature*. By definition, adiabatic wall temperature is the temperature acquired by a wall in a liquid or gas flow if the condition of thermal insulation is observed on it. This temperature is also known as the recovery temperature and denoted as T_r. Mathematically T_r is equal to:

$$T_r = T_\infty (1 + r \frac{k-1}{2} M_\infty^2)$$
(2.2)

r is the recovery factor and it is given by

$$r = \sqrt{Pr}$$
(2.3)

for a laminar boundary layer and it is given by

$$r = \sqrt[3]{Pr}$$
(2.4)

for a turbulent boundary layer [5]. In these equations T_r is the recovery temperature, r is the recovery factor, Pr is the Prandtl number and T_∞ and M_∞ are the free stream conditions for the temperature and mach number. Finally, it is possible to define convective heat transfer as [5];

$$q_w'' = h(T_r - T_w)$$
(2.5)

where q_w'' is the heat flux to surface, h is the heat transfer coefficient, and T_w is the wall temperature.

The temperature profile in the boundary layer of a high velocity gas flow over an adiabatic surface is given in Figure 4.
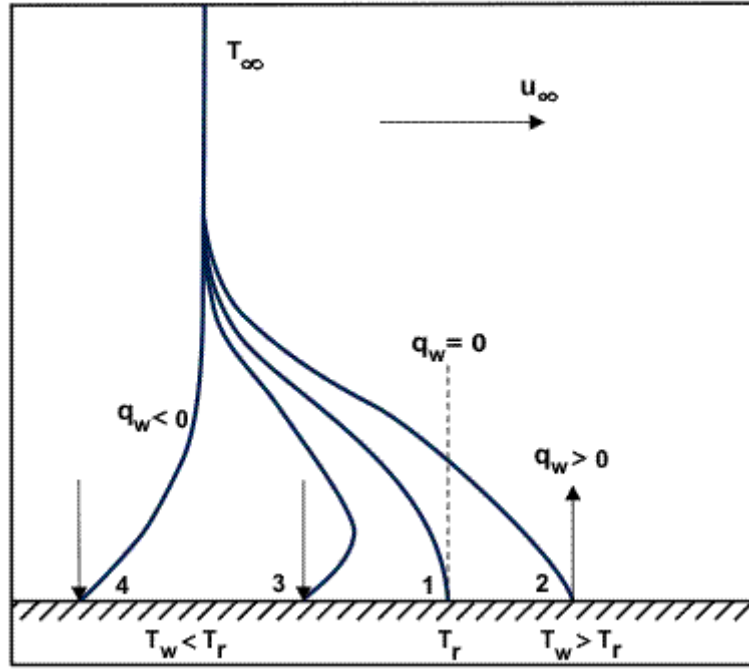
Figure 4: Temperature Profile within Boundary Layer over an Adiabatic Surface [9].

As seen in Figure 4, if $T_w < T_r$, heat is transferred from the flow to the surface and if $T_w > T_r$ heat is transferred from the surface to the flow [9].

Shape of the body is one of the most important parameters that affect the aerodynamic heating as mentioned before. Harry Julian Allen is the one who developed the Blunt Body Theory. In his theory, Allen showed that, a blunt body would have a detached shock wave instead of an attached shock wave, which would decrease the heat transfer to the surface [10].

Shock detachment distance in the blunt body theory, is mainly affected by the density ratio ρ_2/ρ_1. An approximate expression for the shock detachment distance δ on a sphere of radius R is given as follow [2]:

$$\frac{\delta}{R} = \frac{\rho_1/\rho_2}{1+\sqrt{2(\rho_1/\rho_2)}} \tag{2.6}$$

where R is the nose radius, δ is the shock detachment distance, ρ_1 and ρ_2 are the densities of the flow at the up-stream and downstream of the shock wave. Stagnation point heat flux to blunt body is inversely proportional to the square root of the nose radius [11].

$$q_s'' \propto 1/\sqrt{R} \tag{2.7}$$

Calculation of stagnation point convective heat transfer rate is one of the most important studies in the area of supersonic and hypersonic aero-thermodynamics. There are many empirical calculation methods for the stagnation point heating in the literature and three of them are presented in this section.

Scott correlation is one of the empirical equations and it is expressed as follow [5]:

$$q_s'' = \frac{18300(\rho_\infty)^{0.5}}{\sqrt{R}} \left[\frac{u_\infty}{10^4}\right]^{3.05} \tag{2.8}$$

where free stream density, ρ_∞ ,is expressed in kg/m^3, the free stream velocity, u_∞, in m/s, the nose radius, R, in m and the stagnation heat transfer rate, q_s'', in W/cm^2.

Detra correlation is another equation used for stagnation point convective heat transfer rates. It is expressed as follow [5]:

$$q_s'' = \frac{11030}{(R)^{0.5}} \left(\frac{\rho_\infty}{\rho_{SL}}\right)^{0.5} \left(\frac{u_\infty}{u_{CO}}\right)^{3.15} \tag{2.9}$$

In this equation, the nose radius of the sphere in m, density at sea level, ρ_{SL}, in kg/m^3 and u_{CO} is the circular orbit velocity in m/s which is equal to 7950 m/s.

The equation suggested by Fay and Riddel is the reference point for the engineers studying the area of aero-thermodynamics due to its simplicity. Correlation formulae are still in use for thermal analysis of high-speed vehicles. The correlation is expressed as follow [12]:

$$q_s'' = 0.763 Pr^{-0.6}(\rho_e\mu_e)^{0.4}(\rho_w\mu_w)^{0.1} \left(\frac{du_e}{dS}\right)^{0.5} \left[c_p(T_0 - T_W)\right] \tag{2.10}$$

where ρ is the density, μ is the viscosity c_p is the specific heat capacity, T_0 is the stagnation temperature and e denotes conditions at the edge of the boundary layer and w denotes wall conditions.

The velocity gradient term given in equation (2.13) is expressed as follow:

$$\frac{du_e}{dS} = \frac{1}{R}\sqrt{\frac{2(P_e - P_\infty)}{\rho_e}} \tag{2.11}$$

Where P is the pressure and e and ∞ symbols denote edge of the boundary layer and free stream conditions.

Advances in the computer sciences make it possible to differentiate most of the complex equations numerically; therefore, by using CFD techniques many realistic geometries and flight conditions of interest can be used to calculate aerodynamic heating values. Two types of codes are used to model supersonic or hypersonic flows for engineering analyses. The first one is coupled Euler/boundary layer methods which is suitable for high Reynolds number conditions in which viscous layer is very thin compared to shock layer thickness. The second one is parabolic Navier-Stokes Methods which are capable of solving viscous interaction effects related to lower Reynolds numbers and thick viscous layers [2].

2.3 Thermal Protection Systems

Due to high aerodynamic heating values as a result of high flight velocities mentioned above, thermal protection systems should be used since structural parts and electronic equipment in the vehicle have limited operating temperatures. According to cooling process, thermal management of protection systems are classified as passive, semi-passive and active systems. Active systems include pumped coolant, and passive and semi-passive systems include phase change phenomena. Types of thermal protection systems are briefly explained below.

2.3.1 Radiative Systems

This is one of the passive thermal protection systems and in this type of thermal protection system energy input from the high temperature boundary layer at the outside of the vehicle is reradiated to the atmosphere. Only a small amount of heat is conducted to the structure through the insulation. This system does not involve any mass loss and surface temperature can be expressed as follow if surface convective heat flux and surface-reradiated heat fluxes are in equilibrium [13]:

$$T_w = \sqrt[4]{\left(\frac{q_w''}{\sigma\varepsilon}\right)} \tag{2.15}$$

where σ is the Stefan-Boltzmann constant and ε is the emissivity of the surface.

Elevons of the space shuttle mission of NASA, STS-116, are protected by this kind of thermal protection system in 2006 [14]. Schematic representative of system is given in Figure 5.
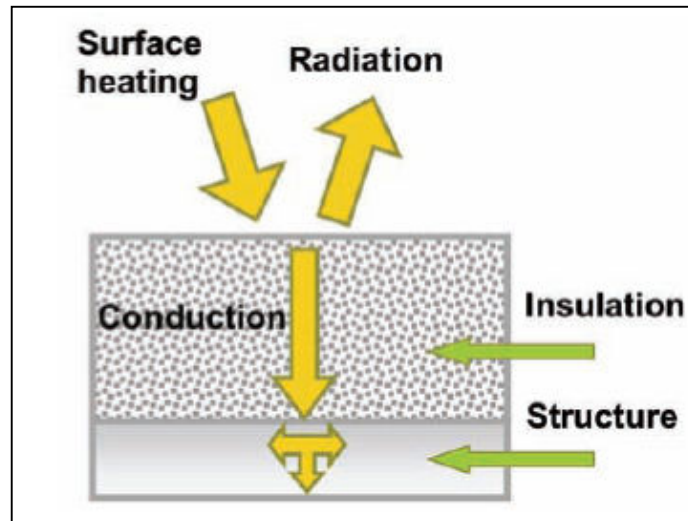
Figure 5: Schematic of Radiative Thermal Protection System [14]

In this system as given in the equation (2.15) operating temperature limit is determined by the used material and maximum heating rate is determined by the operating temperature. Moreover, small increases in the operating temperature limit, increases permitted heating rate rapidly.

Ceramics (oxides, carbides) are commonly used materials as radiative systems and their maximum operating temperatures are nearly 2500 K. Main disadvantage of them is their brittleness and main advantage of this system is the unnecessary material renewal between flights [15].

2.3.2 Heat Sink Systems

In this passive thermal protection system, heat sink absorbs aerodynamic heat during flight without melting or vaporization. The schematic representative of the system is given in Figure 6.
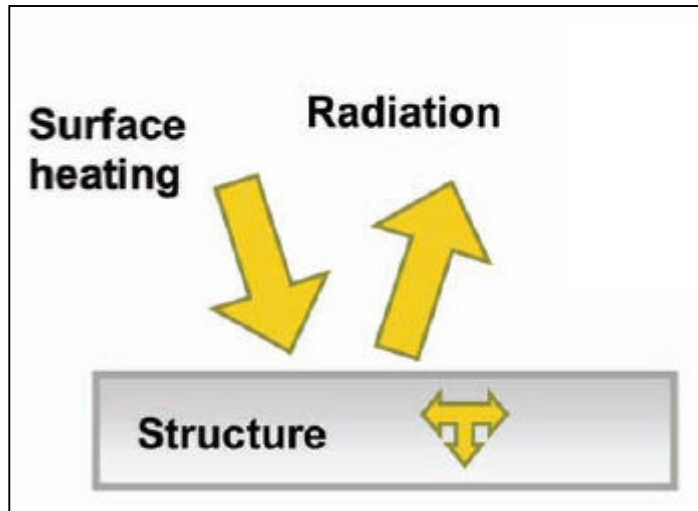
Figure 6: Schematic of Heat Sink Thermal Protection System [14]

The principal advantage of the system is its simplicity and reliability. Thermal material properties of the most of heat sink materials are well known and hand calculations can be made during design phase due to simplicity of the heat absorption process. The large weight of the heat sink materials is main disadvantage of the system [15].

Efficiency of the system mainly depends on the mass, specific heat capacity and limiting temperature of the material. Properties of some commonly used heat absorbing materials are given in Table 1[13].

Table 1: Properties of Heat Absorbing Materials

Material	k, W/m K	ρ, kg/m^3	c kJ/kg K	T_p, K
Copper	368	8950	0.37	1370
Tungsten	150	19300	0.08	3640
Graphite	130	2190	1.68	4000

Leading edges of the rocket powered aircraft *North American X-15* are protected from aerodynamic heating by heat sink thermal protection system [14].

2.3.3 Transpiration and Film Cooling Systems

In this active thermal protection system, gaseous or liquid material is injected into boundary layer outside the wall of vehicle in order to reduce the surface aerodynamic heating. The schematic representative of the system is given in Figure 7 [14].
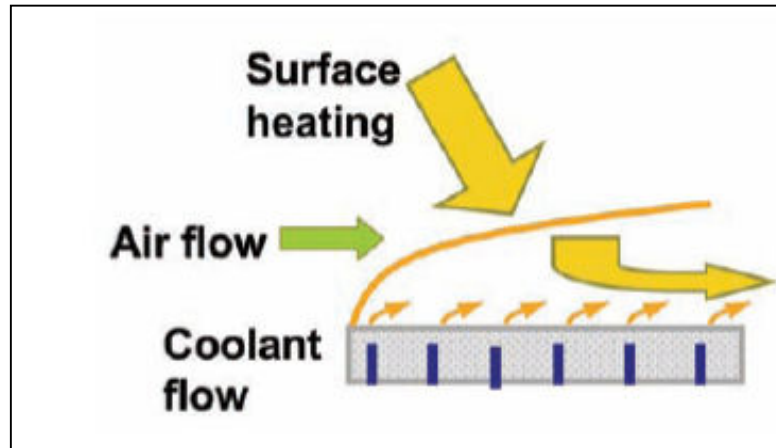
Figure 7: Schematic of Transpiration Cooling Thermal Protection System [14]

If porous inert matrix is used, the system called as transpiration cooling system and if series of discrete slots are used, the system is called as film cooling system [15]. Mass injection into boundary layer decreases net heat flux into surface. Injection process thickens the boundary layer which results in a decrease in the velocity and temperature gradient adjacent to the vehicle wall. Effect of mass injection rate into boundary layer on the surface heat transfer rate is given in Figure 8 [2].
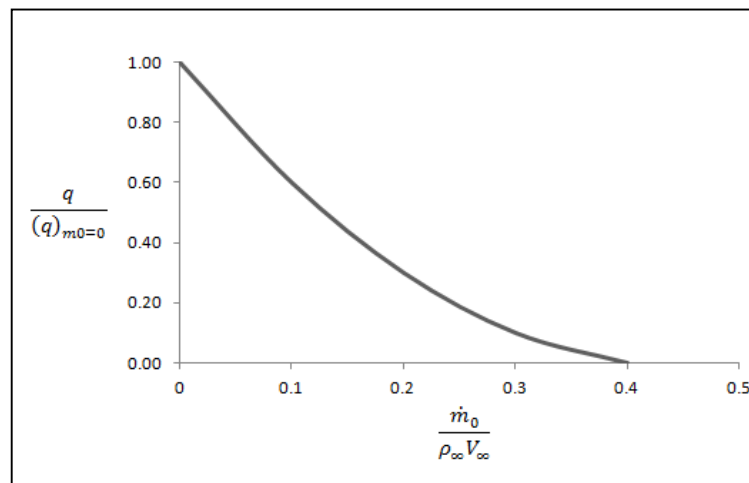
Figure 8: Mass Injection Effect on Stagnation Heat Transfer

However, designer should be careful since mass injection can cause destabilization of flow and this destabilization changes the flow from laminar to turbulent which yields higher aerodynamic heating acting on the surface [15]. As can be seen in Figure 8, an increase in the mass injection rate decreases the surface heat transfer rate. However, maximum rate of mass injection is limited. For high heat fluxes, for long time periods active cooling system should be used. Space shuttle main engines are generally protected by this kind of thermal protection systems [14].

11

2.3.4 Ablative Systems

Ablative systems are the most important type of semi-passive thermal protection systems in which ablation of material occurs. Ablation of an insulation material is a sacrificial method of heat protection since destruction of material is permitted in order to maintain surface temperature between limited temperatures. Most preferred thermal protection systems are the ablative systems because of their light weight, high efficiency and inherent simplicity with reliability [15]. The schematic representative of the system is given in Figure 9.
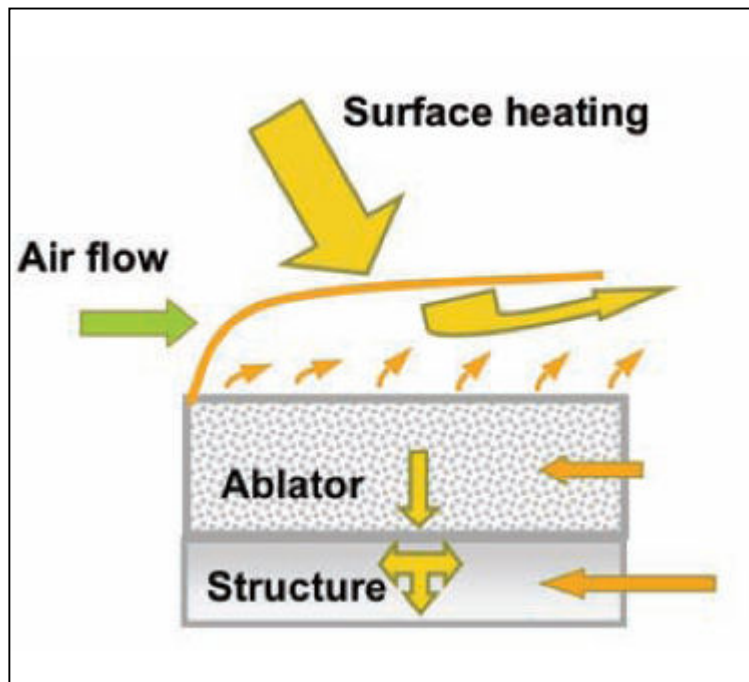
Figure 9: Schematic of Ablative Thermal Protection System [14]

During ablation process, decomposition or phase change of material absorbs large amount of energy and created pyrolysis gases due to decomposition are injected to the boundary layer and *blockage effect* is maintained [15]. Subliming, melting-vaporizing and charring ablators are most commonly used ablative materials in this system.

2.3.4.1 Subliming Ablators

These kind of ablative materials change phases from solid to gas directly and during decomposition high amount of energy is absorbed. Teflon and graphite are the subliming ablators. In this thesis, Teflon characterization and its ablation process are studied. Teflon has high recession rates compared to graphite; therefore, for long-duration flights it is not preferred. Teflon decomposes at nearly 750 K, but graphite sublimes at temperatures as high as 4000 K [14].Therefore, graphite is also used in nozzle of missiles due to its low recession rates and high temperature limits. However, the main disadvantage of graphite is its brittleness and low resistance to thermal stresses [15].

2.3.4.2 Melting-Vaporizing Ablators

These kind of ablative materials melt at elevated temperatures with absorbing energy and then vaporize at vaporization temperature with absorbing latent heat of vaporization. Mass injection to the boundary layer is also performed which causes transpiration cooling. The glassy materials including quartz, Pyrex and fused silica are the examples of the melting-vaporizing ablators. The main disadvantage of these materials is their low emissivity and transparency. Transparency can cause self-heating to the interior by radiation. Therefore, base material should be used to increase their emissivity and to make them opaque. Brittleness of them is also a disadvantage of these kinds of materials [15].

2.3.4.3 Charring Ablators

These kind of ablative materials are generally reinforced composite materials including organic resins as binders. Heating of these materials causes the decomposition at elevated temperatures yielding resin pyrolizations. Gaseous products of pyrolizations are generally hydrocarbons, and they are injected to the boundary layer. As mentioned before, this injection decreases the aerodynamic heating due to thickening of boundary layer. Moreover, resin pyrolysis also produces carbonaceous residue called *char* on the surface. Pyrolysis process is an endothermic process and high amount of energy is absorbed during decomposition. During diffusion of pyrolysis gases toward the surface, they are heated and some amount of energy is also absorbed by this heating process [15]. The zones within the ablative materials are given in Figure 10 [16].
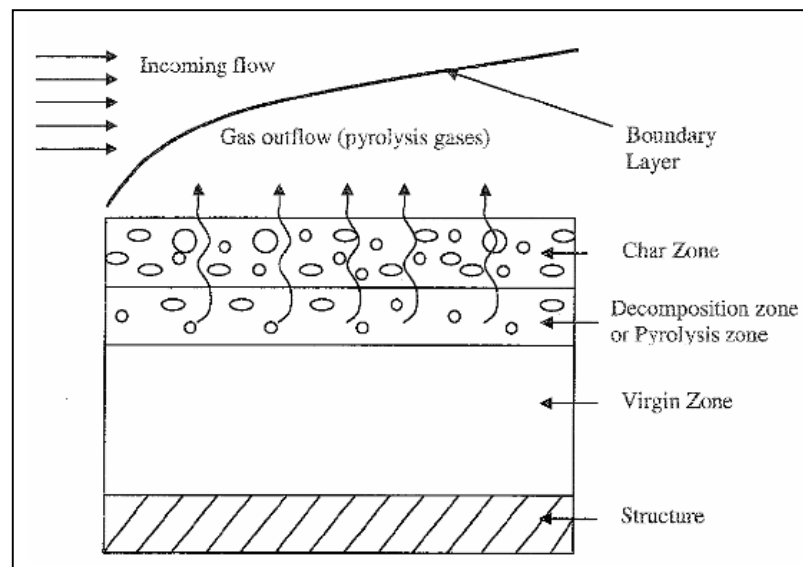
Figure 10: The zones within the charring ablative material [16]

The pyrolysis temperature of ablative material is a function of local pressure and ablation rate and generally it is between 500 K and 800 K [15]. The pyrolysis temperature can be found by TGA testing and this kind of test is conducted in this thesis work.

SLA-561 V (*Super Light Weight Ablator*) which is made by Lockheed Martin and PICA (*Phenolic Impregnated Carbon Ablator*) which is made by NASA Ames Research Center are one of the most common charring ablative materials used for thermal protection systems. Chronology of ablative thermal protection systems for NASA missions is given in Figure 11 [17].
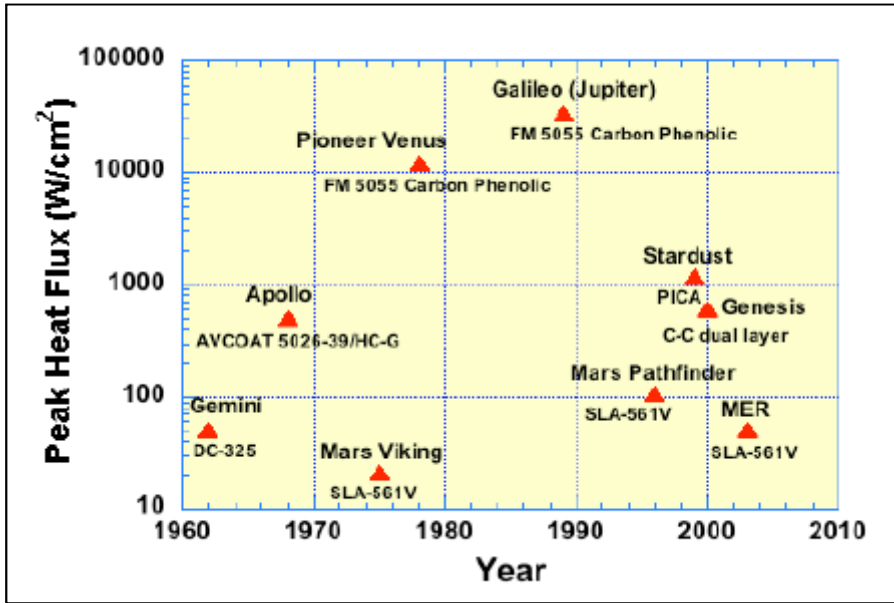
Figure 11: Chronology of Ablative TPS for NASA Missions

CHAPTER 3

LITERATURE SURVEY

Studies on the aerodynamic heating and ablative modeling of thermal protection systems have been continuing since the advent of modern aero-thermodynamics. It is obvious that advances in the modern technology will enable engineers to design higher flight speed vehicles. Higher flight speeds will be possible only with the studies and developments on the area of thermal protection system design. In this chapter, some studies on the aerodynamic heating calculations and thermal protection systems are presented. However, the pool of references in the literature is very limited due to high security of the information on the high-speed vehicle design.

3.1 Survey on Aerodynamic Heating

Lees [18] worked on the aerodynamic heating distribution over blunt-nosed bodies at hypersonic flight speeds. In his study, laminar heat transfer is divided into two limiting cases which are thermodynamic equilibrium condition and diffusion as rate-governing. In the first limiting case, surface heat transfer rate distribution is obtained from surface pressure distribution. Distribution graphs are given for the sphere capped blunt cone. In the second limiting case, atomic recombination rates are neglected and diffusion controlled heat transfer is calculated. In the study, maximum value of the ratio of the rate at which heat is transferred by diffusion and by conduction is found nearly 1.30. In the study, it is also stated that actual physical situation lies between these two limiting cases.

Saravan et al. [12] carried out experiments to obtain convective heating rate distribution on a blunt nose body at hypersonic flight speeds. The tests were conducted at Mach numbers of 5.75 and 8. Platinum thin film gauges are used to measure surface temperatures. Cook-Felderman technique is used to obtain surface heating rates from the measured temperatures. In the study, surface heat fluxes also calculated by using numerical simulations. CFX-Ansys 5.7 commercial package software is used for the simulations. The results of experimental and numerical calculations for the stagnation point heating rates are compared with the Fay and Riddel correlation formulae. The compared results fall within a band of ±10% which is acceptable. Surface heat flux distributions are also given with respect to distance from nose tip. Experimental data and numerical results of surface flux distribution showed a good agreement with each other in the study.

Zoby et al. [19] developed convective heat transfer prediction methods for blunt nosed spacecrafts under hypersonic flight speeds. They presented heat-transfer equations for both laminar and turbulent flows and for both reacting and non-reacting gas flows. The equations were given in detail and results of them for specific flight conditions were compared with experimental results and available analytical solutions. Venusian and Jovian entry conditions are some of the used flight conditions on calculations. They found good agreement between approximately calculated results and available experimental data as well as analytical results.

Quinn and Gong [20] developed a computer program to calculate aerodynamic heating values for high-speed vehicles. In their computer tool, calculations were made for cones flat plates and wedges under different angle of attack values. Laminar or turbulent effect of flow was also considered in the calculations. They used Fay and Riddel correlation for the stagnation point heating which is explained in detail in Chapter 2. For a given flight trajectory and geometry, results of calculations for specified locations on the vehicle surface was compared with the results of in-house batch computer program called AEROHEATING. The agreement between the results of developed tool and AEROHEATING program were presented. They concluded that applied method can be used for thermal simulations of hypersonic air breathing vehicles.

Arnas et al. [21] were presented analytical study of the aerodynamic heating problem. In their study, they simplified equation of state and general conservation equations which are conservation of momentum, conservation of mass and conservation of energy. They simplified the equations since simultaneous exact solution of these equations cannot be achieved mathematically. In their calculations equations were solved by use of similarity parameters, curve fitting techniques and approximate integral method. They solved a case study for adiabatic flat plate and derived convective heat transfer coefficient for aerodynamic heating problem. They also derived Nusselt number relations for laminar and turbulent flows analytically

3.2 Survey on Modeling of Ablation

Candane et al. [22] performed a quasi-one dimensional ablation analysis by using an in-house code. Analyses were conducted for a sharp-nosed re-entry vehicle on which zirconium boride (ZrB_2) and Avcoat had been used as thermal protection materials. They conducted CFD simulations to obtain aerodynamic heating values by using commercial package program FLUENT. Three points were selected at the reentry trajectory and simulations were made under steady state assumption. The calculated aerodynamic heating values were used as input for the ablation code. They validated ablation code with the results of experimental data. The maximum error between the cases they considered and the ablation code were found within 8%. Their study is very similar to this thesis work. Their test data which were compared with the numerical results are given in Table 2. In this thesis, as mentioned before, numerical results are also compared with the test data. However, in this study Teflon material is used as ablative material instead of Avcoat and PICA (Phenolic Impregnated Carbon Ablator) ablative materials.

Table 2: Comparison of Numerical Results with the Test Data

Experimental Models	Density (kg/m³)	Heat Flux (MW/m²)	Test time (s)	Latent Heat (MJ/kg)	Recession (mm)	Calculated recession (mm)
Avcoat	512.60	33.61	10	82.67	7.93	7.68
PICA-1	350.47	29.64	10	366.76	2.21	2.21
PICA-2	360.69	9.65	22	201.57	2.72	2.91
PICA-3	371.32	8.57	25	191.33	2.79	2.99

In the following chapters, test data and calculated recession rates are also compared and similar table is given for Teflon ablation.

Ertürk [15] in his master thesis studied on the modeling of ablation and shape change of thermal protection systems for high-speed air vehicles. Modeling was based on finite element analysis of ablative materials using a commercial analysis program MARC. Element deactivation and latent heat options were used for modeling. Elements having temperature larger than ablation temperature were deactivated to simulate recession. Moreover, effective heat of ablative material was defined as latent heat at ablation temperature. Boundary conditions on the deactivated elements were carried to inner active elements manually during analyses. Therefore, in the study total numbers of elements were limited. Test cases were solved for validation and a case for missile nose ablation was also presented.

Chen and Milos [23] studied on the numerical code named as FIAT (Fully Implicit Ablation and Thermal Analysis) for modeling charring ablation process of PICA and SIRCA (Silicone Impregnated Reusable Ceramic Ablator) materials. In the study, governing equations solved by

FIAT were presented and numerical procedures were explained in detail. Solutions were also compared with the results of another available code CMA (Charring Material Ablation Code) and arc jet test data. They stated that FIAT was numerically more stable than CMA because of the nature of the explicit scheme used in CMA. Case studies were conducted for real flight missions including MARS 2001 and Saturn Entry Probe.

Dec and Braun [24] developed a computer tool to analyze ablative thermal protection system behavior for entry vehicles. In their study, they estimated aerodynamic heating values by using the Sutton-Graves convective heating relation. Ablation process under calculated heat fluxes were modeled under steady state assumption. In this assumption, they used effective heat of ablation for the ablative materials to calculate recession rate of materials. The used equation in their computer tool for recession rate calculations is given below.

$$\dot{s} = \frac{q_w''}{\rho_a.Q_a} \qquad (3.1)$$

where $\dot{s}$ is the recession rate, q_w'' is the hot wall heat transfer rate, ρ is the density of the ablative material and Q_a is the heat of ablation of the ablative material.

They stated that this equation for recession calculation generally over predict the actual recession rate. Therefore, they proposed to use a threshold temperature after which recession of ablative material starts. For verification of their computer tool they examined two flight systems and results of computer tool were compared with the results of CMA computer tool. They observed good agreement between the results.

McAlees Jr. and Maydew [25] modeled ablation of thermal protection system of Talos-Terrior-Recruit (TATER) rocket system which is a three stage solid propellant rocket. They used much kind of computer tools during analyses. The NASA/AMES Flow Field (NAFF) code was used for shock wave and pressure calculations, the BLUNTY code was used to calculate aerodynamic heating values and CMA and ASTHMA (Axisymmetric Transient Heat Conduction Material Ablation) Codes were used to calculate temperature distribution and recession rates of the ablative material. The results of the analyses were compared with the test results. During flight tests, ATJ-S Graphite material was used at the nose tip of the rocket and Dynatherm DE-350 (Sparesyl) was used to protect fin sidewalls and motor case. Recession rates from nose tip were measured by using an acoustic gage and temperature histories of specified locations were measured by thermocouples. They compared the results, and concluded that followed method was suitable to model thermal protection systems of high-speed air vehicles.

Lin [26] studied on the one-dimensional quasi-steady ablation process of semi-infinite charring ablative materials theoretically. In the study governing equations including mass and energy conservation equations are presented and temperature distributions for virgin and char zone are derived. A transient numerical code for the analyses of the ablation process called as CAMAC is also developed. In the study comparison of the results of theoretical values are compared with the results of CAMAC and good agreement between the results are observed. It is stated that the results can be used as a verification tool for the transient numerical models for charring ablators.

Milos [27] studied on the ablation measurement of the heat shield of the Galileo Probe during the hypersonic entry into the Jovian atmosphere on Dec.7, 1995. In his study, 10 analog resistance ablation detector (ARAD) sensors were used to measure the recession values at different locations on the probe. Unfortunately, data quality was good only for the second half of the entry. Measured recession values were compared with the results of preflight predictions. Preflight predictions were made by using COLTS (a viscous shock layer code developed by NASA) and TOPIC (the thermodynamic outer planets insulation code). It is showed that all predictions overestimated recession at the nose tip and underestimated recession over most of the frustum. It is stated that

errors between the experimental and numerical results were due to the differences between the preflight and actual trajectories and atmosphere structure of the Jupiter.

Milos et al. [28] studied on the transient thermal analyses of the Galileo Probe by using the data of four thermometers taken during entry into Jovian atmosphere. In the analyses ablation, pyrolysis and heat conduction into the body were taken into consideration. FIAT, MAT code and REKAP codes were used for the analyses. Following the analyses, surface heating values which produce the measured temperatures and recession rates were determined to compare with the results of preflight predictions. In the study, they observed an agreement between the temperature and recession data at the frustum section however; some differences for the aft cover section were explained. It is stated that the reason for the difference was the unexpectedly low heat conduction into the heat shield.

Nompelis et al. [29] developed a numerical code for performing full trajectory analyses of ablating materials. The code is capable of solving fluid and solid response equations in a coupled manner. In the paper mathematical formulation of ablation modeling was presented and discretization of the equations was also presented. Two case studies were solved by using algorithm. The first one was the spherically blunted conical graphite in an arc jet facility and the second one was the axisymmetric sphere-cone body in a ballistic trajectory in the Earth's atmosphere. The results of case studies were presented and it was stated that the results were in a good agreement with the results obtained by existing axisymmetric code.

Torre L et al. [30] studied on the thermal analysis techniques which are used to characterization of the ablative materials. In the study, DSC and STA (simultaneous thermal analysis) were used to evaluate the heat of ablation of ablative material under nitrogen and air atmosphere. Moreover, degradation kinetics of a silicon based ablative material was also developed by using TGA. The results of the experiments were used as input for a numerical algorithm to model the behavior of a thermal protection system under aerodynamic heating. In this thesis, similar characterization study for the Teflon material was conducted by using DSC and TGA and detailed explanation of the characterization is given in Chapter 4.

Mohammadiun and Kianifar [31] studied on the numerical modeling of ablation process of a non-charring ablative material. In paper, governing equations including the effect of chemical reactions, mass transfer and heat transfer to the surface were presented. Newton-Raphson methods with the TDMA algorithm were used to solve the equations. Discretization of the governing equations was also presented. In order to check the validity of the algorithm a 1-D nonlinear case was solved and result of the analysis was compared with the analytical solution of the case. A good agreement between the results was showed, and then, more complex problem for the entry conditions was solved and results were compared with the results of taken from literature for the same problem. A consistency was also graphically presented for the entry problem.

Beaudet et al. [32] worked on the ablative performance of the two kinds of composite materials which are carbon (C) reinforced and silicon carbide (SiC) reinforced ceramic matrix composites (CMC). Oxyacetylene torch tests were performed on the materials according to ASTM E 285-80 standard. Mass loss and recession of the samples were measured and compared. It was showed that carbon reinforced composite (CRC) was more sensitive to mass loss compared to SiC reinforced composite (SiRC).The reason was that during ablation of SiRC, SiO_2 liquid film is created and melting of this liquid film is endothermic process which yields a decrease in net heat flux to the material. In the study, SEM microstructures of the materials were presented, and it was showed that CRC has a lower porosity compared to SiC after oxyacetylene tests. Moreover, differences in the ablation mechanisms of the two different composite materials were also explained in the study.

CHAPTER 4

MATERIAL CHARACTERIZATON OF TEFLON

In this thesis, experimental and numerical studies are based on Teflon. Therefore, to obtain required material properties, characterization study was conducted. In this chapter, results of material characterization studies of Teflon are presented.

4.1 What is Teflon?

Teflon, also known as polytetrafluorethylene (PTFE) is a synthetic fluoropolymer. Its chemical structure is given in Figure 12 [33].
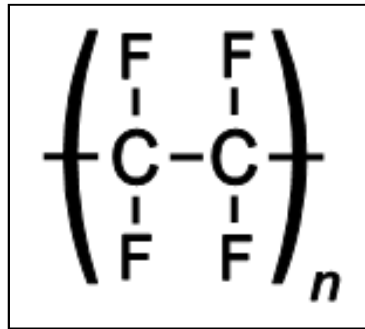
Figure 12: Chemical Structure of Teflon

Teflon is inert to most of the chemicals and it is one of most slippery material in existence. It has resistance to ozone, acetic acid, ammonia and sulfuric acid. It is non-stick, few of materials can permanently adhere on it and it has low friction coefficient. Teflon is also a non-wetting material.

Moreover Teflon can withstand higher temperatures. Due to its attractive properties, it is used in many applications. In this thesis, Teflon which is an ablative material for thermal protection systems of a rocket is studied. Conducted material tests are explained below in detail.

4.2 Thermogravimetric Analysis (TGA) of Teflon

TGA is a technique in which the mass of specimen is measured as a function of temperature or time under controlled temperature and atmosphere [34]. During test, specimen resides on a pan which is in a furnace. Furnace is heated or cooled depending on the purpose of the test. Weight of the specimen is monitored and mass loss history is saved. During test purge gases are used in order to avoid reaction between the sample and air and to control moisture content of the atmosphere. Generally nitrogen and argon are used as a purge gas. Specimen weight is generally between 2 mg and 50 mg and maximum test temperature depends on the capability of the device. Schematic drawing of TGA parts are given in Figure 13 [35].
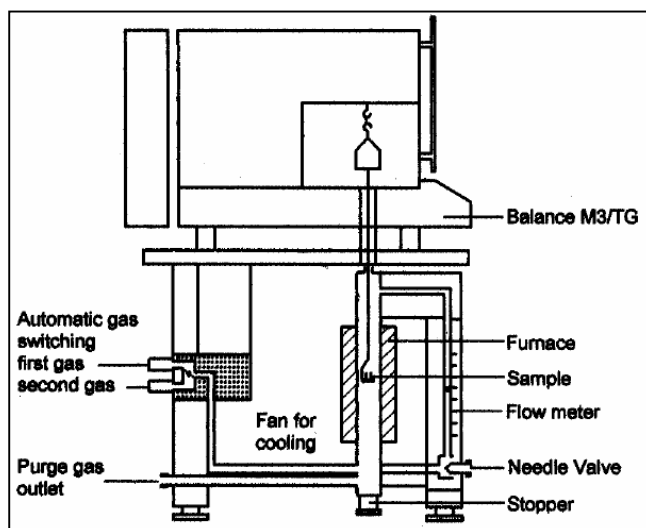
Figure 13: Schematic Drawing of TGA Test System [35]

TGA can be made to find oxidative stability, moisture and volatiles content, thermal stability and decomposition kinetics of the materials.

TGA measurements for this thesis were made in METU Central Laboratory by using Perkin Elmer Pyris 1 TGA device. To examine the effects of heating rate and test atmosphere on the decomposition temperature, several experiments were conducted. List of measurements are given in Table 3.

Table 3: List of TGA Measurements

Test Number	Heating Rate (°C/min)	Sample Atmosphere
1	10	Nitrogen
2	10	Air
3	10	Oxygen
4	20	Oxygen
5	30	Oxygen
6	40	Oxygen

Results of measurements are given separately and also given together to examine the effects better. Weight loss and their derivative curves are given together. Derivative curves indicate rate of change on the weight loss curves.
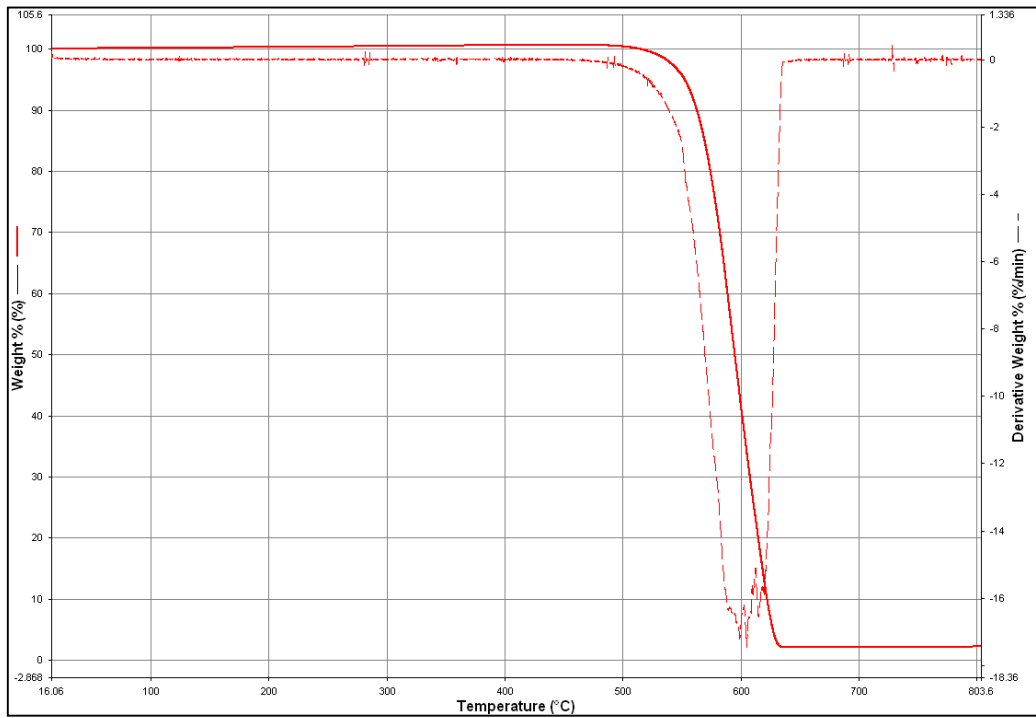
Figure 14: Result of TGA under Nitrogen Atmosphere at Heating Rate of 10 °C/min
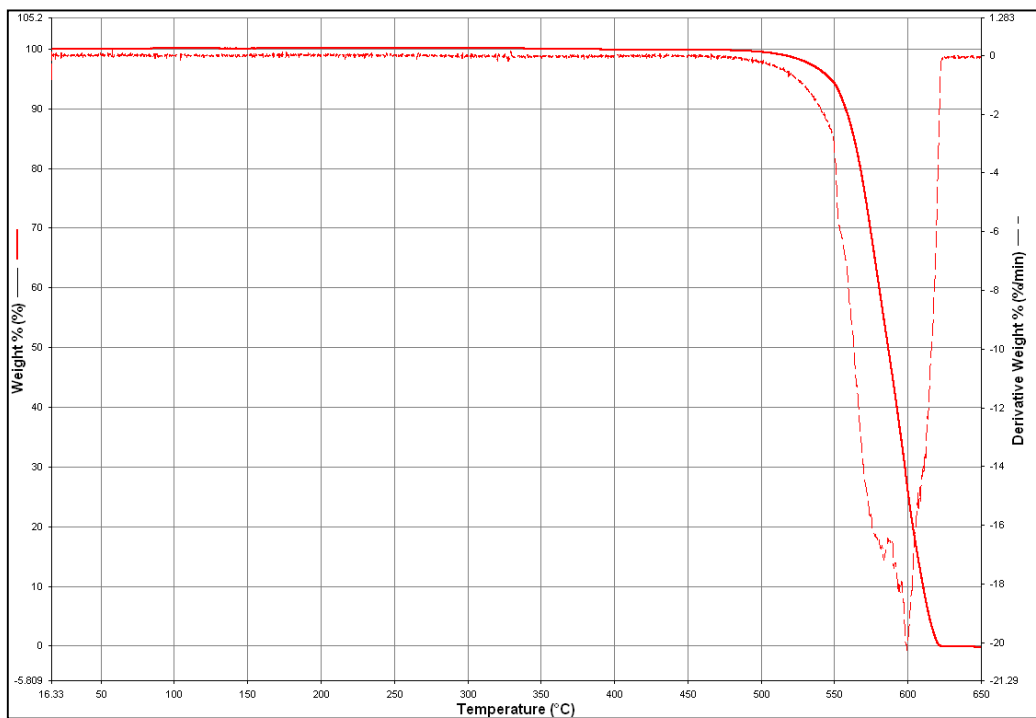
Figure 15: Result of TGA under Air Atmosphere at Heating Rate of 10 °C/min
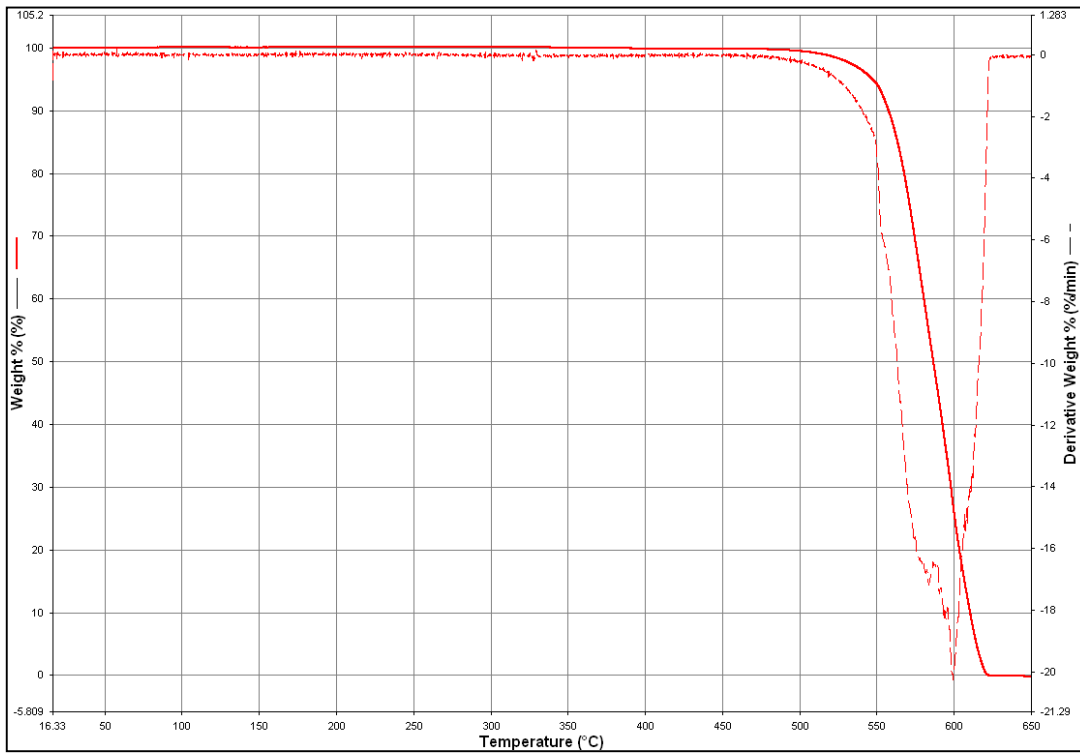
Figure 16: Result of TGA under Oxygen Atmosphere at Heating Rate of 10 °C/min
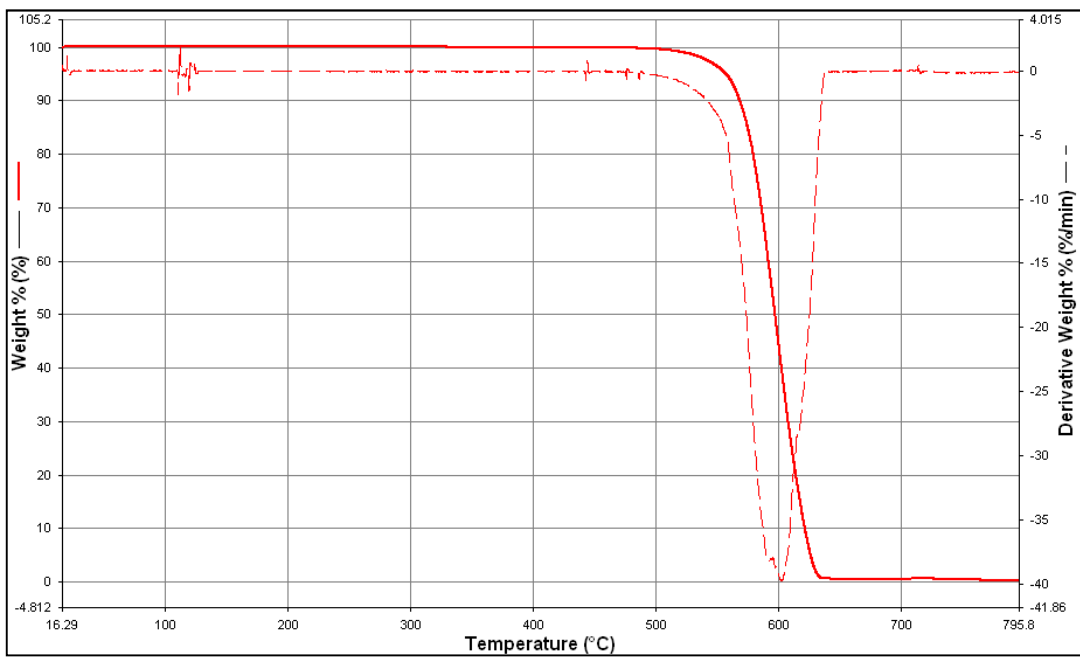
Figure 17: Result of TGA under Oxygen Atmosphere at Heating Rate of 20 °C/min
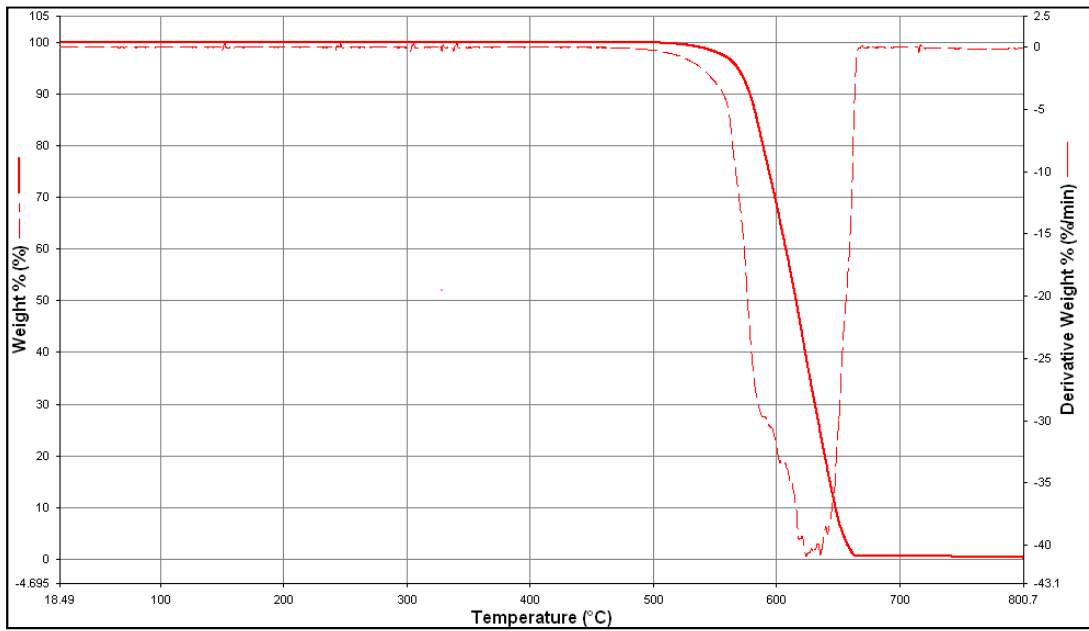
Figure 18: Result of TGA under Oxygen Atmosphere at Heating Rate of 30 °C/min
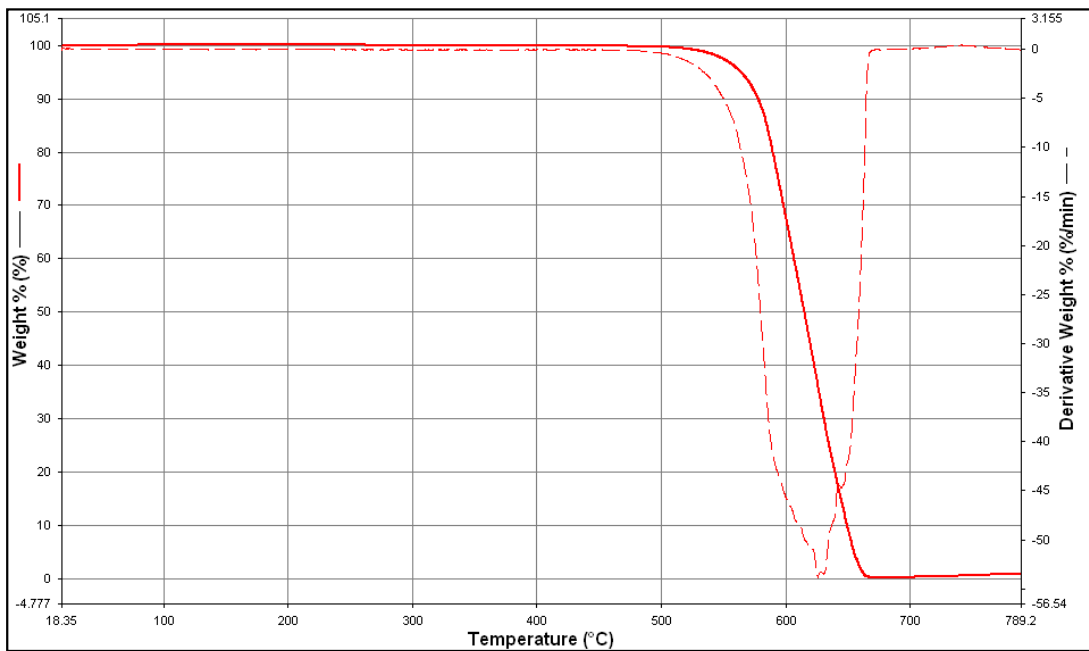
Figure 19: Result of TGA under Oxygen Atmosphere at Heating Rate of 40 °C/min

As mentioned before, to examine the results better, measurement results are given together in a same graph in Figure 20 and Figure 21.
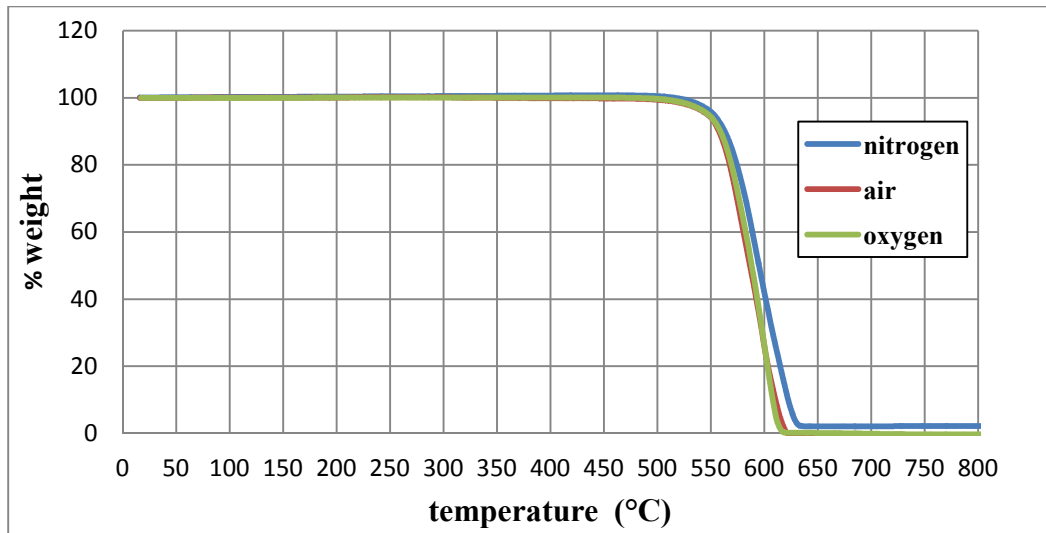
Figure 20: Effect of Test Atmosphere on the Decomposition Temperature of Teflon at Heating Rate of 10 °C/min
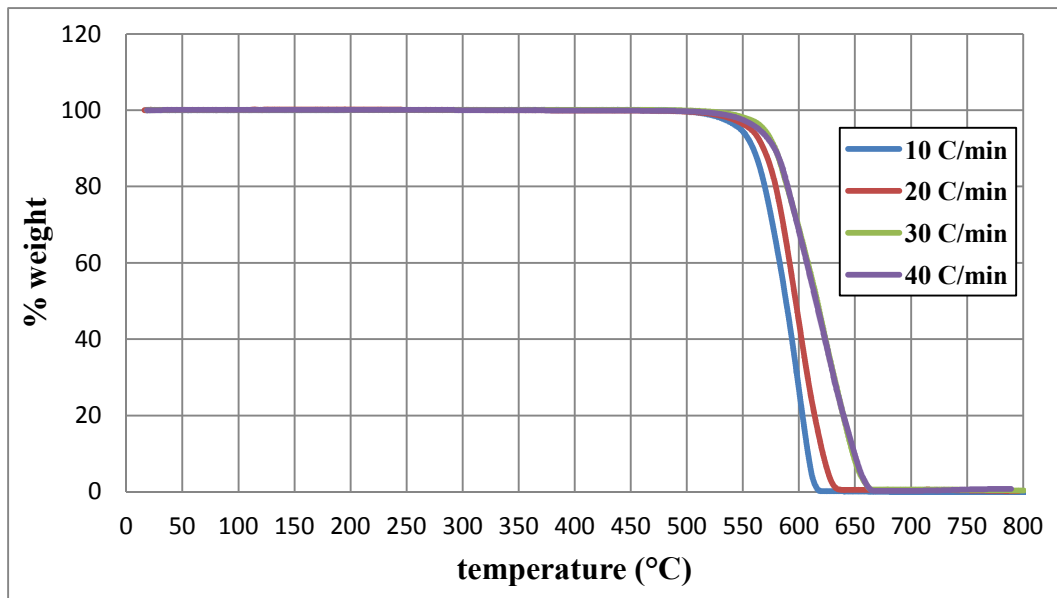
Figure 21: Effect of Heating Rate on the Decomposition Temperature of Teflon under Oxygen Atmosphere

As can be seen from the results, sample atmosphere affects decomposition temperature slightly but effect can be negligible and increasing heating rate shifts curves to the right. But decomposition temperature differs only 30 °C. Therefore in the ablation analyses, as an approximation, decomposition temperature of Teflon will be taken as a constant value of 580 °C. An increase in heating rate provides larger instantaneous thermal energy. Therefore, larger time is required for the purge gas to reach equilibrium with the furnace due to heat transfer limitations. Moreover, higher heating rate has a short reaction time at the same time and in the same temperature region, therefore; the temperature needed for the sample to decompose is also higher. This is the main reason why curves shift to the right [36, 37]. The principal products of decomposition are carbon tetrafluoride (CF_4) and small amount of hexafluoropropylene (C_3F_6) [38]. However, if there is oxygen in the decomposition atmosphere, carbon monoxide (CO) and carbon dioxide (CO_2) is also produced [38]. Therefore, weight lose is larger in air and oxygen atmosphere compared to nitrogen atmosphere as seen in Figure 20.

4.3 Differential Scanning Calorimetry (DSC) Analysis of Teflon

Differential Scanning Calorimetry is a technique in which specific heat capacity (c_p) change of a material is measured at various temperatures. The sample is heated or cooled during test and heat flow into specimen is measured. Glass transitions, phase changes and curing detection are also possible by DSC [39].

In the test set-up there exist two pans which are sample pan in which specimen exists and reference pan. Reference pan can be empty or a reference material can be in the pan. Specific heat capacity of the reference material must be well-defined over the ranges of temperatures. During test, temperatures of the two pans are increased at a same specific rate such as 10 °C/min. To keep the pans at same temperature, heat flow to the pans should be different and by measuring the differences in the heat flow, specific heat capacities of the specimen are found. Purge gases are used to avoid reaction of specimen with the air and to keep the moisture content of atmosphere in control as in TGA testing. Schematic drawing of a DSC device is given in Figure 22 [40].
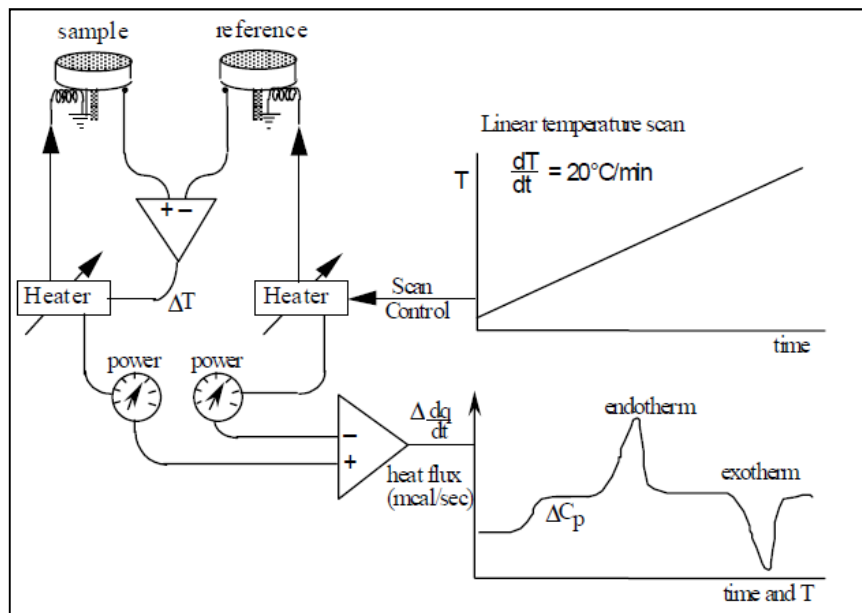
Figure 22: Schematic Drawing of DSC Test System [40].

As mentioned before, different kinds of transitions and phase changes can be investigated with DSC testing. Interpretations of typical DSC transitions are given in Figure 23 [41].
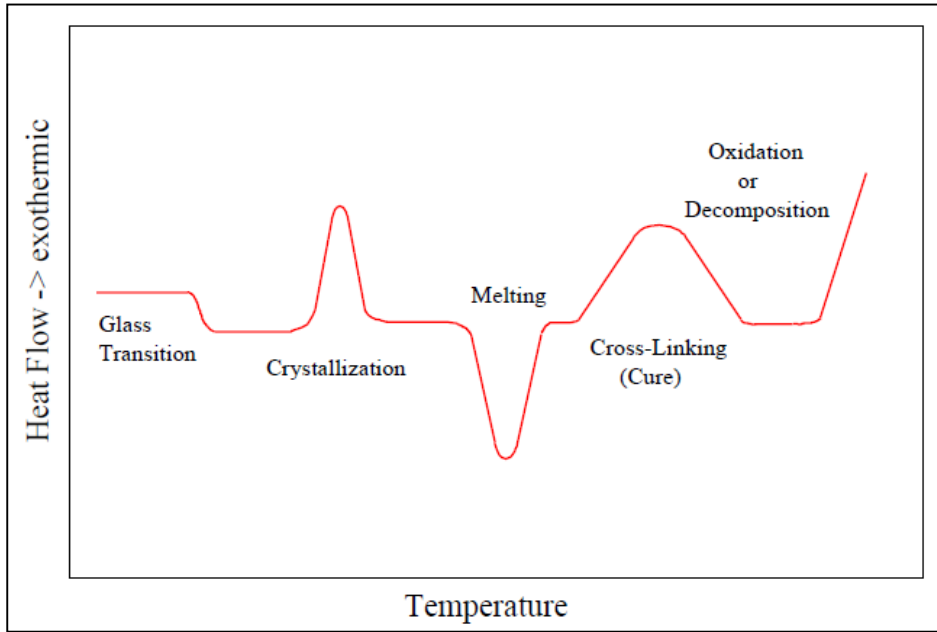
Figure 23: General Shape of Typical DSC Transitions [41].

Heat flow output of DSC test of Teflon is given in Figure 24. As can be seen, melting of Teflon occurs at nearly at 325 °C and heat of fusion is nearly 37 J/g.
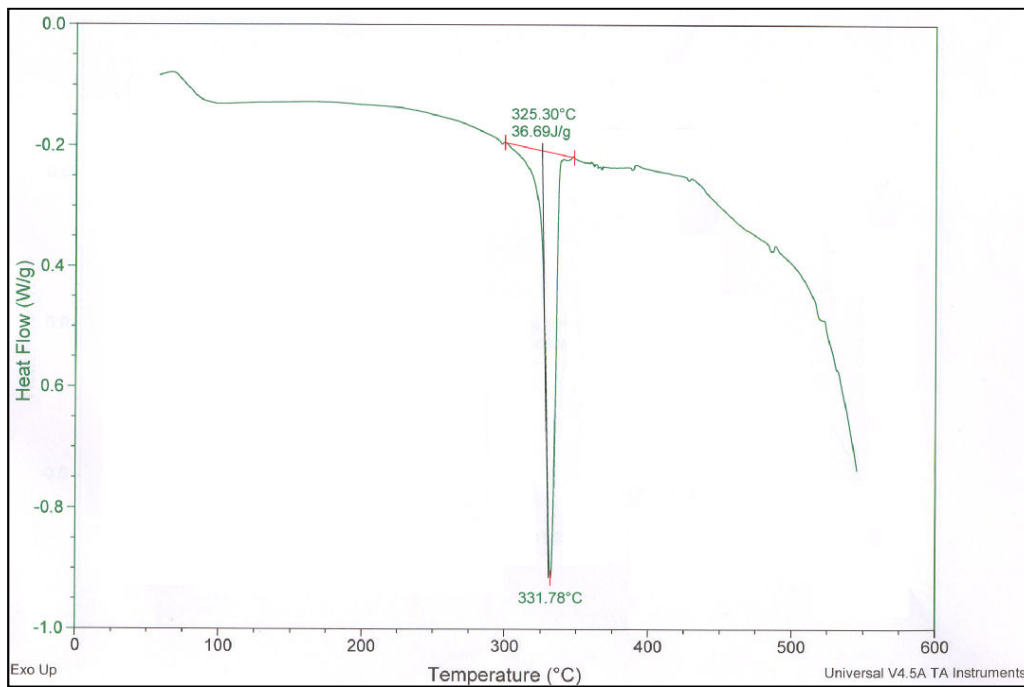
Figure 24: DSC Transition Curve of Teflon

Specific heat capacity is the amount of heat required per unit mass to increase the temperature of a substance by one degree [42]. DSC test result for the c_p measurement is given below. As can be seen, specific heat capacity of Teflon depends on the temperature and at melting region, c_p increases rapidly.

26
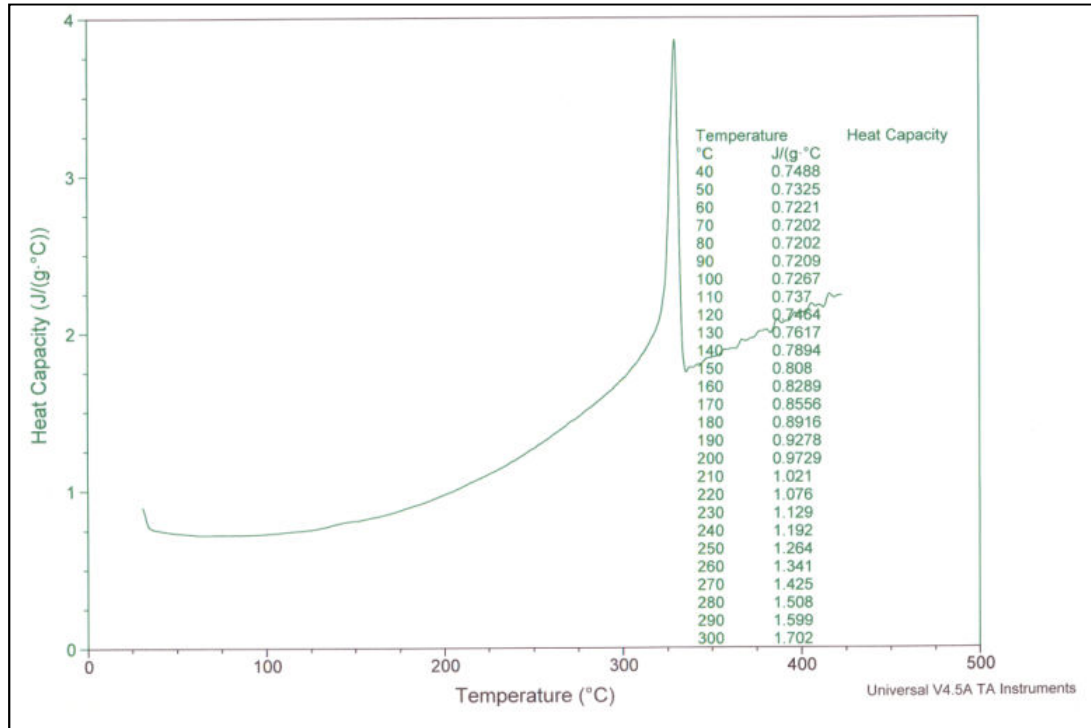
Figure 25: Specific Heat Capacity of Teflon at Various Temperatures.

For the numerical simulations thermal conductivity of the Teflon is assumed to be constant and it is equal to 0.3 W/m K [43]. However, as mentioned in Chapter 9, a method can be used to measure the conductivity of materials by using DSC test equipment.

Heat of vaporization of Teflon is taken from reference [44] as 6.56e6 J/kg. In the numerical simulations heat of vaporization is converted to specific heat capacity of the material. For the transformation the equation given below is used. Starting and ending temperatures of vaporization are taken from Figure 14. In this equation Q_a is the heat of ablation and T_s and T_f are the starting and ending temperatures of phase change [45].

$$c_{eff} = c_p + \frac{Q_a}{\Delta T} \quad , \quad T_s < T < T_f \tag{4.6}$$

This equation can also be seen on the DSC test results. As seen on the Figure 24 and Figure 25, specific heat capacity of Teflon increases during phase change region. Finally by using Figure 25, equation (4.6) and Q_a value of Teflon, specific heat capacity of Teflon for thermal simulations is taken as given in Table 4.

Table 4: Specific Heat Capacity of Teflon Used in Thermal Simulations

Temperature (K)	Specific Heat Capacity (J/kg K)
300	779
405	766
500	1104
556	1538
582	1830
596	2298
602	3860
610	1753
640	1952
694	2229
793	2229
893	67829

For this table, TGA result of Figure 15 is used. As seen in Figure 15, start and end temperatures of decomposition are nearly 793 K (520 °C) and 893 K (620 °C). In the ablation simulations, average temperature of the decomposition is used for the ablation temperature. These temperatures are calculated by using the starting and ending temperatures of decomposition. Calculated average temperatures are given in Table 5.

Table 5: Average Temperatures of Decomposition for Teflon Under Different Test Conditions

Test Number	Test Atmosphere	Heating Rate (°C/min)	Average Temperature of Ablation (K)
1	Nitrogen	10	≈850
2	Air	10	≈840
3	Oxygen	10	≈840
4	Oxygen	20	≈850
5	Oxygen	30	≈863
6	Oxygen	40	≈863

CHAPTER 5

COMPUTATIONAL DOMAINS AND GOVERNING EQUATIONS

Thermal analyses are conducted using ANSYS Software for the Teflon specimens that are exposed to oxyacetylene ablation tests and blunt nose section of a supersonic rocket. Detailed information about oxyacetylene ablation tests and their results are given in Chapter 7 and thermal analyses for the specimens and blunt noses are given in Chapter 8. However, in this chapter, detailed information about computational domain and applied boundary conditions on the numerical analyses is given. Moreover, since thermal analyses are conducted by using ANSYS software, heat flow fundamentals and thermal analysis capabilities of ANSYS are given in Appendix section.

5.1 Computational Domains and Boundary Conditions

Cylindrical-shaped specimens are used for the ablation tests. These specimens have 0.01 meter height and 0.03 meter diameter. Since specimens are axisymmetric, axisymmetric PLANE55 type elements are used in the analyses. Therefore, 2-D analyses became possible instead of 3-D analyses. In Chapter 8 detailed information about results of analyses under different mesh sizes and time steps are given; however, representation of computational domain of the Teflon specimens is given in Figure 26.
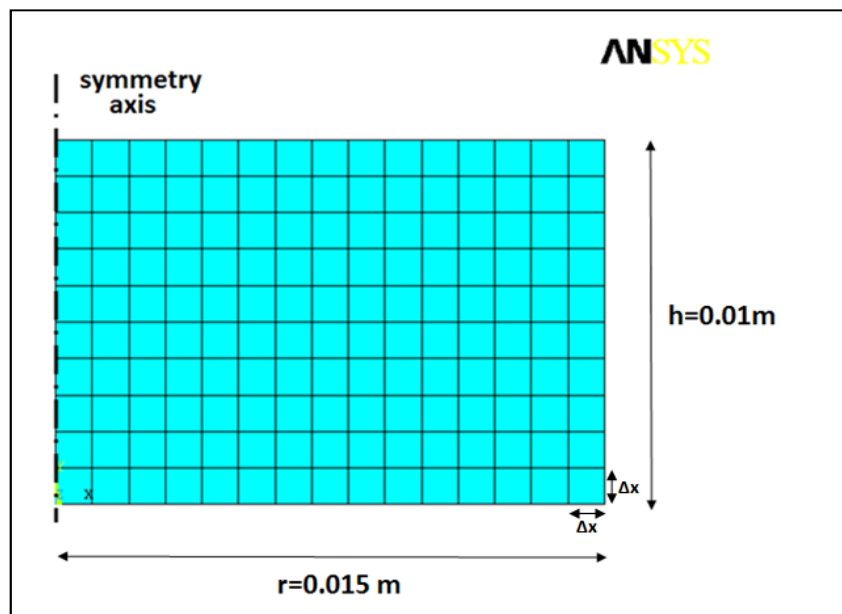
Figure 26: Computational Domain for the Ablation Simulations of Teflon Specimens

The same method is used for the ablation simulation of the blunt nose section of a supersonic rocket. Due to axisymmetry of the nose section, axisymmetric analysis model by using PLANE 55 elements is prepared. Results of ablation simulation of nose section are given in Chapter 9 in detail; however, representation of computational domain of the blunt nose section is given in Figure 27. In the simulations of both Teflon specimens and nose section, heat flux is applied as boundary condition. For Teflon specimen constant heat flux applied on the upper surface and for nose section time and coordinate dependent heat flux applied to the outer surface. In both kind of analyses, inner walls are

assumed adiabatic and heat transfer to the surroundings is neglected. Used heat flux values and their determination are mentioned in Chapter 7 and Chapter 8 in detail.
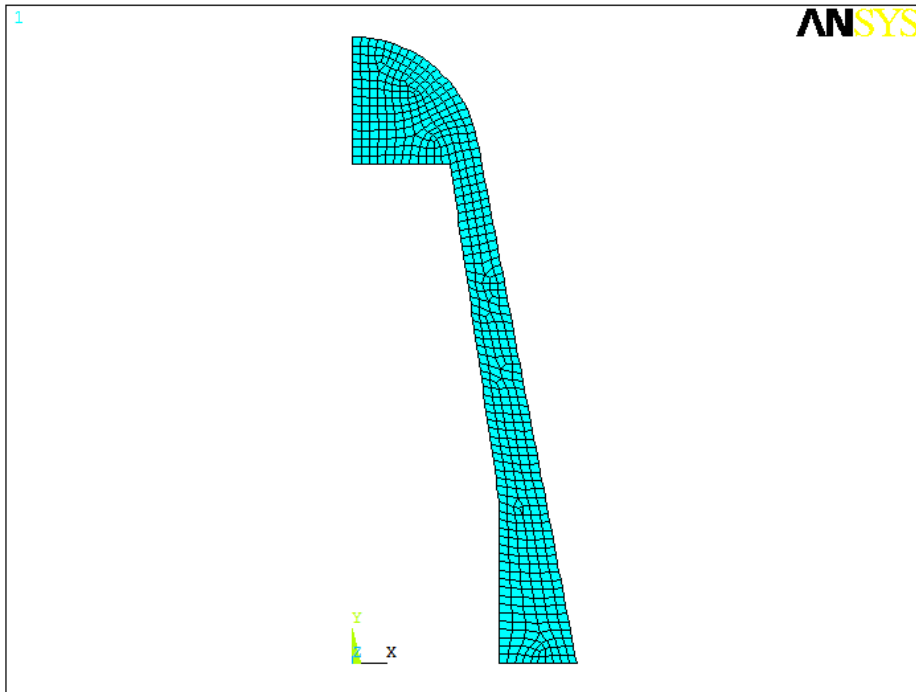
Figure 27: Computational Domain for the Ablation Simulation of Blunt Nose Section of a Supersonic Rocket

5.2 Governing Equations

ANSYS uses equation (5.1) during thermal analyses. This equation can be derived by using first law of thermodynamics and it can be written in the global Cartesian system as [46]:

$$\rho c_p \left(\frac{\partial T}{\partial t} + v_x \frac{\partial T}{\partial x} + v_y \frac{\partial T}{\partial y} + v_z \frac{\partial T}{\partial z} \right) = q''' + k_x \left(\frac{\partial^2 T}{\partial x^2} \right) + k_y \left(\frac{\partial^2 T}{\partial y^2} \right) + k_z \left(\frac{\partial^2 T}{\partial z^2} \right) \tag{5.1}$$

where q''' is the heat generation rate per unit volume, v_x, v_y and v_z are the velocity components of the flow, k_x, k_y and k_z are the conductivies at x, y, z directions ,T is the temperature, c_p is the specific heat capacity at constant pressure, ρ is the density and t is the time. ANSYS converts this equation into matrix and vector form during solution [46]. In Appendix section detailed information about solution technique, verification of ANSYS and thermal analysis capabilities of ANSYS are given by using references [47, 48].

CHAPTER 6

FINITE ELEMENT APPROACH TO ABLATION PROBLEM

In this chapter, the approach to modeling the ablation process by using finite element method is explained.

6.1 General Concepts

As mentioned in literature survey chapter, most of the finite element approaches to ablation problems are based on the numerical coding of the physical events of the process. However, there is commercial package software products used to model ablation phenomena. Marc solver of MSC Company and SINDA/FLUINT solver of C&R Technologies are example of some commercial software products. Moreover, Charring Material Thermal Response and Ablation Program (CMA) of Aerotherm Company is other commonly used product for ablation modeling. Simulation tools which are widely used to model ablation process in the field of aerospace are given in Table 6 [49].

Table 6: List of Currently Available Ablation Simulation Tools [49]

Name	Contact	Owner	Users	Applications
Amaryllis	T. van Eekelen	Samtech, Belguim	EADS Astrium, ESA	Design
CAMAC	W.-S. Lin	CSIST, Taiwan	Taiwan Ins. of Sci. Tech.	Unknown
CAT	N. N. Mansour	NASA ARC, USA	NASA ARC	Analysis
CHALEUR	B. Blackwell	SNL, USA	SNL	Design
CHAP	P. Keller	Boeing, USA	Boeing	Design
CMA	R. Beck	Aerotherm, USA	NASA, SNL	Design
CMA/SCMA	C. Park	Tokyo Univ., Japan	JAXA	Design
CMA/KCMA	P. Reygnier	ISA, France	ISA/ESA	Analysis
COYOTTE2	D. W. Kuntz	SNL, USA	SNL	Design
FABL	J. Merrifield	Fluid Grav. Eng. Ltd., UK	ISA/ESA/FGE	Analysis
FIAT	Y.-K. Chen	NASA ARC, USA	NASA, SpaceX	Design
FIAT3D	Y.-K. Chen	NASA ARC, USA	NASA ARC	Analysis
HERO	M. E. Ewing	ATK, USA	ATK	Analysis
ITARC	M. E. Ewing	ATK, USA	ATK	Design
libAblation	R. R. Upadhyay	Univ. of Tex. Aust., USA	UTA	Analysis
MIG	S. Roy	Univ. of Flo., USA	Univ. of Florida	Analysis
MOPAR	A. Martin	Univ. of Mich., USA	UKY/Univ. of Michigan	Analysis
NEQAP	J. B. Scoggins	N. Carol. St. Univ., USA	NCSU	Analysis
NIDA	G. C. Cheng	Univ. Alab. Birm., USA	UAB	Analysis
PATO	J. Lachaud	NASA ARC, USA	Univ. Calif. Santa Cruz	Analysis
PRESENT	J. Dec	NASA LaRC, USA	NASA LaRC	Analysis
STAB	B. Remark	NASA JSC, USA	Fluid Gr. Eng.	Design
TITAN	F. S. Milos	NASA ARC, USA	NASA	Analysis
TMU	A. R. Bahramian	T. Modares Univ., Iran	TMU	Analysis
US3D	G. Candler	Univ. of Minn., USA	UM	Analysis

6.2 Modeling Considerations

In this thesis, ANSYS software is used for the modeling of ablation problem. The algorithm is developed on the APDL program language. APDL stands for ANSYS Parametric Design Language and by using this language; it is possible to build models or to automate common tasks in terms of parameters [50].

In this thesis, an approach to ablation problem is developed. In the method, when the average nodal temperature of an element reaches the temperature of ablation, it is *killed* and an amount of energy equal to latent heat of vaporization is removed from the material. Element kill option of the ANSYS is used for the removal of the material from the heating surface.

During analyses, when an element is killed, actually ANSYS does not remove element from the body. Instead, stiffness or conductivity of the element is multiplied by the severe reduction factor which is nearly equal to zero. Therefore, the mass and energy of the deactivated element are not included in the solution of the model [46]. Moreover, a deactivated element can also be included in the analyses by using element birth option of the ANSYS in the later analysis steps. Element birth/death options of ANSYS are verified in VM194 model [48].

6.3 Material Removal Strategy

Material removal from the model is based on the temperature of the element. As mentioned before, when temperature of an element reaches to the ablating temperature, it is killed and removed from the solution. Since a quad element has 4 or 8 nodes (if it is triangular, it has 3 or 6 nodes) temperature calculation of an element is slightly complex. Mean of all nodal temperatures of an element is calculated, and it is checked with the ablating temperature. If average of the nodal temperatures is greater than the ablating temperature, then the element is killed. For example, if we have a temperature distribution on the element as given in Figure 28, the average value of the nodal temperatures is 732.5K and if the ablating temperature is below 723.5, the element will be killed otherwise it won't be killed.
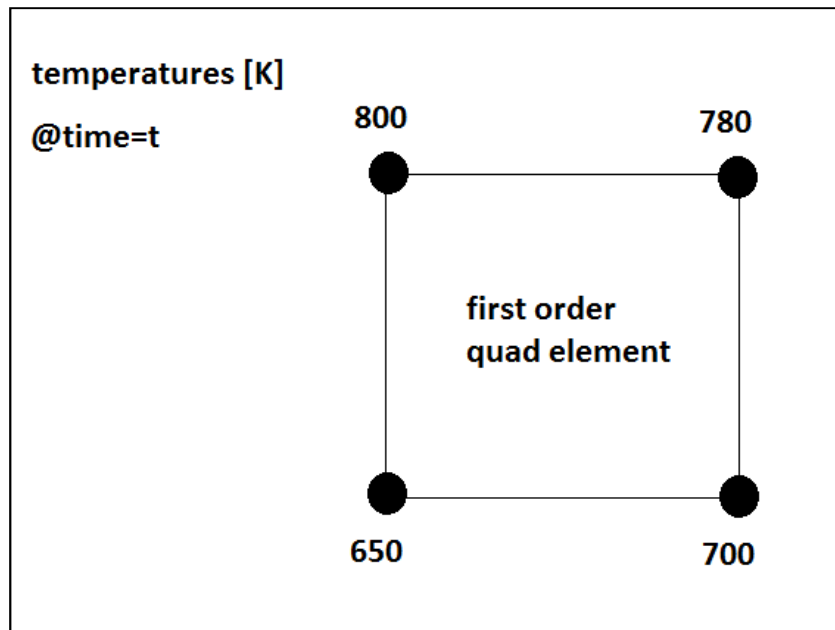
Figure 28: Schematic Representation of an Element with Nodal Temperatures

If deactivated element has any boundary condition acting on it, a problem arises. Therefore, boundary condition should be moved from the deactivated element to the active element at the inner side. This process is also taken account in the algorithm and by using available commands, boundary conditions are moved from the deactivated elements.

6.4 Flow Chart of the Algorithm

The analyses are conducted according to flow chart shown in Figure 29.
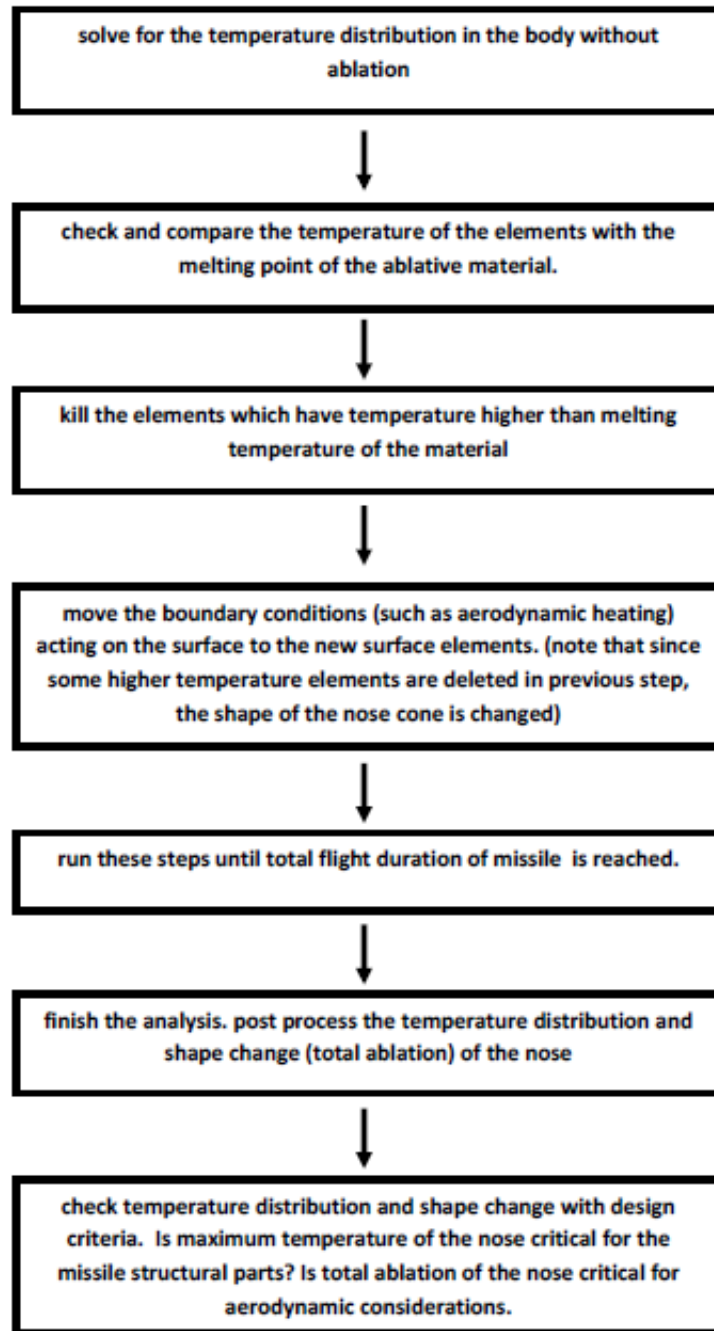
Figure 29: Procedure for the ablation analysis

6.5 Commands of Numerical Algorithm

In the numerical algorithm, ANSYS APDL commands are used to achieve procedures given in Figure 29. In this section, detailed information about algorithm is given.

The first step of the algorithm is defining the geometry of the model. As given in Figure 26, axisymmetric analysis model is a rectangle. Therefore, a rectangle model is defined. To define a rectangle, key points for the vertices are defined by using *K, NPT, X, Y, Z* command. In this command, NPT is the keypoint number, and *x, y, z* is the keypoint location. Then by using *A, P1, P2, P3, P4* command a rectangle area is created by connecting key points, P1, P2, P3 and P4. The second step of the algorithm is defining element type and mesh size and meshing the geometry. Element type is defined by using *ET, ITYPE, Ename* command. In this command *ITYPE* is the element type number and *Ename* is the name of the element. Since model is axisymmetric, element option is changed from planar to axisymmetric by using *KEYOPT* command. Mesh size is defined by using *ESIZE, SIZE* command. In this command, *SIZE* is the length of the element. Finally meshing is achieved by using *AMESH* command. Commands for geometry definition and meshing are given in Figure 30.

```
k,1,0,0.01                  ! Define keypoints

k,2,0,0

k,3,0.015,0

k,4,0.015,0.01

a,1,2,3,4                   ! Connect the keypoints to form area

ET,1,Plane55                ! Defining element type

KEYOPT,1,3,1                ! switching element option from planar to axisymetric

esize,0.0001                ! Mesh size

amesh,all                   ! Meshing geometry
```

Figure 30: Commands for Geometry Definition and Meshing

The third step of the algorithm is defining material properties. To define material properties *MPDATA, Lab, MAT*, command is used. In this command Lab is the name of material properties (*EX* for elastic modulus, *C* for specific heat capacity etc.) and *MAT* is the material number. *MPTEMP* command is used for the temperature dependent material properties.

34

```
MP,Dens,1,2155          ! Define density

mp,kxx,1,0.3            ! Define conductivity

MPTEMP,                 ! Define specific heat capacity

MPTEMP,1,300

MPTEMP,2,405

MPTEMP,3,500

MPTEMP,4,556

MPTEMP,5,582

MPTEMP,6,596

MPTEMP,7,602

MPTEMP,8,610

MPTEMP,9,640

MPTEMP,10,694

MPTEMP,11,793

MPTEMP,12,893

MPDATA,C,1,,779

MPDATA,C,1,,766

MPDATA,C,1,,1104

MPDATA,C,1,,1538

MPDATA,C,1,,1830
```

Figure 31: Commands for Defining Material Properties

The next step of the algorithm is applying boundary condition. As mentioned before, a heat flux is applied to the upper face of the model. *SFL, LINE, Lab, VALI* command is used to apply heat flux to the upper face of the model. In this command *LINE* is the line number that will be used, Lab is the type of the boundary condition (*PRES* for the pressure, *HFLUX* for the heat flux etc.) and *VALI* is the value of the boundary condition. The next step of the algorithm is to create a set from nodes which are associated with the other lines. The purpose of creating set is to be able to unselect them from analysis model during applying boundary conditions to all exterior nodes. By this method, in all analysis steps, boundary condition will only be applied to the upper surface of the model. To select nodes which are associated with the other lines, first those lines are selected by using *LSEL* command. Then nodes on these lines are selected by using *NSLL* command. Set is created by selected nodes by using *CM* command. Commands for these steps are given in Figure 32.

```
SFL,4,HFLUX,2.3e6          ! apply heat flux on line 4.


LSEL,S,LINE,,1,3,1          ! selecting lines on which there is no applied heat flux.

NSLL,S,1                   !selecting nodes associated with the selected lines.

CM,CM_1,NODE              ! creating a set from selected nodes.Name of set is CM_1.
```

Figure 32: Commands for Defining Boundary Conditions and Creating a Nodal Set

The next step of the algorithm is defining analysis options for the simulations. *ANTYPE, Antype* command is used to define analysis type that will be performed. In this command, *Antype* determines analysis type (0 for static analysis, 1 for buckling analysis, 2 for modal analysis, and 4 for transient analysis). Maximum number of iterations is specified by using *NQIT* command. Solution methodology is changed to full Newton-Raphson method by using *NROPT, FULL* command. And initial temperature of the model is applied by using *TUNIF* command. Solution is started by using *SOLVE* command.

```
ANTYPE,4               !analysis type is transient

NROPT,FULL,            ! full newton-raphson

NEQIT ,100             ! Max no. of iterations

OUTRES,ALL,ALL,        !write results in all steps

TUNIF,300,             !initial temperature is 300 K

SOLVE                  ! start the solution
```

Figure 33: Commands for Defining Analysis Options

The next step of the algorithm is to define sub steps according to specified time step size. For this procedure, a do-loop is used. *DO, Par, IVAL, FVAL, INC* command is used to define a do-loop. In this command *Par* is the parameter name (i, j, etc.), *IVAL* is the initial value of the parameter, *FVAL* is the final value of the parameter and INC is the increment size of the parameter. In the algorithm INC is used as time step size and *FVAL* is used as total duration of test time and *Par* is used as time of analysis. At each sub step, external heat flux should be applied to the upper surface of the geometry (or external surface of the nose cone of the rocket). For this procedure, first applied boundary conditions deleted after killing elements which satisfy ablation criteria by using *EKILL* command. Then only upper surface nodes are selected and boundary conditions are applied again.

```
SFDELE,ALL,HFLUX        ! delete applied boundary condition

NSEL,S,EXT              ! node select all exterior nodes

CMSEL,U,CM_1            ! unselect nodes that is in set created before

SF,ALL,HFLUX,2.3e6      ! apply boundary condition to all selected exterior nodes
```

Figure 34: Commands for Selecting Surface which is Exposed to Heat Flux

36

In each sub step, killed elements are selected by using ablation criterion. As mentioned before, average temperature of an element is compared with the ablation temperature of the material. At each sub step, a table is created from the elements which have temperature larger than ablation temperature. Then these elements are selected by using *ESEL* command and then killed by using *EKILL* command.

```
ETABLE, ABLATED, TEMP,,        ! create an element table with results of temperature

ESEL, S, ETAB, ABLATED, 850    ! select all elements from table above 850 K

EKILL, ALL                     ! kill all selected elements

ESEL, S, LIVE                  ! select all live elements
```

Figure 35: Commands for Simulation of Ablation

These all commands are written in a .txt file and then input file is read by ANSYS for the simulations.

CHAPTER 7

OXYACETYLENE ABLATION TESTINGS OF TEFLON SPECIMENS

In this chapter, results of oxyacetylene testing of Teflon specimens are given. The results are compared with the theoretical values calculated by using equation (5.6). The results are also used for the comparison with the analyses results.

7.1 Oxyacetylene Ablation Testing

Oxyacetylene testing is generally used for determining ablation performance of the ablative materials. In this test, high amount of surface heat flux is applied on the surface of the ablative material over a period of time and then total amount of recession of the surface is measured. Total decrease in the mass of the specimen is also measured. Heat flux is gained by burning of oxygen and acetylene mixture. The net surface flux is a function of volumetric flow rates of gases. ASTM standard E-285-80 *Standard Test Method for Oxyacetylene Ablation Testing of Thermal Insulation Materials* deals with this type of testing. Before test, net heat flux applied to surface of the specimen should be known. Test period mainly depends on characteristics of ablative materials. If temperature of ablation is too low, test period should not be too long and if ablation temperature is high test period can be longer. Moreover, during test, pyrolysis gases are created which are generally hazardous to human health. Therefore, precautions against pyrolysis gases should be taken into account. Schematic of test equipments are given in Figure 36 [51].
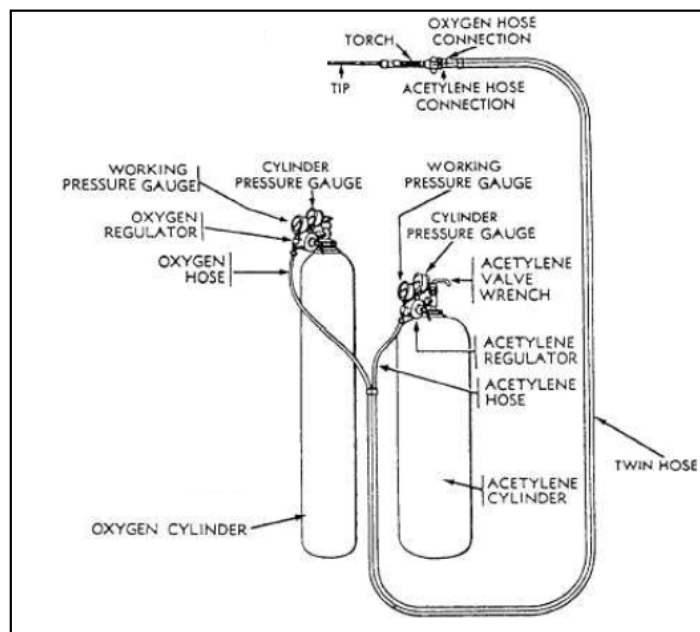
Figure 36: Oxyacetylene Testing Equipment [51]

7.2 Determination of Heat Flux of Oxyacetylene Ablation Testing Device

As mentioned before, heat flux acting on the surface of the specimen should be known to examine the results correctly. Therefore, a study was conducted to determine the heat flux of the testing system. An AISI 4140 steel bar was produced and one of the tips is exposed to heat flux over 80 seconds. Temperature increase histories at different locations were collected by using K type thermocouples and measured temperature values were compared with the analysis result of the bar. Analyses were conducted under various heat flux values and heat flux value, under which analysis result and test result are nearly same, was determined as a heat flux of oxyacetylene test equipment. The produced bar and its analysis models are given in Figure 37.
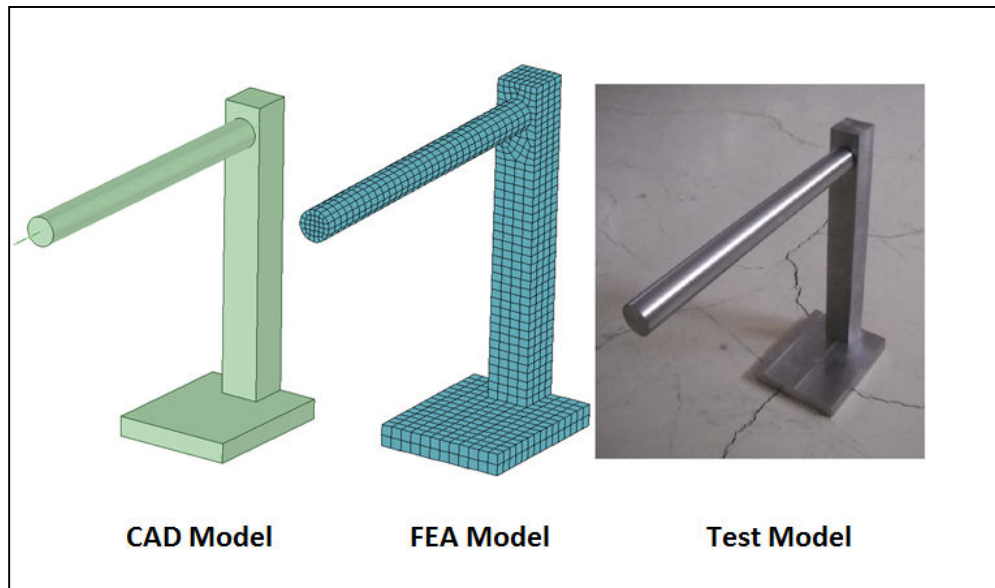
Figure 37: CAD, FEA and Test Model of Bar Used in Oxyacetylene Testing

Temperature measurements were made on the surface of the test model under oxyacetylene testing. The locations are 20, 40 and 60 mm away from the tip of the bar. Omega brand K type thermocouples were used for the temperature measurements. Thermal simulation of bar heating was made on commercial software MSC MARC. Brick elements with 8 nodes were used for the modeling. Used FEA model for the simulation is also given in Figure 37. When 2.3×10^6 W/m^2 heat flux value used in the analysis, comparison of test results and analysis results for three points are given in Figure 38. In the analysis, material properties for the AISI 4140 steel was taken from reference [52].
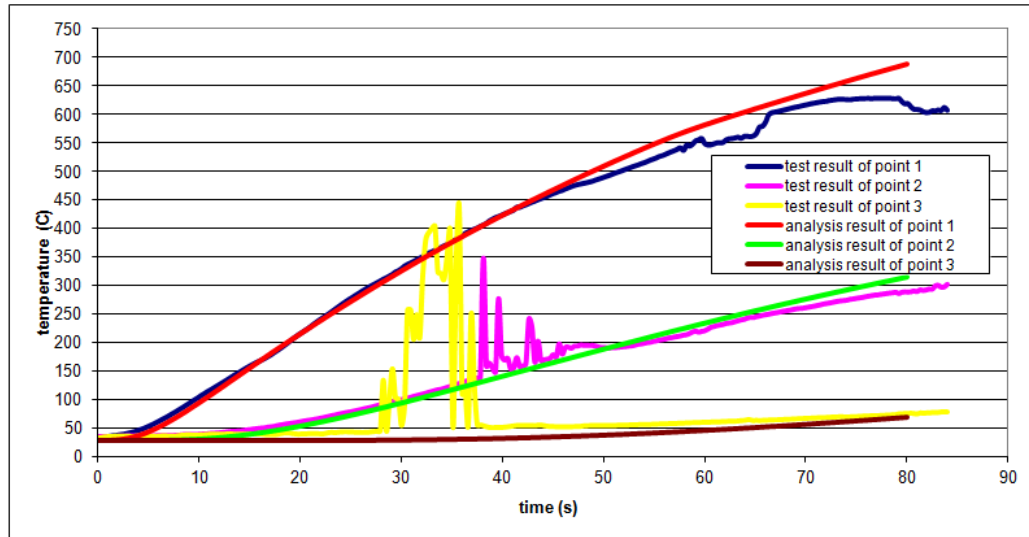
Figure 38: Comparison of Test Results and Analysis Results of Bar Heating Test

As seen at Figure 38, when 2.3×10^6 W/m^2 heating value is used in the analysis, test results and analysis results are in a good agreement. In the test results there are oscillations between 30th and 50th seconds of test time. These are due to electrical noises seen during data acquisition and their effects on the general trend of the temperature graphs are neglected.

The obtained heat flux value is used to determine the theoretical mass loss of the Teflon specimens under oxyacetylene testing. For theoretical calculations, Equation 3.1 is used.

7.3 Teflon Specimens for Oxyacetylene Testing

Teflon specimens were prepared in a cylinder shape for tests. Their diameter is 30 mm and height is 10 mm. They were mounted at test case which is 10 mm away from the nozzle of the oxyacetylene test equipment. The general view of Teflon specimens and their locations during tests are given in Figure 39 and Figure 40.

Figure 39: Teflon Specimens Used for Oxyacetylene Tests

Figure 40: Teflon Specimen on the Test Set-Up

7.4 Oxyacetylene Test Results and Theoretical Results

Oxyacetylene tests were conducted under different period of times. Before and after each test, weights of the specimens were measured. The measured recession distances were compared with the analytically calculated ones. They were calculated by using weight loss, cross sectional area of the specimen and density of the Teflon. Equation (3.1) is used for the calculations. Sum of the results are given in Table 7.

Table 7: Comparison of Test Results with Analytical Results

Specimen	exposing time to heat flux (s)	weight before test (g)	weight after test (g)	weight loss (g)	mean weight loss (g)	recession (mm)	calculated recession (eq.3.1) (mm)	%error
1	5	15.1513	13.9292	1.2221		0.804	0.813	-1.11%
2	5	15.3742	14.1145	1.2597		0.822	0.813	1.05%
3	5	15.1494	13.8937	1.2557	1.245	0.827	0.813	1.61%
4	5	15.1817	13.9495	1.2322		0.810	0.813	-0.43%
5	5	15.1693	13.9151	1.2542		0.825	0.813	1.42%
6	10	15.3407	12.908	2.4327		1.585	1.627	-2.56%
7	10	15.1722	12.7395	2.4327		1.600	1.627	-1.64%
8	10	15.1836	12.7237	2.4599	2.471	1.618	1.627	-0.54%
9	10	15.1783	12.6516	2.5267		1.662	1.627	2.16%
10	10	15.1529	12.6522	2.5007		1.647	1.627	1.24%
11	15	15.1695	11.4974	3.6721		2.415	2.440	-1.02%
12	15	15.1500	11.4984	3.6516	3.691	2.404	2.440	-1.51%
13	15	15.1686	11.4192	3.7494		2.463	2.440	0.93%
14	20	15.2328	10.4283	4.8045		3.156	3.254	-3.00%
15	20	15.1808	10.3067	4.8741	4.829	3.204	3.254	-1.53%
16	20	15.1486	10.3397	4.8089		3.165	3.254	-2.72%
17	30	15.1844	7.8877	7.2967		4.797	4.881	-1.73%
18	30	15.1684	7.7464	7.422	7.381	4.885	4.881	0.09%
19	30	15.1860	7.7628	7.4232		4.880	4.881	-0.02%
20	40	15.1660	5.0796	10.0864	10.086	6.635	6.508	1.95%

As can be seen in Table 7, test results are in a good agreement with the calculated results. This agreement also satisfies the heat flux measurement studies and heat of vaporization of Teflon, since they were used to calculate recession as given in Equation 3.1. The maximum absolute value of error is only 3%.

Before applying heat flux to the specimens, the system is started and high temperature flame is obtained. But in this duration, high temperature flame can affect the specimen temperature and may cause some sublimation. To check this situation, temperature measurement from specimen is conducted before applying heat flux on it. In this way, effect of radiation is examined. As seen in Figure 41, if flame direction is not turned to the specimen, temperature of the specimen does not increase.
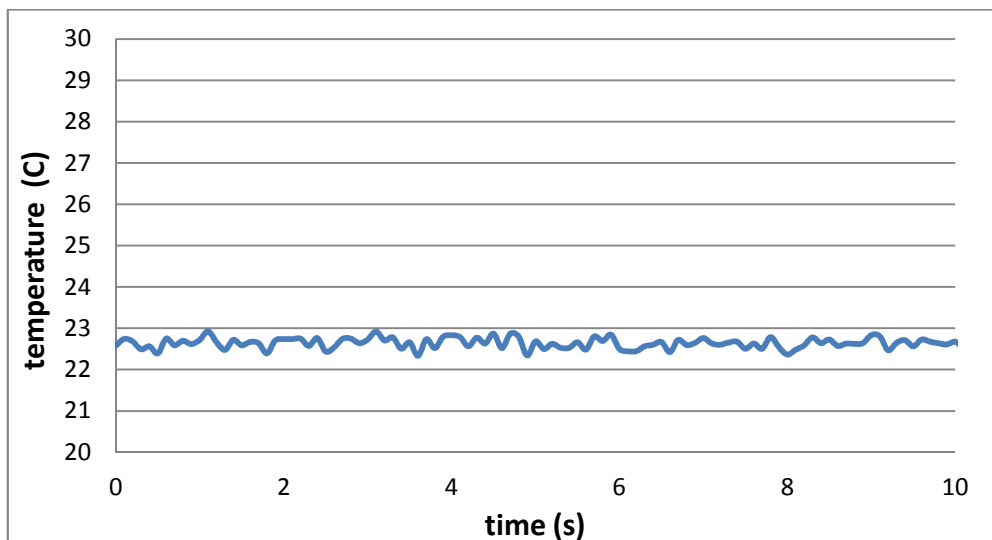
Figure 41: Temperature of the Specimen before Flame is Applied on it.

CHAPTER 8

SIMULATON OF THERMAL ABLATION

In this chapter, results of numerical simulations of oxyacetylene tests of Teflon specimens are given. The measured recession values are compared with the calculated recession values which are obtained from numerical simulations. Moreover, developed numerical algorithm was applied to the blunt nose section of a supersonic rocket to find the recession values of the nose section under aerodynamic heating.

8.1 Numerical Simulations of Oxyacetylene Tests

The simulations were conducted by using ANSYS as mentioned before. The analysis models were prepared by using the axisymmetry of the specimens. PLANE55 type elements were used in the analyses. Since specimens are in a cylinder shape, prepared models have 0.01 m height and 0.015 m radius. ANSYS uses y axis as the axis of symmetry. The sample representative of the solution domain and boundary conditions are given in Figure 42.
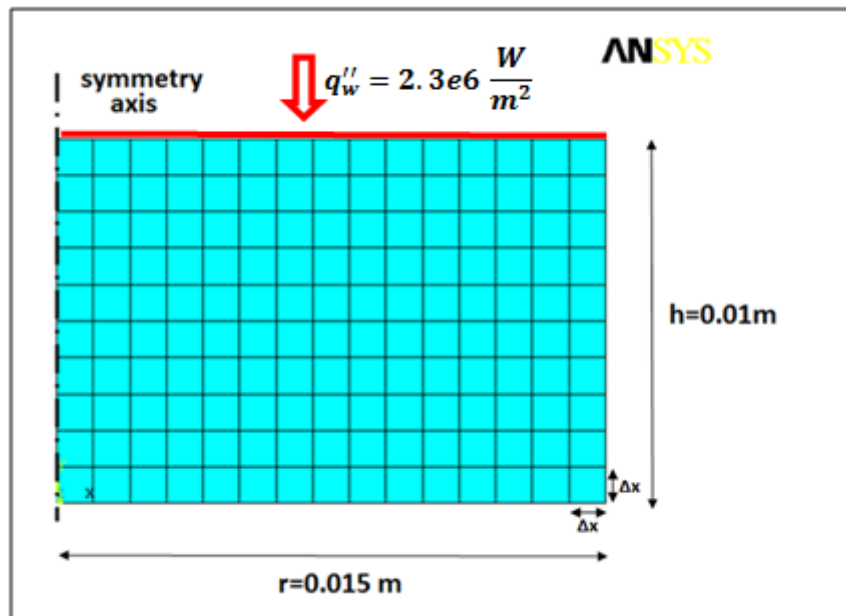
Figure 42: Solution Domain of Sample Analysis Model

8.1.1 Determination of Time Step Size

ANSYS Mechanical APDL uses implicit scheme for the discretization of the differential equations related to heat transfer [46]. In this scheme, at each time level, equations are solved simultaneously in order to determine the nodal temperatures. For linear problems, the implicit solution is always stable; that is, the time step size can be arbitrarily large [46], however, for nonlinear problems small time step size is recommended due to convergence difficulties [46, 53]. Moreover, time step size must be kept reasonably small to obtain results sufficiently close to the exact solution of the partial differential equation [54]. In transient heat transfer analysis, there is a relationship between the minimum time increment and the element size [55]. To avoid inaccurate results or unstable solutions, a proper choice of the initial time step is required [55]. An initial time step is dependent on a number of factors, including the spatial size of the element mesh and the thermal diffusivity of the material. A general guideline for the minimum initial time step is given as follow [53]:

$$\Delta t = \frac{\Delta^2}{n\alpha} \tag{8.1}$$

where Δ is mesh size and α is thermal diffusivity. ANSYS recommends 4 for n [47], ABAQUS recommends 6 [55] and NASTRAN recommends 10 [53]. If time increment is smaller than this value, spurious oscillations which are non-physical can be seen in the solutions. This causes problems especially if temperature dependent material properties are defined. Moreover, small time step can lead to locally inaccurate solutions [55]. In order show these effects, analyses are conducted. In these analyses, an axisymmetric model with 1 mm mesh size is created. Heat flux is applied to the upper surface of the geometry. Transient analyses with different time step sizes are conducted and temperature history of point A is collected over 10 seconds. Representative of model is given in Figure 43.
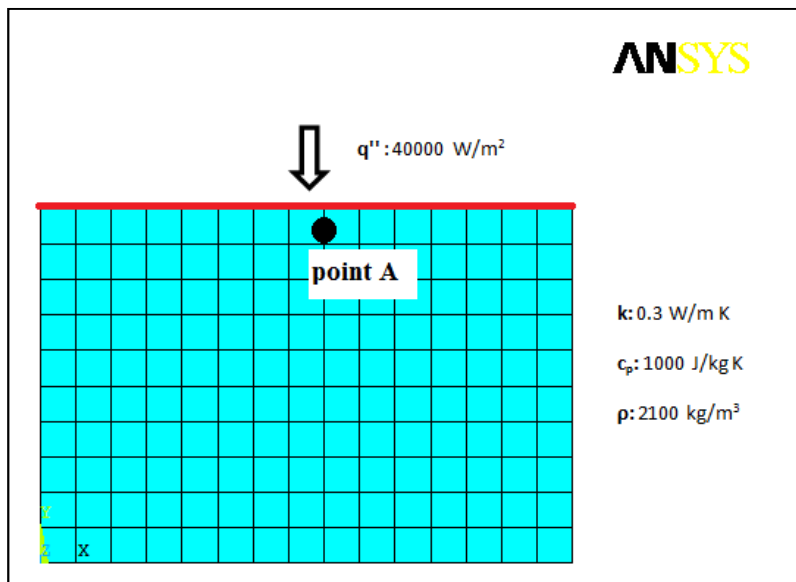
Figure 43: Analysis Model and Material Properties of the Sample Problem

By using Equation (8.1) recommended time step size by ANSYS is calculated as 1.75 s. Effect of larger time step on the temperatures of point A is given in Figure 44.
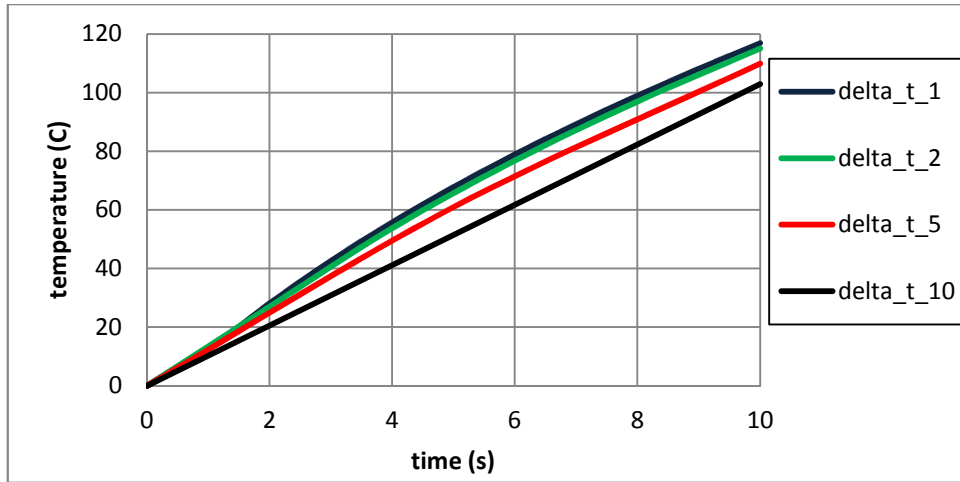
Figure 44: Effect of Larger Time Step Sizes on the Temperature of Point A.

As seen in Figure 44, increase in the time step size causes accuracy losses on the results. However, as mentioned before, ANSYS recommends selecting time step size large enough to prevent unwanted oscillations and temperatures outside of the physically possible range. Effects of smaller time step sizes on the results of the solution are given in Figure 45.
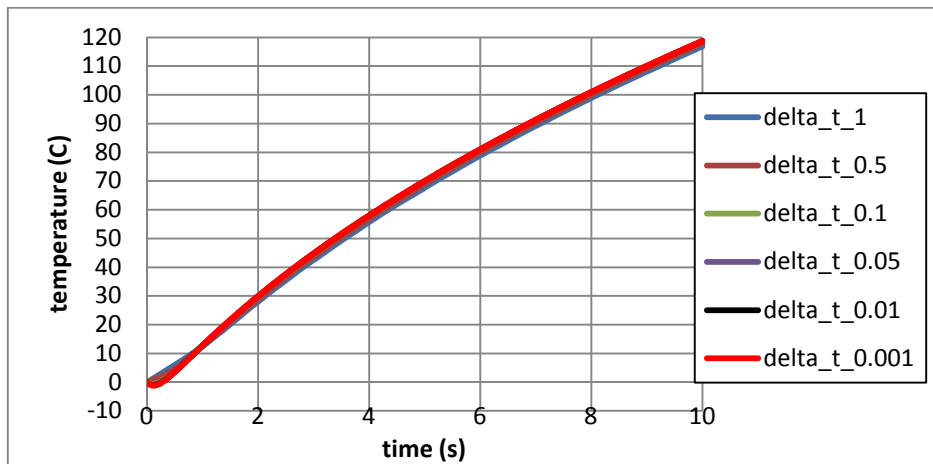
Figure 45: Effect of Smaller Time Step Sizes on the Temperature of Point A.

If the results at the initial time points are examined, it is seen that there are temperatures outside of the physically possible range. Detail view of beginning of graph is given in Figure 46.
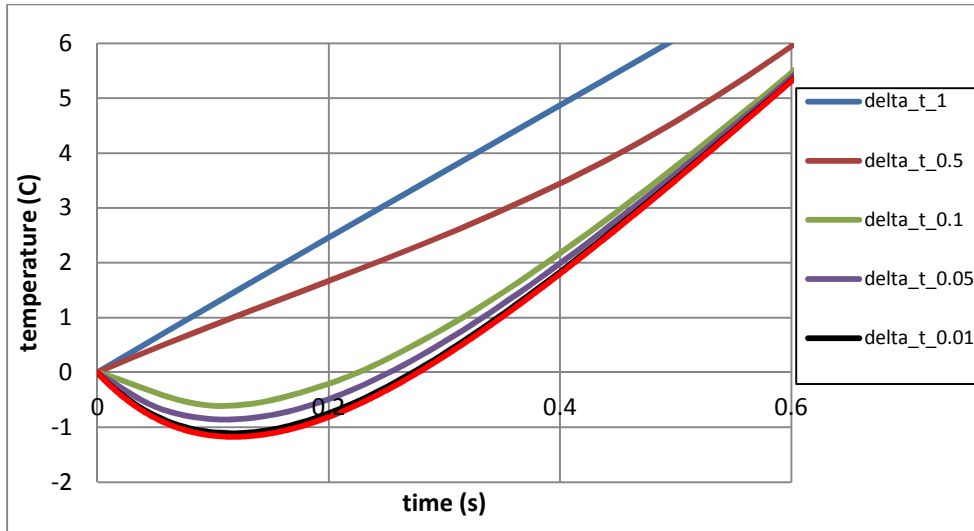
Figure 46: Results of First 0.6 Seconds of Solution

As seen in Figure 46, smaller time step size than recommended value, causes temperatures outside of the physically possible temperature range. As a result, two goals must be simultaneously attained: the mesh must have sufficient resolution for the problem and the time step must be determined to get proper mathematical transient behaviour for that mesh [56]. Detailed information about thermal capabilities and solution technique of ANSYS is given in Appendix section. For Δ is equal to 0.1 mm and material properties of Teflon (k=0.3 W/m K, ρ=2155 kg/m^3 and c_p from Table 4) recommended Δt by ANSYS is calculated by as nearly 1.2s. Therefore, in the ablation simulations Δt is taken as 1.2s.

8.1.2 Results of Ablation Simulations of Oxyacetylene Tests

The simulations were conducted for different test cases and results of simulations were compared with the average value of recession measured after tests. In the simulations time step was used as 1.2 seconds as mentioned above and mesh size was used as 0.1 mm. The comparisons of numerical results with the experimental results are given in Table 8. For the percent error calculation, equation (8.2) is used.

$$\% \ Error = \frac{|experimental \ recession - calculated \ recession|}{|experimental \ recession|} x100 \qquad (8.2)$$

48

Table 8: Comparison of Numerical Results with the Experimental Results

No	Total Exposed Time to Heat Flux (s)	Average of Experimental Recessions (mm)	Calculated Recession (mm)	% error (-)
1	10	1.622	1.59	1.9%
2	15	2.427	2.48	2.3%
3	20	3.175	3.26	2.6%
4	30	4.854	5.01	3.2%

As can be seen in Table 8, percent error increases with the increasing test duration However, maximum percent error does not exceed % 3.2 which is an acceptable level. The errors are due to absence of the material properties such as thermal conductivity at high temperature levels, errors which are coming from discretization (meshing), experimental errors of the DSC and TGA test results and uncertainties, seen on the oxyacetylene test results etc. However, since calculated recession values are larger than measured values, to be on the safe, results of numerical algorithm are acceptable.

8.1.3 Effects of TGA Results on the Oxyacetylene Test Simulations

As mentioned in Chapter 4 "Material Characterization of Teflon", in order to find the ablation temperature of Teflon, TGA studies were conducted. TGA studies showed that heating rate and test atmosphere affect the ablation temperature of Teflon slightly. To see the effects of test results on the simulation results, simulations were made by using different ablation temperatures. Results of simulations are given in Table 9.

Table 9: Oxyacetylene Simulation Results for Different Ablation Temperature of Teflon

Test Number	Test Atmosphere	Heating Rate (°C/min)	Average Temperature of Ablation (K)	Calculated Recession (mm)
1	Nitrogen	10	≈850	1.59 mm
2	Air	10	≈840	1.61 mm
3	Oxygen	10	≈840	1.61 mm
4	Oxygen	20	≈850	1.59 mm
5	Oxygen	30	≈863	1.54 mm
6	Oxygen	40	≈863	1.54 mm

As seen in Table 9, increase of ablation temperature, decreases surface recession as expected. However, since average ablation temperatures are very close to each other, recession values are very similar.

8.1.4 Effects of Thermal Conductivity of Teflon on the Oxyacetylene Test Simulations

It is mentioned that thermal conductivity of Teflon is used as 0.3 W/m K, taken from reference [43]. However, in some studies, thermal conductivity of Teflon is given as 0.25 W/m K [57]. Therefore, to see the effect of thermal conductivity on the simulation results, analyses are repeated with different conductivity values. In the simulations, total simulation time is selected as 10 seconds.

Table 10: Effects of Thermal Conductivity on the Simulation Results

No	Thermal Conductivity (W/m K)	Average of Experimental Recessions (mm)	Calculated Recession (mm)	% error (-)
2	0.25	1.622	1.50	7.5%
3	0.30	1.622	1.59	2.6%

As seen in Table 10, increase in the thermal conductivity, increases the total recession since temperature of the inner sides becomes larger.

8.2 Ablation Simulations of Blunt Nose of a Rocket

8.2.1 Rocket Nose Ablation Analysis

As mentioned before, developed numerical algorithm was applied to the blunt nose section of a supersonic rocket to find the recession values of the nose section under aerodynamic heating. The used nose section is given in Figure 47.
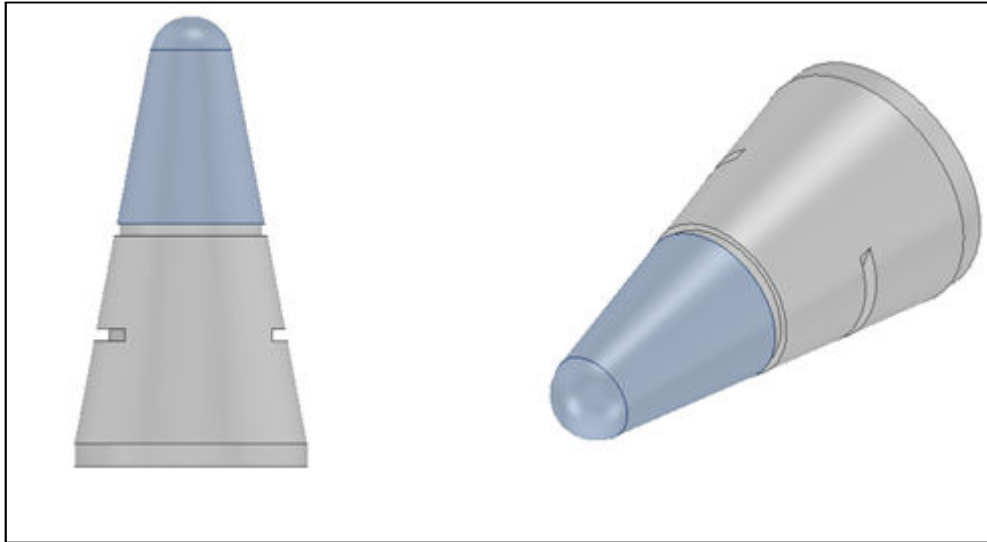
Figure 47: CAD Model of Nose Section

The simulations were conducted for the Teflon part of the nose section. Models were prepared as axisymmetric around y axis in ANSYS. The cross sectional view of nose section and its analysis model is given in Figure 48.
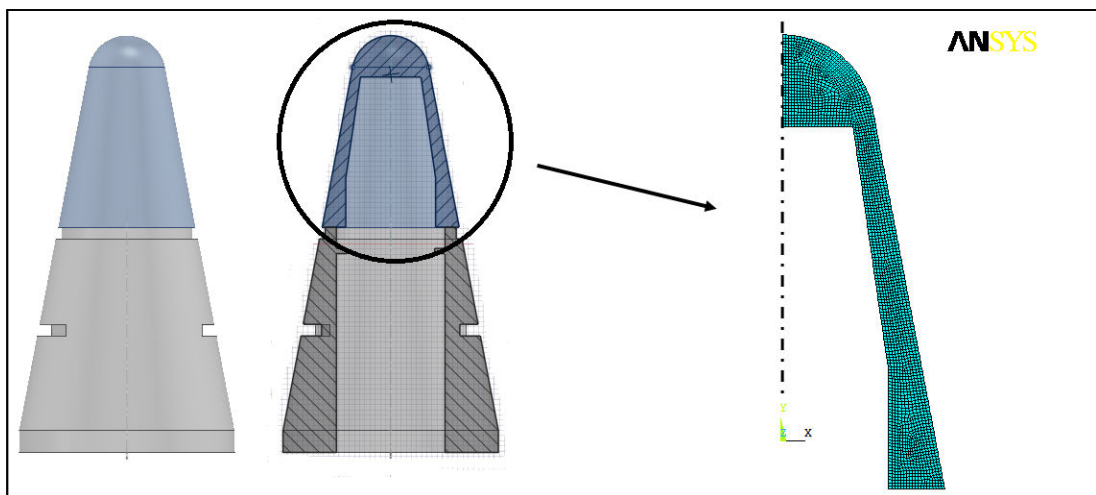
Figure 48: Teflon Part of Nose Section and Its Axisymmetric Analysis Model

In the analyses, aerodynamic heating was used as boundary condition for the nose section. During the flight period, aerodynamic heating acts on the surface of the section and peak values of heating are seen at the stagnation point which is the tip of the nose section. Aerodynamic heating data over 120 seconds of flight period is given in Table 11.

Table 11: Aerodynamic Heating Data Used in the Simulations (W/m²)

y coord. (m)					time (s)				
0.0000	0	5	10	18	20	40	60	100	120
0.0000	0	10886	43204	122027	139811	31550	12702	13096	14206
0.0190	0	11927	47336	133699	153185	34568	13917	14349	15565
0.0390	0	13820	54850	154922	177500	40055	16126	16626	18036
0.0590	0	17417	69126	195244	223698	50480	20323	20953	22730
0.0616	0	18932	75137	212221	243150	54870	22090	22775	24706
0.0629	0	20758	82385	232695	266608	60163	24221	24973	27090
0.0641	0	26050	103385	292007	334564	75498	30395	31338	33995
0.0653	0	32209	127829	361047	413666	93349	37581	38747	42032
0.0665	0	38925	154486	436339	499931	112815	45418	46828	50798
0.0676	0	45929	182281	514846	589879	133113	53590	55253	59937
0.0686	0	52986	210288	593951	680513	153566	61824	63743	69146
0.0696	0	59897	237716	671422	769274	173596	69888	72057	78165
0.0705	0	66492	263891	745351	853978	192710	77583	79991	86772
0.0713	0	72626	288237	814116	932764	210489	84741	87370	94777
0.0720	0	78177	310268	876341	1004058	226577	91218	94048	102021
0.0726	0	83042	329574	930871	1066536	240676	96894	99901	108370
0.0731	0	87135	345819	976754	1119105	252539	101670	104825	113711
0.0735	0	90388	358730	1013222	1160888	261968	105466	108738	117957
0.0738	0	92749	368100	1039686	1191209	268810	108220	111579	121038
0.0739	0	94180	373781	1055731	1209592	272959	109890	113301	122906
0.0740	0	94660	375684	1061106	1215751	274349	110450	113877	123531

As mentioned before, aerodynamic heating is the maximum at the stagnation point which is at the tip of the nose(y=0.074 m). Heating values decrease through the back of the nose. The ratio of the aerodynamic heating on the surface of the nose to the stagnation point is given in Figure 49.
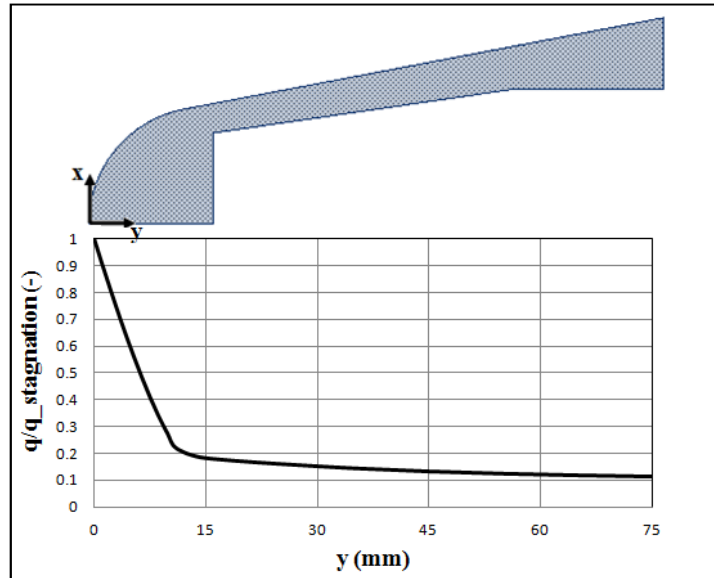
Figure 49: Change of Ratio of Aerodynamic Heating of a Point to the Stagnation Point Heating With Respect to Coordinate of the Point

In the analyses, change of aerodynamic heating due to ablation of the nose section is neglected. Due to change of the nose shape and blowing effect of the vaporized Teflon gases, aerodynamic heating decreases in real flight conditions; however, in the analyses, by neglecting the decrease on the aerodynamic heating, recession rates are found larger than that of real cases which bring extra safety to the design. At 120th second of flight, temperature distribution on the nose and its final shape is given in Figure 50.
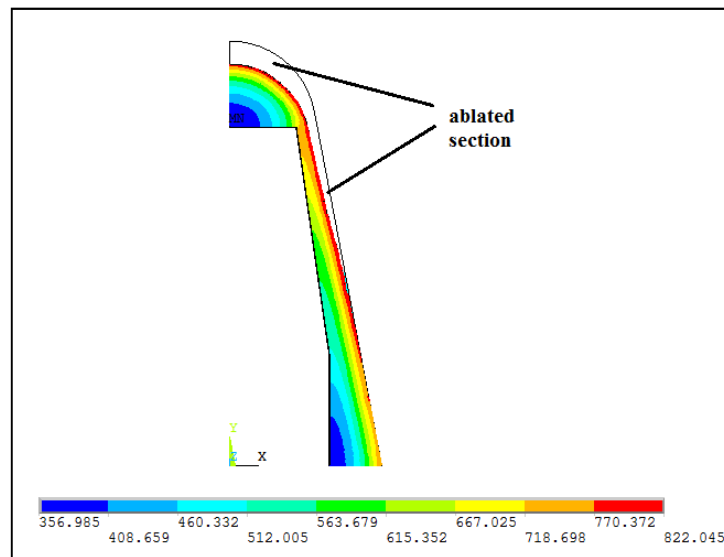
Figure 50: Temperature Distribution and Shape Change of Nose at the End of Flight after Ablation Simulation

As can be seen in Figure 50, calculated recession is maximum at the nose tip as predicted since aerodynamic heating is maximum at this location due to stagnation condition. Recession and temperature values decrease through the back of the nose due to decrease on the aerodynamic heating as given in Figure 49. Maximum recession at the nose is nearly 4.2 mm. Recession history of the nose tip is given in Figure 51.
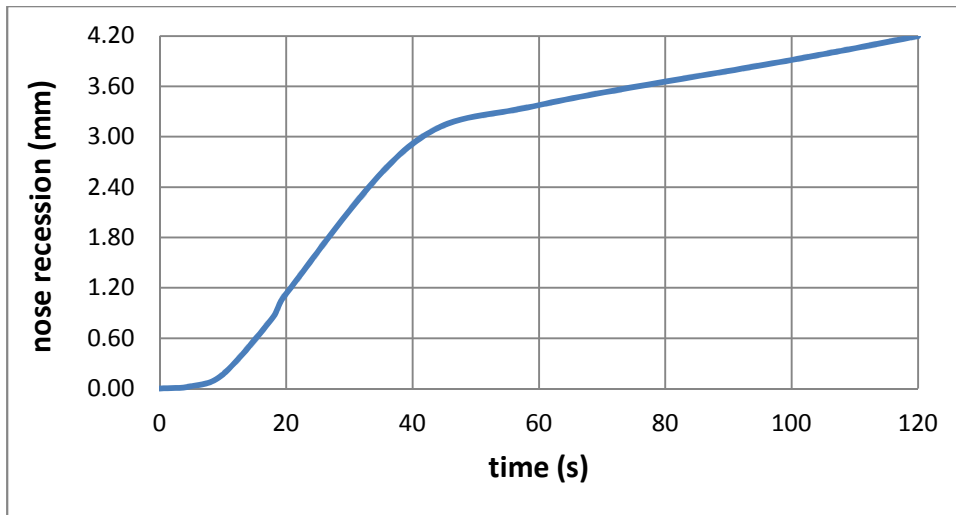
Figure 51: Recession of Nose Tip During Flight Duration

In order to see the effects of the ablation on the solutions, nose analysis was also conducted without using ablation criteria. In other words, without using developed algorithm, only transient thermal analysis was conducted under same aerodynamic heating values. The temperature distribution of the non-ablated nose at the end of the flight is given in Figure 52.
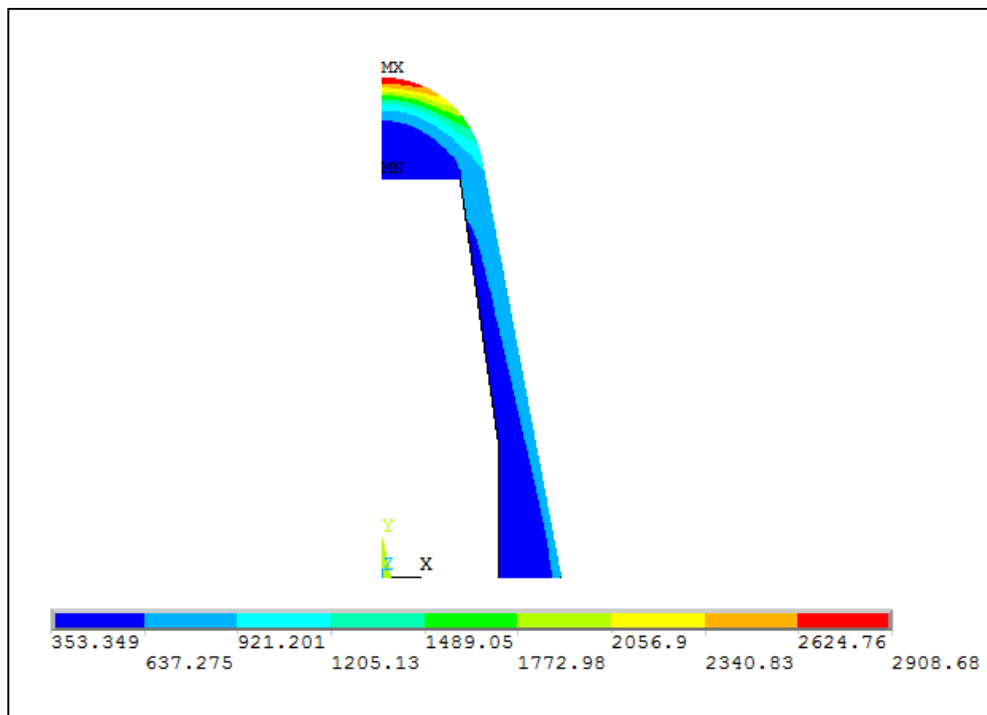
Figure 52: Temperature Distribution and Shape Change of Nose at the End of Flight after Simulation in which Ablation is Ignored

As can be seen in Figure 52, nearly 2900 K temperature level is seen at the nose tip, however, as given in Figure 14, Teflon vaporizes at nearly 850 K and it is not possible for the Teflon to reach these elevated temperature levels. Therefore, ablation simulation is necessary for the insulation materials, especially for the nose or leading edge materials which are exposed to high aerodynamic heating loads.

8.2.2 Effects of TGA Results on the Rocket Nose Simulations

To see the effects of ablation temperature on the total recession of the nose cone, simulations are conducted by using different temperatures of ablation. Temperatures are taken from TGA results. Calculated stagnation point recessions are given in Table 12.

Table 12: Nose Cone Ablation Simulation Results for Different Ablation Temperatures of Teflon

Test Number	Test Atmosphere	Heating Rate (°C/min)	Average Temperature of Ablation (K)	Calculated Stagnation Point Recession (mm)
1	Nitrogen	10	≈850	4.20 mm
2	Air	10	≈840	4.45 mm
3	Oxygen	10	≈840	4.45 mm
4	Oxygen	20	≈850	4.20 mm
5	Oxygen	30	≈863	3.82 mm
6	Oxygen	40	≈863	3.82 mm

As seen in Table 12, increase of ablation temperature, decreases stagnation point recession as expected.

8.3 Effect of Ablation on the Trajectory of the Rocket

As mentioned before, ablation is necessary to decrease the aerodynamic heating effects on the rocket. However, shape change of the nose section of a missile can prevent success of the mission since shape change effect the trajectory. Therefore, to see the effect of ablation on the trajectory flight simulations are conducted.

Aerodynamic prediction software packages provide a design tool to generate aerodynamic performance estimates [58].Some of these tools are Missile DATCOM, PANEL3D, PRODAS V3,SET 3D and NEAR MISL3 [58]. For the simulations, Missile DATCOM and an in-house code are used. Dynamic coefficients are calculated by using Missile DATCOM and trajectory is calculated by using an in-house code. Missile DATCOM is a semi-empirical aerodynamic prediction codes that calculate aerodynamic forces, moments and stability derivatives as a function of angle of attack and Mach number. Simulation configuration can be axisymmetric or nonaxisymetric. Flight conditions and aerodynamic parameters range from subsonic to hypersonic speeds, angles of attacks up to 90 deg. and control surface deflections from -35 to 35 deg [59].

For the simulations two different missile configurations with two different nose geometries are used. These nose geometries are original geometry and ablated geometry that is given in Figure 50. These geometries represent two extreme cases. One is original geometry and other one is the ablated geometry at the end of the flight. In reality ablation will be transient during flight. Therefore; actual trajectory will be between trajectories calculated by use of these geometries. Other parameters

(propellant temperature, firing angle, atmospheric conditions, and fin shapes etc.) are taken same value for the two configurations. Schematic representations of configurations are given in Figure 53.
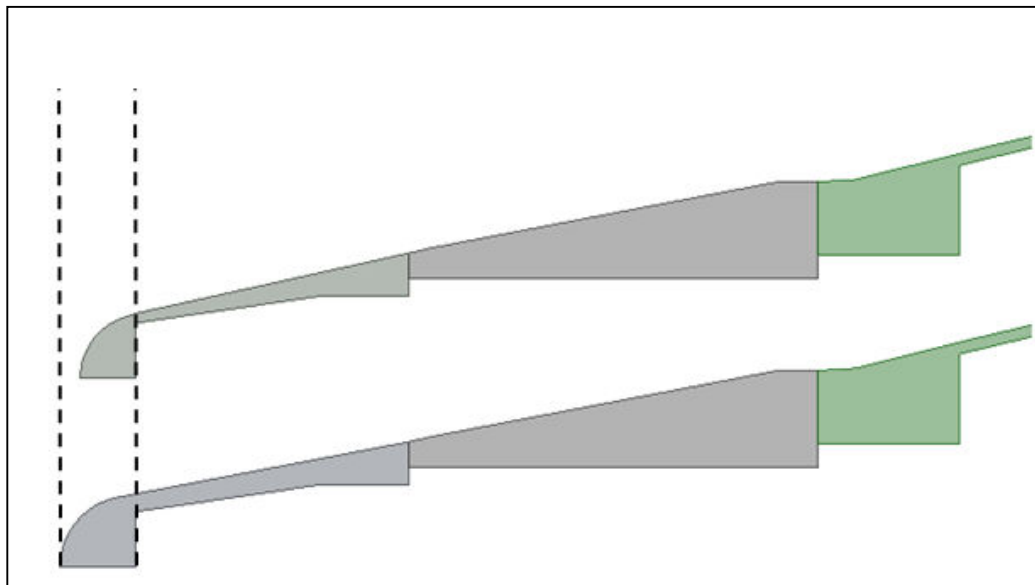
Figure 53: Axisymmetric Representations of Nose Cone of Two Rocket Configurations

Results of trajectory simulations are given Figure 54.
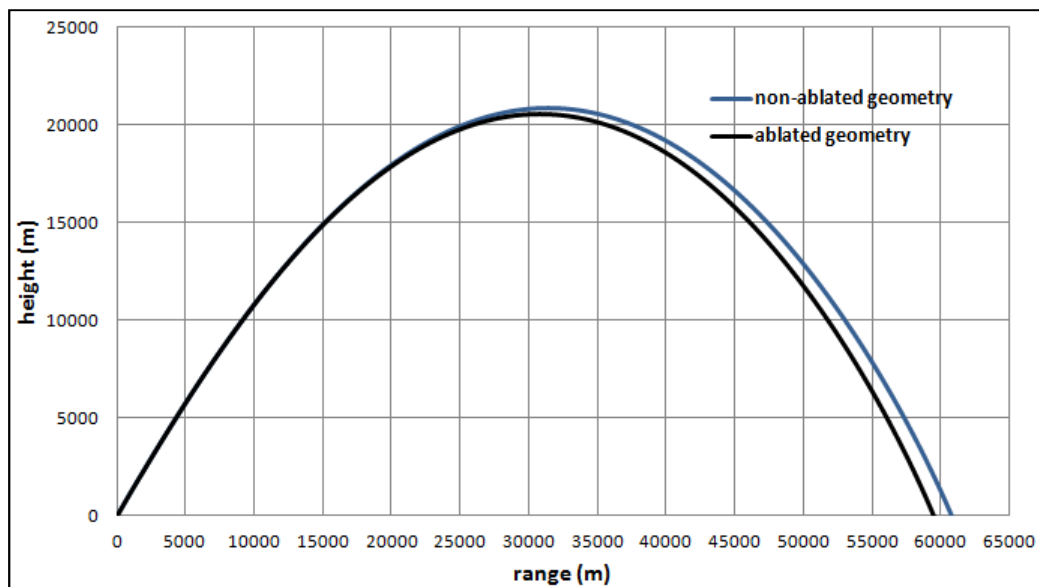
Figure 54: Comparison of Trajectories of Two Rockets Which Have Ablated and Non-ablated Nose Geometries

As can be seen in Figure 54, nearly 4 mm recession of the nose tip can decrease total range nearly 2000 m. Since ablation increases bluntness of the nose, drag coefficients increase. This is the main reason of differences seen in the trajectories. 2000 m. distance is not a value that can be neglected during the design of the rockets or missiles. Therefore, ablation calculation is an obligation for a designer. As mentioned before, actual trajectory will be between these two trajectories since two

extreme geometries are used in the simulations. Therefore; 2000 meters is the maximum possible range difference.

As mentioned before, shape of the nose cone will change continuously from original geometry to the final geometry during flight period. Therefore, flight trajectory will be between these calculated trajectories. To show this fact, third simulation is conducted. In this simulation, for the first 5 seconds of flight, original nose geometry is used and for the rest of the flight, ablated geometry is used. As expected, trajectory is found between two extreme trajectories as given inFigure 55.
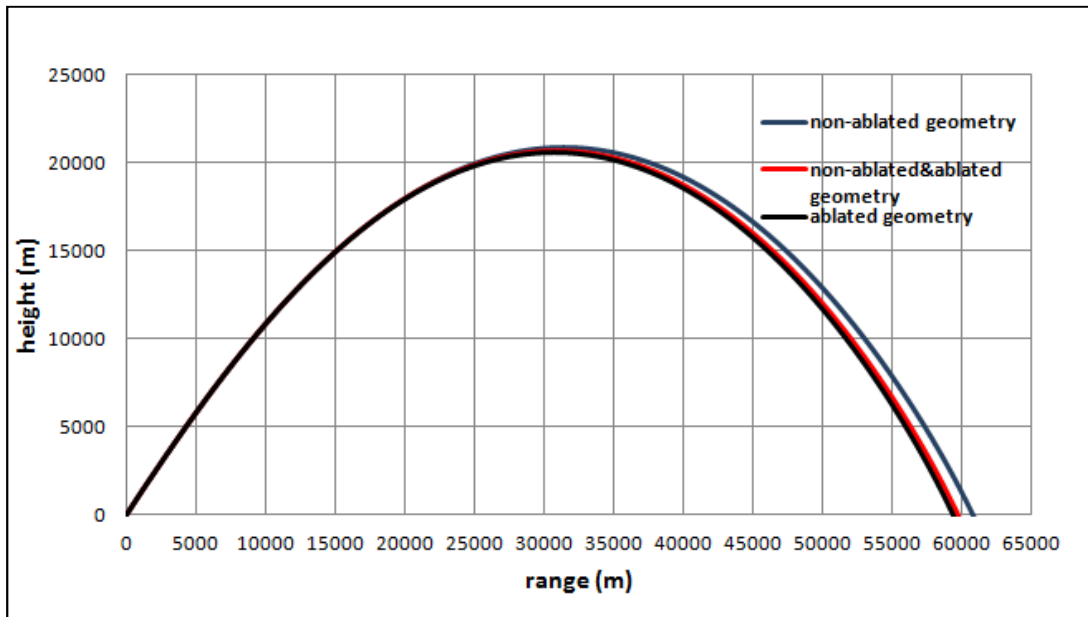
Figure 55: Trajectory of Rocket when Ablated and Non-ablated Geometries are Used Simultaneously in the Simulation

8.4 Effect of Ablation on the External Flow on the Rocket

To see effect of shape change of the nose cone on the external flow around rocket, CFD analyses are conducted. In the analyses, ANSYS Fluent software is used. In the analyses, two different axisymmetric models are used. These models have nose geometries which are ablated and non-ablated. Geometries are same with the geometries used in the trajectory simulations given in Figure 53. Flight velocity is used as 4.2 M and free stream temperature is 275 K in the analyses. Schematic representations of results are given below.
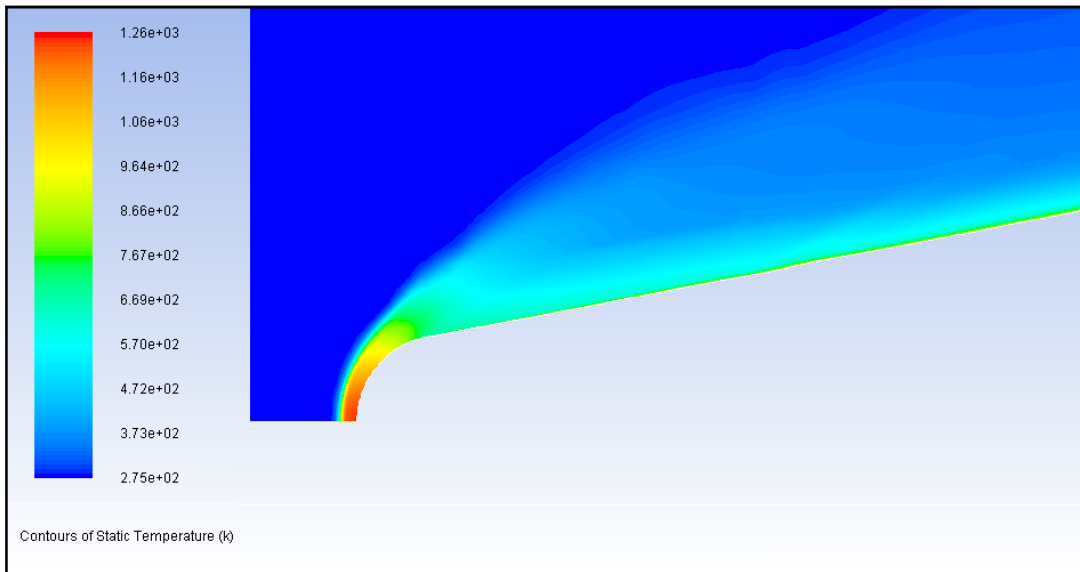
Figure 56: Temperature Distribution in Flow for Non-Ablated Nose Geometry (K)
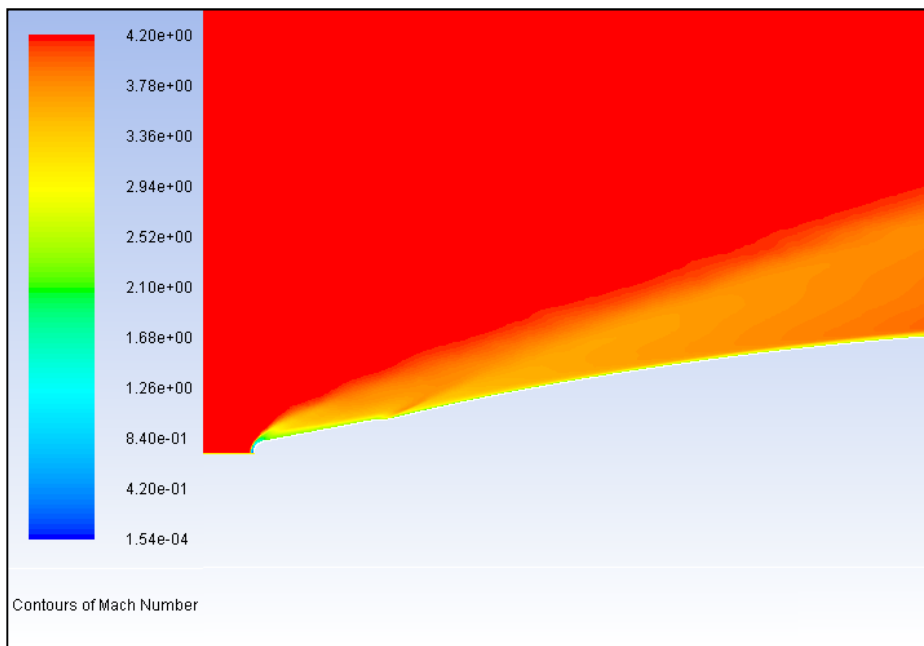
Figure 57: Mach Number Distribution in Flow for Non-Ablated Nose Geometry
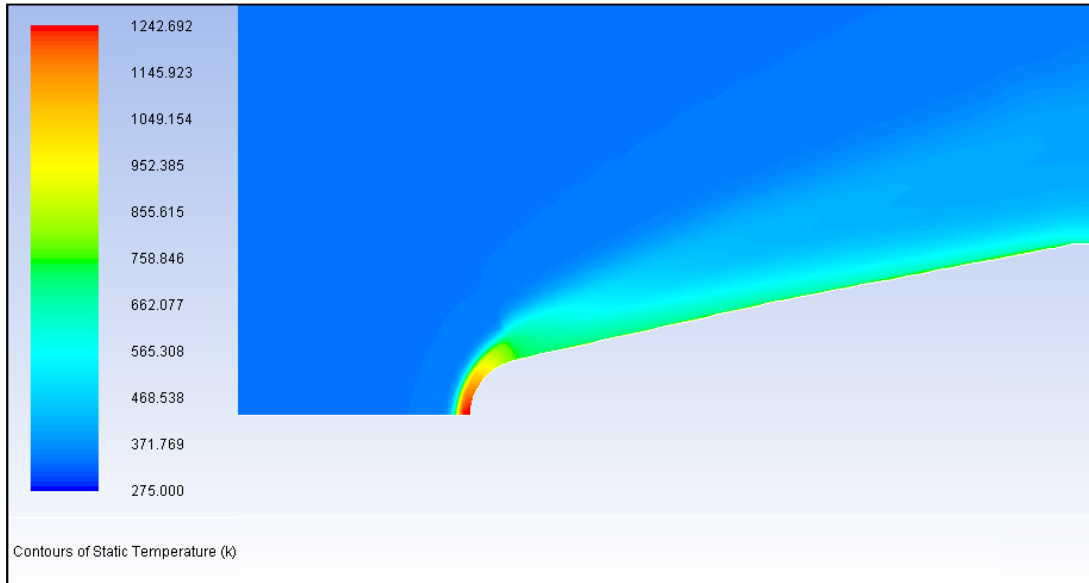
Figure 58: Temperature Distribution in Flow for Ablated Nose Geometry (K)
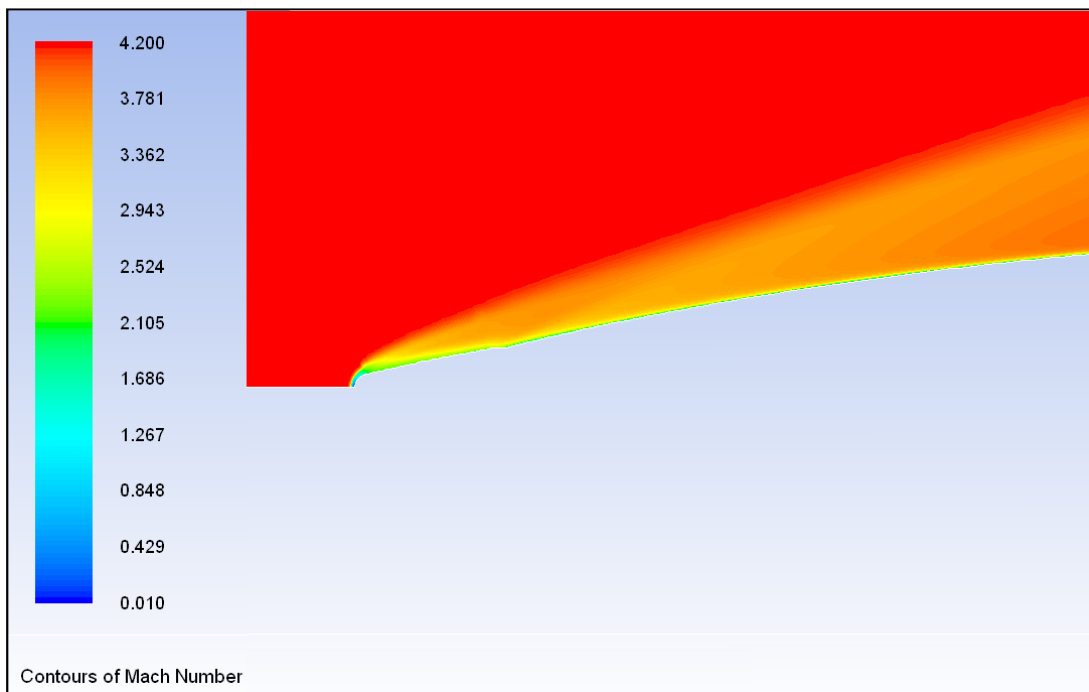
Figure 59: Mach number Distribution in Flow for Ablated Nose Geometry

In the results, it is seen that stagnation point temperatures are nearly same for rockets which have different nose geometries. Stagnation point temperature is defined as [60]:

$$T_O = T_\infty (1 + \frac{k-1}{2} M_\infty^2) \tag{8.3}$$

As mentioned before, T_∞ is used as 275 K and M_∞ is used as 4.2. If these values are substituted in Eq.8.1, stagnation point temperature is calculated as 1245 K. Differences between this value and results are less than 2%.

Moreover, in the introduction section of this thesis, blunt body theory is mentioned. This theory states that bluntness of body increases distance between body and shock wave. To see the bluntness effect on the shock wave location, Mach number distribution along a line is plotted. By this method, it is aimed to see the position of shock wave. Schematic representations of line and Mach number distribution along this path are given below.
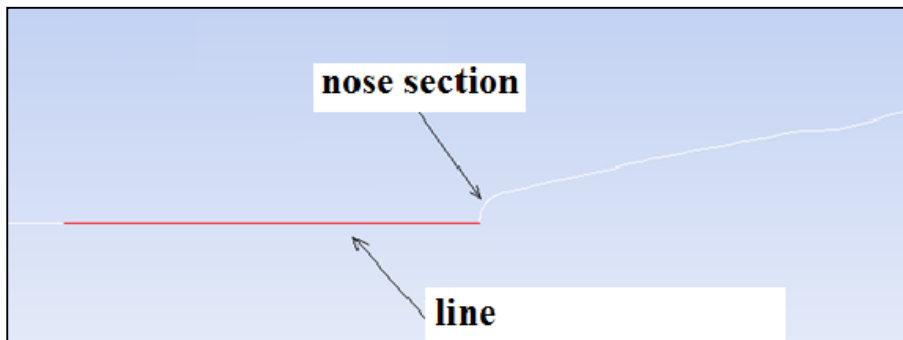
Figure 60: Schematic Representation of Path
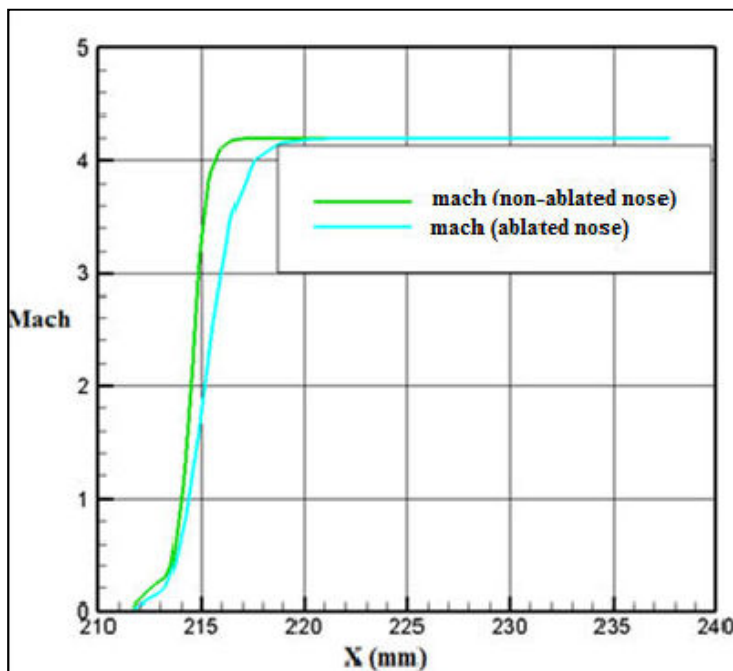
Figure 61: Mach Number Distribution Along Path for Two Different Nose Geometries

As expected, since ablation increases bluntness, position of point at which flow regime changes from supersonic to subsonic (M=1) is pushed away from nose tip.

CHAPTER 9

SUMMARY AND CONCLUSIONS

In this chapter, general summary of the thesis and some conclusion remarks are presented. In addition, recommendations for future work are given.

9.1 GENERAL CONCLUSIONS

In this thesis, background information about aero-thermodynamics, from the air ionization due to high-speed flow to the blunt body theory for the air vehicles, was supplied and detailed information about thermal protection systems was presented. Moreover, advantages and disadvantages of the different types of thermal protection systems and their applications were explained. It is believed that this thesis will be a reference guide for an engineer who works on the field of aerodynamic heating analyses of the missiles or satellites.

In this thesis, literature review for the aerodynamic heating and ablation modeling were presented and each of the studies from the literature was explained in detail. The most recent and the most beneficial sources were selected in this area. Therefore, this thesis includes list of studies which are useful references for the engineers working on ablation phenomena.

Teflon, which is used widely in the area of aerospace, was characterized for thesis study and results of density measurement, TGA and DSC thermal analyses were presented in detail. By using these tests, specific heat capacity of material up to 500 °C, melting temperature, latent heat of melting and sublimation temperature were found. Moreover, by using different heating rates and test atmospheres during TGA tests, effects of these parameters were examined on the sublimation temperature of Teflon. These material properties were used in the thermal and ablation analyses of Teflon.

Oxyacetylene ablation tests were conducted for Teflon specimens. A total number of 20 tests under different exposing times to flame were performed and weight loss and recession distance for each specimen were measured. Before the analytical calculations, heat flux of the test set up was measured by using temperature response of a steel bar to oxyacetylene flame. Then, analytically calculated recession distances were compared with the average test results in Table 7 and it was showed that maximum difference between experimental and analytical results was only %3. Therefore it is clear that use of analytical methods to predict recession rates is possible as mentioned in reference [24] and a academic study by using this method was conducted and presented at 52nd AIAA Structures, Structural Dynamics and Materials Conference on 4-7 April 2011 in Denver ,USA [61].

A numerical algorithm for the ablation modeling was developed by using APDL (ANSYS Parametric Design Language). In the algorithm element death option of the ANSYS was used and material removal strategy of the algorithm for modeling the ablation was explained in detail in this thesis. Moreover, thermal analysis capabilities of the ANSYS were also given briefly. Mesh and time step dependencies of results were studied by using different mesh size and time steps. 10 seconds exposed time test result of oxyacetylene ablation test was used as a reference and it was showed that by using proposed time step by ANSYS (equation A.18) for mesh size of 0.1 mm, maximum %3.2 error was observed. Reasons of the differences are the experimental errors on the experimentally found material properties by using DSC and TGA and applied heat flux during oxyacetylene tests. As seen in Table 7, under same exposing times to flame, measured recessions show variances. Moreover, lack of material properties such as thermal conductivity at higher temperatures and errors coming from discretization are one of the reasons.

Numerical algorithm was applied on the nose section of a supersonic rocket. Change of stagnation point heating during flight period and heat transfer rate distribution over nose which are used as an input value for the analyses were presented. Axisymmetry of the model was used in the analyses and for the end of flight period, temperature distribution and final shape of the nose section was presented. As predicted, maximum recession was seen at the nose tip of the section due to stagnation point aerodynamic heating. Nearly 4.2 mm recession was observed on the nose tip. Moreover, effect of ablation temperature on the recession was examined by using different TGA results.

In order to see the effect of ablation on the trajectory of the rocket, two flight simulations were conducted by using two different nose cone geometries. One of the geometries is the original geometry and other geometry is the ablated geometry that is found by using ablation simulation at the end of the flight. Dynamic coefficients for the flight were obtained by using Missile DATCOM package software and trajectory calculations were made by using an in-house code. Results of simulations showed that ablation shortens the rocket range. Nearly 2000 meters difference was seen on the ranges of the rockets that have two different nose geometries. Therefore, it is possible to say that ablation simulations are necessary to find the ranges of the rockets during design phases.

Effect of ablation on the external flow around the rocket was examined by CFD analyses. CFD analyses were conducted by using Fluent package software. In the analyses, it was showed that change of nose shape does not change the total stagnation temperature; however, location of shock depends on the nose geometry. Bluntness of the geometry pushes shock wave as expected. Distance between the shock wave and the nose tip increases with the increasing bluntness of the nose.

9.2 RECOMMENDATIONS FOR FUTURE WORK

In this thesis, material characterization of Teflon and numerical and experimental studies on the ablative behavior of the Teflon are presented. However, the approaches can be further improved with the additional efforts. These improvements can be done as explained below.

As mentioned before, subliming ablative material modeling was performed in this thesis, but ablation of charring ablative materials can also be modeled under aerodynamic heating. However, for this kind of modeling, more material properties and boundary layer conditions are required. Charring ablative materials are also widely used as thermal protection systems, and it is compulsory to model it for some types of missiles.

In this thesis, material removal from base material was only due to thermal degradation. However, due to high shear stress caused by flow adjacent to the surface, mechanical erosion of the material is also possible. Therefore, shear removal of the material can be modeled numerically. For this kind of modeling, material shear strength should be determined by performing required tests

In this thesis, flow calculations over the rocket were not included in the analyses; therefore, changes in the aerodynamic heating values due to shape change and blowing effect of ablation are neglected. But, to get the effect of shape change on the aerodynamic heating, an iterative study can be done such that at every time step aerodynamic heating values are recalculated by CFD analyses by using changed shape. Then ablation analyses can be performed under new heating values. This order should be followed up to the end of flight.

In this thesis, DSC analyses are performed for material characterization. DSC device is generally used to find specific heat capacity and phase change parameters of the materials. However, by following some special methods, thermal conductivity of the material can also be measured by DSC [62].The details are explained in reference [62].

REFERENCES

[1] Bianchi, D., *Modeling of Ablation Phenomena in Space Applications*, Ph.D. Thesis, University of Roma, 2007.

[2] Thornton. E.A., *Thermal Structures and Materials for High Speed Flight*, Progress in Astronautics and Aeronautics AIAA, Volume 140, 1992.

[3] Anderson, Jr. J. D., *Fundamentals of Aerothermodynamics, 3rd Edition*, McGraw Hill Inc., 2001.

[4] Bart., G. C., *On Aerial Navigation*, Nicholson's Journal of Natural Philosophy, 1810.

[5] Bertin J.J., *Hypersonic Aerothermodynamics*, AIAA Education Series, 1994.

[6] U.S. Centennial of Flight Commission, http: //www.centennialofflight.gov. last visited on March 2012.

[7] Chou, D.C., Smith, F.T., *Aerodynamic Heating of Supersonic Blunt Bodies*, Army Research Office, Report No: AD/Q-001 135, 1974.

[8] Achard, T.R., *Fundamental Relationships for Ablation and Hyperthermal Heat Transfer*, Structure Division of the Air Force Flight Dynamics Laboratory, Report No: AFFDL-TR-66-25, 1965.

[9] Thermopedia^{TM}, www.thermopedia.com, last visited on June 2012.

[10] Vincenti, W.G., Boyd, J.W., Bugos, G. E., *H. Julian Allen: An Appreciation*, Annual Review of Fluid Mechanics, Vol.39, pp 1-17, 2007.

[11] Santos W.F.N., *Leading-Edge Bluntness Effects on Aerodynamic Heating and Drag of Power Law Body in Low-Density Hypersonic Flow*, Journal of the Braz. Soc. of the Mech. Sci.& Eng., Vol. XXVII, No.3, 2005.

[12] Saravanan S., Jagadeesh, G., Reddy, KPJ., *Convective heat-transfer rate distributions over a missile shaped body flying at hypersonic flight speeds*, Experimental Thermal and Fluid Science, Vol.33, pp.782-790, 2009.

[13] Ertürk, G., *Shape Change and Ablation Modeling of Thermal Protection Systems of High-Speed Aerospace Vehicles*, M.Sc. Thesis, Middle East Technical University, 2003.

[14] Glass, D.E., *Ceramic Matrix Composite (CMC) Thermal Protection Systems (TPS) and Hot Structures for Hypersonic Vehicles*, 15th AIAA Space Planes and Hypersonic Systems and Technologies Conference, AIAA-2008-2682, 2008.

[15] NASA, *Entry Thermal Protection*, Report No: NASA SP-8014, 1968.

[16]Aykan, F.S., *Numerical Analysis of Ablation Process on a Two Dimensional External Surface*, M.Sc. Thesis, Middle East Technical University, 2005.

[17] Lamb. B., Venkatapathy, E., *Thermal Protection System Technology and Facility Needs for Demanding Future Planetary Mission*, International Workshop on Planetary Probe Atmospheric Entry and Descent Trajectory Analysis and Science, Lisbon Portugal, 2003.

[18] Lees, L., *Laminar Heat Transfer Over Blunt-Nosed Bodies at Hypersonic Flight Speeds*, Journal of Jet Propulsion, Vol.26,No.4, pp.259-269,274, 1956.

[19] Zoby E.V., Moss, J., N., Sutton, K., *Approximate Convective-Heating Equations for Hypersonic Flows*, Journal of Spacecraft and Rockets, Vol.18, No1., pp 64-70, 1981.

[20] Quinn R.D., Gong, L., *Real-Time Aerodynamic Heating and Surface Temperature Calculations for Hypersonic Flight Simulation*, NASA Technical Memorandum 4222, August 1990.

[21] Arnas, A. Ö., Daisie, D. B., Gunnar, T., Seth, A.N., Jason, R.W., Michael, J. B., Bret, P. V., *On the Analysis of the Aerodynamic Heating Problem*, Journal of Heat Transfer, Vol 132, December 2010.

[22] Candane, S.R., Balaji, C., Venkateshan, S.P., *Ablation and Aero-thermodynamic Studies on Thermal Protection Systems of Sharp-Nosed Re-entry Vehicles*, Journal of Heat Transfer, Vol.129, pp. 912-916, 2007.

[23] Chen Y.K and Milos F.S., *Ablation and Thermal Response Program for Spacecraft Heatshield Analysis*, Journal of Spacecraft and Rockets, Vol.36, No.3, pp.475-483, 1999.

[24] Dec, J.A., and Braun R.D., *An Approximate Ablative Thermal Protection System Sizing Tool for Entry System Design*, 44th AIAA Aerospace Sciences Meeting and Exhibit, , Reno, Nevada, AIAA 2006-780, Jan. 2006.

[25] McAlees Jr., Samuel and Maydew, C.R., *Aerothermodynamic Design of High Speed Rockets*, Journal of Spacecraft, Vol 22,No 3, pp. 309-315, May-June 1985.

[26] Lin, W., *Quasi-steady Solutions for the Ablation of Charring Materials*, International Journal of Heat and Mass Transfer, Vol.50, pp. 1196-1201, 2007.

[27] Milos F.S., *Galileo Probe Heat Shield Ablation Experiment*, Journal of Spacecraft and Rockets, Vol 34, No.6, 1997.

[28] Milos, F.S., Chen Y.K., Squire T.H and Brewer, R.A., *Analysis of Galileo Heatshield Ablation and Temperature Data*, Journal of Spacecraft and Rockets, Vol.36, No.3, 1999.

[29] Nompelis, I., Candler G.V., Conti, R.J., *A Parallel Implicit CFD Code for the Simulation of Ablating Re-Entry Vehicles*, AIAA 2009-1562, 2009.

[30] Torre, L., Kenny J.M., Maffezzoli A.M., *Degradation Behaviour of a Composite Material for Thermal Protection Systems Part 1-Experimental Characterization*, Journal of Materials Science, Vol. 33, pp. 3137-3143, 1998.

[31] Mohammadiun H., Kianifar A., *Numerical Modeling of Non-Charring Material Ablation with Considering Chemical Reaction Effects, Mass Transfer and Surface Heat Transfer*, European Journal of Scientific Research, Vol.54, No.3, pp.435-447, 2011.

[32] Beaudet, J., Cormier, J., Dragon, A., Rollin, M., Benoit, G., *Ablation Properties of C Fibers and SiC Fibers Reinforced Glass Ceramic Matrix Composites upon Oxyacetylene Torch Exposure*, Materials Sciences and Applications, Vol. 2, pp.1399-1406, 2011.

[33] W.M. Laurence., *the Effect of Temperature and Other Factors on Plastics and Elastomers*, 2nd Edition, William Andrew Inc., 2008.

[34] PerkinElmer, Inc., *Thermogravimetric Analysis (TGA), A Beginner's Guide*, 2010.

[35] Rawlinson C., *Differential Scanning Calorimetry-Cooking with Chemicals*, School of Pharmacy, University of Bradford, 2006.

[36] Slopiecka, K., Bartocci, P., Fantozzi, F., *Thermogravimetric analysis and kinetic study of poplar wood pyrolysis*, 3rd International Conference on Applied Energy,16-18 May 2011,Perugia,Italy.

[37] Quan,C., Li,A.,Gao,N., *Thermogravimetric analysis and kinetic study on large particles of printed circuit board wastes*, Waste Management, Vol.29, No.8., pp.2353-2360, 2009.

[38] National Fire Protection Association, *SFPE Handbook of Fire Protection Engineering*, 3rd Edition, 2002.

[39] PerkinElmer Inc., *Differential Scanning Calorimetry(DSC), A Beginner's Guide*, 2010.

[40] Colby College., www. colby.edu/chemistry/PChem/lab/DiffScanningCal.pdf, last viewed on May 2012

[41] Colorado State University, http:/ /www1. chm.colostate.edu /Files/CIFDSC/ dsc2000.pdf last viewed on May 2012

[42] Borgnakke, C., and Sonntag, R. C., *Fundamentals of Thermodynamics, 7th Edition*, John Wiley and Sons, 2009.

[43] Blumm, J., Lindemann, A., Meyer, M., Strasser, C., "Characterization of PTFE Using Advanced Thermal Analysis Techniques", http://www.netzsch-thermal-analysis.com/download/P-022_315.pdf last viewed on June 2012.

[44] Camberos J.A., Roberts L., *Analysis of International Ablation for the Thermal Control of Aerospace Vehicles*, Joint Institute for Aeronautics and Acoustics, Report No: JIAA TR-94, August 1989.

[45] Jafari,A., Seyedein S.H., Haghpanahi M., *Modeling of Heat Transfer and Solidification of Droplet/Substrate in Microcasting SDM Process*, IUST International Journal of Engineering Science,Vol.19, No.5-1, pp.187-198,2008.

[46] ANSYS, Inc., *ANSYS 14.0 Help, Version 14.0*, 2011.

[47] ANSYS, Inc., *Thermal Analysis Guide, Release 12.1*, 2009.

[48] ANSYS Inc., *Verification Manual for the Mechanical APDL Application*, 2009.

[49] Lachaud, J., Magin,T.E., Cozmuta, I., Mansour, N.N., *A Short Review of Ablative Material Response Models and Simulation Tools*, 7th European Symposium on the Aerothermodynamics, 9-12 May 2011,Brugge, Belgium

[50] ANSYS Inc., *ANSYS Parametric Design Language Guide, Release 12.0*, 2009

[51] Tokentools., http://www.tokentools.com.au/library/ILLUS.htm., last visited on May 2012.

[52] Rice, R.C., Jackson, J. L., Bakuckas, J., Thompson, S., *Metallic Materials Properties Development and Standardization*, U.S. Department of Transportation Federal Aviation Administration, Report No: DOT/FAA/AR-MMPDS-01, 2003.

[53] MSC Software. *MSC Nastran Thermal Analysis User's Guide*, 2002

[54] Özışık, M.N., *Finite Difference Methods in Heat Transfer,* CRC Press, Inc., 1994.

[55] Dassault Systems, *Abaqus Analysis User's Manual*, 2011.

[56] Stout, R., Billings, D., *Accuracy and Time Resolution in Thermal Transient Analysis,* International ANSYS Conference, 2002.

[57] R J Chase Company, Inc., http://www.rjchase.com/ptfe_handbook.pdf., last visited on November 2012.

[58] Maurice, A.F., *Aerodynamic Performance Predictions of a SA-2 Missile Using Missile DATCOM*, M.Sc. Thesis, Naval Postgraduate School, 2009.

[59] Sooy, T.J., Schmidt, R.Z., *Aerodynamic Predictions, Comparisons and Validations Using Missile DATCOM (97) and Aeroprediction 98 (AP98)*, Journal of Spacecraft and Rockets, Vol. 42., No.2, 2005.

[60] Aksel, M. H., Eralp, O.C., *Gas Dynamics*, Prentice Hall, 1994.

[61] Simsek, B., Kuran, B., Tunc, T., and Yüncü, H., *Thermal Reliability Prediction of External Insulation System in Supersonic Speeds Using Surrogate Models*, AIAA Paper No.2011-2038, 2011.

[62] Çeçen V., *Thermal Properties and Mechanical Anisotropy in Polymer Composites*, Ph.D. Thesis, Dokuz Eylul University, September 2006.

APPENDIX A

SOLUTION TECHNIQUE AND THERMAL ANALYSIS CAPABILITIES OF ANSYS

In this Appendix section, detailed information about solution procedure and thermal capabilities of ANSYS are given.

A.1. Solution Technique of Governing Equation

As mentioned before, ANSYS solves equation (A.1), given below, during thermal analyses.

$$\rho c_p \left(\frac{\partial T}{\partial t} + \{v\}^T \{L\}T \right) = \{L\}^T ([D]\{L\}T) + q''' \tag{A.1}$$

where;

$$\{L\} = \begin{Bmatrix} \frac{\partial}{\partial x} \\ \frac{\partial}{\partial y} \\ \frac{\partial}{\partial z} \end{Bmatrix} = vector\ operator \tag{A.2}$$

and,

$$\{v\} = \begin{Bmatrix} v_x \\ v_y \\ v_z \end{Bmatrix} = velocity\ vector\ for\ mass\ transport\ of\ heat \tag{A.3}$$

In these equations, {L} can be interpreted as grad operator and {L}^{T} can be interpreted as divergence operator. Moreover, [D] is the conductivity matrix and it is written as [46]:

$$[D] = \begin{bmatrix} k_x & 0 & 0 \\ 0 & k_y & 0 \\ 0 & 0 & k_z \end{bmatrix} \tag{A.4}$$

By premultiplying equation (5.2) by a virtual change in temperature, integration over the volume of the element and by doing some manipulations the following equation is reached. The full derivation is not given in this thesis but it can be found at reference [46]

$$[C_e^t]\{\dot{T}_e\} + ([K_e^{tm}] + [K_e^{tb}] + [K_e^{tc}])\{T_e\} = \{Q_e^f\} + \{Q_e^c\} + \{Q_e^g\} \tag{A.5}$$

In Equation (5.6) , $[C_e^t]$ is the element specific heat (thermal damping) matrix, $[K_e^{tm}]$ is the element mass transport conductivity matrix, $[K_e^{tb}]$ is the element diffusion conductivity matrix, $[K_e^{tc}]$ is the element convection surface conductivity matrix, $\{Q_e^f\}$ is the element mass flux vector, $\{Q_e^c\}$ is the element convective surface heat flow vector and $\{Q_e^g\}$ is the element heat generation load.

Heat flow evaluations are calculated from the element thermal gradients at the integration points. The element thermal gradients at the integration points are [46]:

$$\{a\} = \{L\}T = \left[\frac{\partial T}{\partial x}, \frac{\partial T}{\partial y}, \frac{\partial T}{\partial z}\right]^T \tag{A.6}$$

where $\{a\}$ is the thermal gradient vector, $\{L\}$ is the vector operator. By using shape functions Equation (A.6) can be written as [46]:

$$\{a\} = [B]\{T_e\} \tag{A.7}$$

where $[B]$ is the shape function derivative matrix evaluated at the integration points and $\{T_e\}$ is the nodal temperature vector of an element. Then, the heat flux vector at the integration points may be computed from the thermal gradients [46]:

$$\{q\} = -[D]\{a\} = -[D][B]\{T_e\} \tag{A.8}$$

In Equation (A.8) $\{q\}$ is the heat flux vector.

 As a result to find the nodal temperatures ANSYS can use Newton-Raphson procedure and then by using nodal temperatures heat flow in the material can be found.

During ablation simulations, ANSYS used Newton-Raphson procedure to solve the governing equations mentioned above. For a set of simultaneous equations, yielded by the finite element discretization process:

$$[K]\{u\} = \{F^a\} \tag{A.9}$$

where $[K]$ is the coefficient matrix, $\{u\}$ is the vector of unknown DOF(degree of freedom) values and $\{F^a\}$ is the vector applied loads. If the coefficient matrix, [K] is itself a function of the unknown DOF values (i.e. if material properties are temperature dependent), then Equation (A.9) is a nonlinear equation and Newton-Raphson method is an iterative process of solving the nonlinear equations. It can be written as [43]:

68

$$[K_i^T]\{\Delta u_i\} = \{F^a\} - \{F_i^{nr}\} \tag{A.10}$$

$$\{u_{i+1}\} = \{u_i\} + \{\Delta u_i\} \tag{A.11}$$

In thermal analyses, $[K_i^T]$ is the conductivity matrix, $\{u_i\}$ is the temperature vector and $\{F_i^{nr}\}$ is the resisting load vector calculated from the element heat flows. More than one, Newton-Raphson iterations can be needed to obtain a converged solution. Schematic representative of iteration and its next iteration for Newton-Raphson procedure is given in Figure 62.
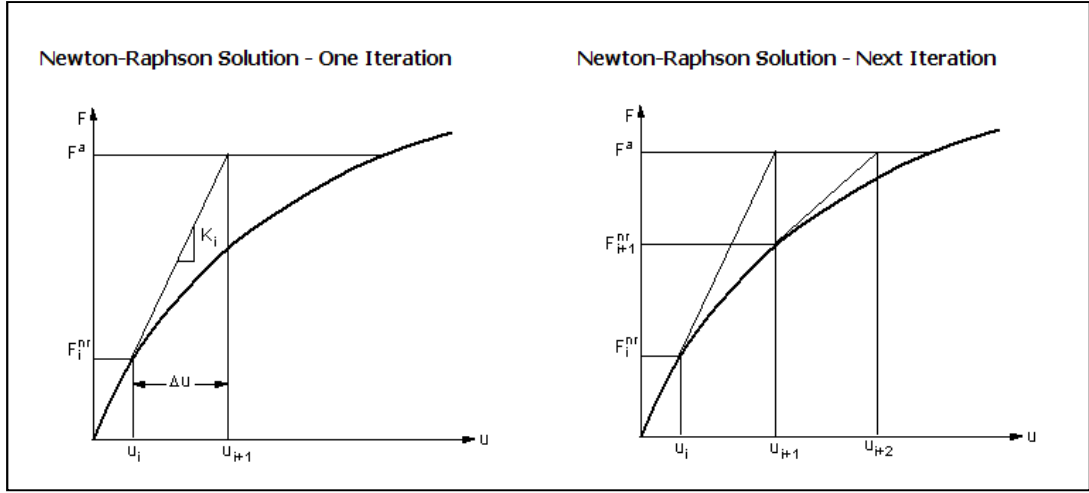
Figure 62: Schematic Representation of Newton-Raphson Iterations [43]

Until convergence criteria is achieved, previously mentioned Newton-Raphson iterations are performed. Numbers of iterations are limited by the maximum number of allowed iterations determined by the user or the program. Convergence is achieved when [46]:

$$\|\{R\}\| < \varepsilon_R R_{ref} \quad \text{(out-of-balance convergence)} \tag{A.12}$$

and/or

$$\|\{\Delta u_i\}\| < \varepsilon_u U_{ref} \quad \text{(DOF increment convergence)} \tag{A.13}$$

where {R} is the residual vector and it can be written as:

$$\{R\} = \{F^a\} - \{F^{nr}\} \tag{A.14}$$

$\{\Delta u_i\}$ is the DOF increment vector, ε_R and ε_u are the tolerances and R_{ref} and U_{ref} are the reference values. ANSYS uses out-of-balance convergence by default and default tolerance values are 0.001. Moreover, $\|vector\|$ is a vector form which is a scalar measure of the magnitude of the vector. In ANSYS there are three norms to use for the $\|\{R\}\|$ value [46].

1. Infinite Norm: $\quad \|\{R\}\|_\infty = max|R_i|$ $\hfill$ (A.15)

2. L1 Norm: $\quad \|\{R\}\|_1 = \sum|R_i|$ $\hfill$ (A.16)

3. L2 Norm: $\quad \|\{R\}\|_2 = (\sum R_i^2)^{1/2}$ $\hfill$ (A.17)

For DOF increment convergence Δu can be substituted for R in the above equations. By default, ANSYS uses L2 norm [46].

A.2. Thermal Analysis Capabilities of ANSYS

ANSYS is a general purpose software which is used to simulate interactions of all disciplines of structural, vibration ,fluid mechanics, heat transfer and electromagnetic.

The main idea of the thermal analysis in ANSYS is to calculate nodal temperatures and to obtain other thermal quantities such as thermal gradients and thermal fluxes, by using nodal temperatures. Heat transfer calculations come from heat balance equations which are obtained from the principle of conservation of energy [47].

Three primary modes of heat transfer, conduction, convection and radiation can be modeled by using ANSYS.

Convection can be modeled as a boundary condition on solid elements or shell elements. Input values of convection modeling are the convection film coefficient and the bulk fluid temperature. Film coefficient can also be defined as a function of temperature. Moreover, by using FLOTRAN CFD elements details of convection such as fluid velocities, local values of film coefficient and temperature distribution in both fluid and solid region can be modeled [47].

Radiation can be modeled by using ANSYS in four different ways. These methods will not be expressed in detailed in this thesis study [47].

- modeling by using the radiation link element.
- modeling by using surface elements with radiation option
- modeling by generating radiation matrix and using it as a superelement in a thermal analysis
- modeling by using the Radiosity Solver Method.

In addition to the three modes of heat transfer phase change and internal heat generation can also be modeled by using ANSYS. Moreover, two types of thermal analyses, steady state thermal analysis and transient thermal analysis are supported by ANSYS. In the steady state thermal analysis temperature distribution are determined under steady state loading conditions and in the transient thermal analysis the temperature distribution are found under conditions varying over a period of time [47].

Used element types are the one of the most important parameters in Finite Element Analysis. Nearly 40 types of elements can be used for thermal analysis in ANSYS. Some types of elements are described and schematic views of them are given below.

Table 13: 2-D Solid Elements Supporting Thermal Analyses [47]

Element	Dimension	Shape or Characteristic	DOFs
PLANE35	2D	Triangle,6-node	Temperature at each node
PLANE55	2D	Quadrilateral,4-node	Temperature at each node
PLANE75	2D	Harmonic,4-node	Temperature at each node
PLANE77	2D	Quadrilateral,8-node	Temperature at each node
PLANE78	2D	Harmonic,8-node	Temperature at each node

Table 14: 3-D Solid Elements Supporting Thermal Analyses [47]

Element	Dimension	Shape or Characteristic	DOFs
SOLID70	3D	Brick,8-node	Temperature at each node
SOLID87	3D	Tetrahedron,10-node	Temperature at each node
SOLID90	3D	Brick,20-node	Temperature at each node

Table 15: Radiation Link Elements Supporting Thermal Analyses [47]

Element	Dimension	Shape or Characteristic	DOFs
LINK31	2D or 3D	Line,2-node	Temperature at each node

Table 16: Convection Link Elements Supporting Thermal Analyses [47]

Element	Dimension	Shape or Characteristic	DOFs
LINK34	3D	Line,2-node	Temperature at each node
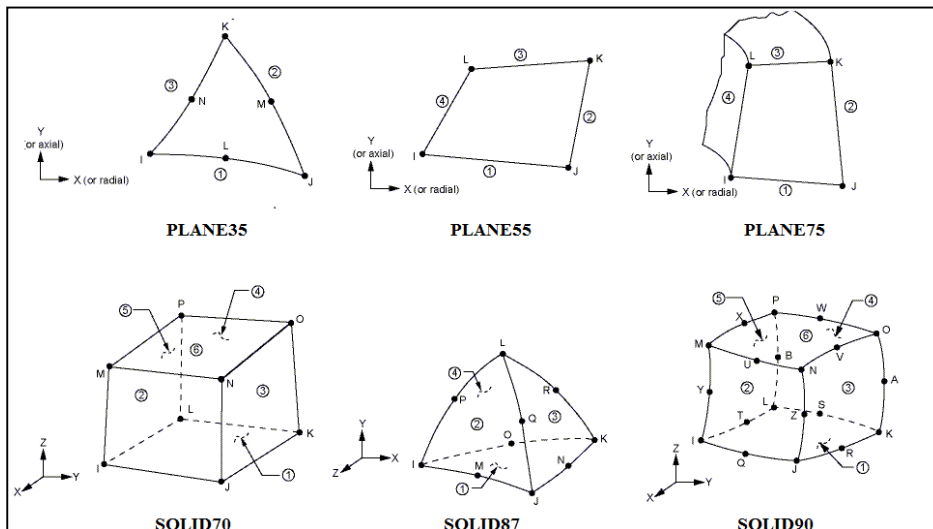
Figure 63: Schematic Representative of Some Thermal Elements [46]

For steady state and transient thermal analysis, three tasks exist. These tasks should be followed step by step.
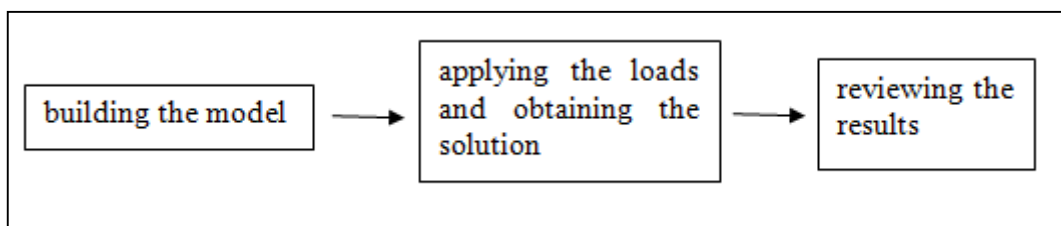
Figure 64: Three Main Steps of Thermal Analyses

First step includes meshing process and defining the material properties. Conductivity, specific heat capacity, density, enthalpy, emissivity and heat generation rate can be defined as a material property. All of the properties can be temperature dependent and conductivity can be defined as isotropic or orthotropic.

Moreover, if it is required, contact definition between contacting surfaces is also possible in this step. Second step, includes applying the boundary conditions and initial conditions. Moreover, required analysis options are also set in this step. Determination of time stepping (in transient analyses only) and convergence criteria and choice of the solver are the most important actions followed in this step. A third step includes plotting temperature distribution or other thermal quantities.

During transient thermal analyses determination of time stepping is very important to obtain correct results. To obtain good results there is relationship between the largest element size in the direction of heat flow and the smallest time step. Generally smaller mesh size with the same time step gives better results however; smaller time step with the same mesh size gives worse results [47]. The following relationship is recommended by ANSYS for determining the time step or mesh size (Δ) [47].

$$TS = \frac{\Delta^2}{4\alpha} \qquad\qquad (A.18)$$

Thermal analysis capabilities of ANSYS are demonstrated in *verification manual* [48]. In this manual different types of thermal analyses such as temperature distribution along a tapered fin (VM98), liquid solid phase change (VM104), heat transferred to a flowing fluid (VM126) are conducted and results are compared with the reference results.